POLITECNICO DI TORINO

Master Degree in Mechanical Engineering

Master's Degree Thesis

Model Order Reduction for Nonlinear Vibrations of Geometrically Nonlinear Structures

Academic Supervisor:
Prof. Stefano ZUCCA
Dr. Loic SALLES
Prof. Eugenio BRUSA

Graduate:
Mr. Pierluigi LONGOBARDI

ACADEMIC YEAR 2018-2019

Abstract

During the last decades the size of finite element models, used in industrial and research applications, is constantly growing. The increased of computational power and the accuracy of FEM software are leading an interest in nonlinear behaviour of the structures. However, the solution of large set of nonlinear equations is still computationally expensive. The idea of any Model Order Reduction (MOR) is to reduce the number of degrees of freedom of a given structure, so that it is possible to drastically decrease the number of unknowns of the full model into a subset of equations faster to solve. The aim of this work is to formulate a reduced order basis (ROB) without computing the solution of full model. In this way, all the equations will be projected on ROB able to capture the nonlinearity of the whole system. Therefore, the idea is to project a large system of equations onto a smaller subspace to create a lower dimensional space of reduced unknowns. In this thesis, the "nonlinear static condensation" and the "modal derivatives" have been presented to efficiently formulate a subspace of nonlinear differential equations of a geometrically nonlinear model. Moreover, it has been developed a method to analyse the dynamics of the 3D finite element turbofan jet engine compressor and fan blades. The nonlinear forced response (NFR) of the structure can be fast computed projecting of all the equations on a reduced order basis. The computational procedure has been designed to be adapted to a tip rubbing problems, so that it has been possible to consider the contact and geometric nonlinearities (large deformations) during the developing of the in-house code. The flexibility of the code allows to include both the geometric nonlinearities or the contact. The blade-casing interaction in turbofan jet engines can lead the structure to large deformations and this phenomenon cannot be neglected during the structural analysis.

Acknowledgements

Firstly, I would like to thank my thesis supervisor Dr. Loic Salles for giving me the unforgettable opportunity to work within the Rolls-Royce Vibration University Technology Centre at Imperial College London. The door of his office was always open whenever I had a doubt or question about my research project. I would also like to thank Ms. Alessandra Vizzaccaro who contributed to the completion of this work with patience and work ethic. They consistently allowed this project to be my own work, steering me in the right direction whenever they thought I needed it. Without their passionate participation this thesis could not have been successfully conducted.

I am also grateful to Prof. Stefano Zucca and Prof. Eugenio Brusa, as my supervisors from Politecnico di Torino. Even from a distance, their support has been essential to organize the work and to prepare the thesis.

I would also like to show my gratitude to Prof. Olivier Thomas and Prof. Aurélien Grolet for hosting me at Arts et Métiers ParisTech in Lille for an interesting workshop on structural dynamics of geometrically nonlinear structures. It was a very stimulating meeting in which new ideas and interesting perspectives for the thesis came up.

Last but not the least, I would like to thank my parents Antonio and Antonella, my two brothers Gianmarco and Gianluca for supporting me with wise advice and for always being by my side.

Contents

List of Tables

List of Figures

Chapter 1

Introduction

The structural dynamics engineering has dramatically change over the last twenty years. The companies must fulfil always more stringent requirements to put competitive products on the market and to develop cutting-edge technologies. Nowadays, several numerical analysis tools are available to efficiently predict the dynamics behaviour of the structure. Nevertheless, the computational costs are still too high to solve a large set of nonlinear differential equations, therefore better numerical methods with high accuracy and flexibility are strongly needed. The logical response to this problem is the model order reduction (MOR), where the full model of the structure may be approximated into a reduced model of less computational complexity. There is a huge range of applications from the automotive sectors to the aerospace industries where most of the structure behaves nonlinearly. Due to the stringent requirements of the aerospace industry, where lightweight materials with high stiffness to weight ratio are commonly used, the nonlinear effects cannot be neglected during the dynamics design of the structure.

In this project has been developed a method to analyse the dynamics of the 3D finite element turbofan jet engine compressor and fan blades, so that the nonlinear forced response (NFR) of the structure can be fast computed projecting of all the equations on a reduced order basis. The computational procedure has been designed to be adapted to a tip rubbing problems, so that it has been possible to consider the contact and geometric nonlinearities during the developing of the in-house code. The flexibility of the code allows to include either the geometric nonlinearities or the contact. The idea of developing a code capable to capture the nonlinearities of the contact and the large deformations came up from a real problem found on a turbofan jet engine (1.1) at the level of compressor stages. The rubbing between the blades and the casing of the engine can lead the structure to large deformations that cannot be neglected during the structural analysis.
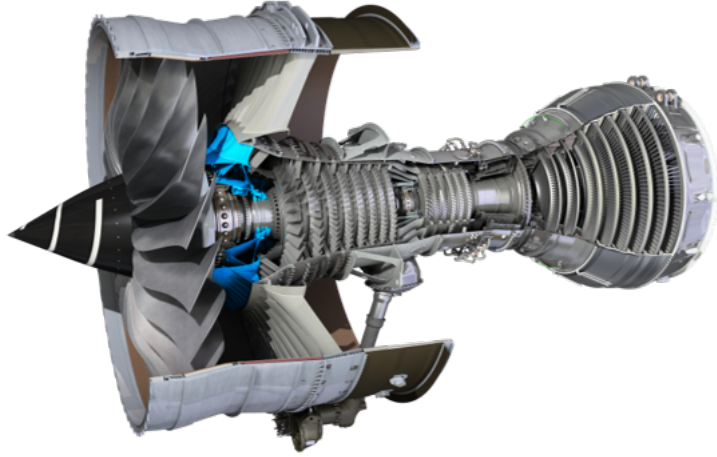
Figure 1.1: Assembly Rolls-Royce Trent 7000

The tip rubbing is a phenomenon that must be taken under control because it is one of the major responsible of the engine failure and maintenance due to the small gap between the tip blade and the liner (≈ 0.2 mm). The logical response to this problem would have been to increase the clearance between the blade and the engine casing; unfortunalely this would cause the engine to a dramatically reduction of its performances due to the leakages at the blade tip. Moreover, the fatigue loads acting on the blade tip can also lead to a premature failure or cracking of the blade.

Figure 1.2: Linear Modeshape vs. Nonlinear Modeshape

The model order reduction applied in linear structural dynamics cannot catch the nonlinearities of the structure at high oscillation amplitude. Therefore, the linear modal analysis describes an unrepresentative behaviour of the structures with large deformations (1.2).
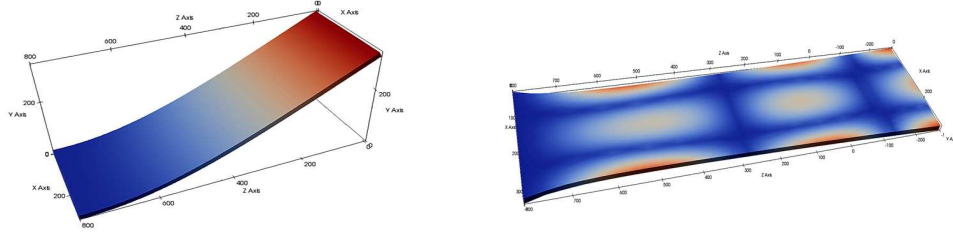
Figure 1.3: Bending (out-of-plane) and Membrane (in-plane) Modeshapes

In case of linear modeshape the structure tends to increase its length, which is a justified approximation only for small amplitudes. On the other hand, the nonlinear modeshape well represents the behaviour of the structure with large deformations. In addition, the linear analysis does not take into consideration the bending-membrane coupling (1.3); the risk is to overpredict the response leading the structure to a conservative design.

The idea of any Model Order Reduction (MOR) is reducing the number of degrees of freedom of a given structure, so that it is possible to reduce the number of unknowns of a large model into a subset of equations faster to solve. In this project have been used the Reduced Order Models (ROMs) where, projecting a large system of equations in a smaller subspace, has been possible to create a lower dimensional space of reduced unknowns.

Overall, the objective of the project is to develop a reduced order model (ROM) for nonlinear vibrations of geometrically nonlinear structures including contact and large deformations, so that the nonlinear forced response (NFR) of the structure can be fast computed projecting all the equations on a reduced order basis (ROB) able to capture the nonlinearities of the whole system.

1.1   Outline

The thesis has been written following the same logic of the implemented open-source code to trace the nonlinear force response of the geometrically nonlinear structure. In order to reduce the computational time to solve the nonlinear problem, it has been used a reduced order model technique named non-intrusive (indirect) method. This latter is a displacement-based indirect method, where the nonlinear coefficients of the quadratic and cubic stiffness have been calculated imposing a series of static nodal displacement fields (linear and nonlinear) to determine the nodal forces fields of the structure. Therefore, this technique can be used within any finite element software performing the nonlinear static analysis. In this way it has been possible to evaluate the nonlinear stiffness tensors starting from a structural finite element model.

Once the nonlinear stiffness tensors have been calculated, the nonlinear set of ordinary differential equations must be solved. In nonlinear dynamics is common to use numerical methods to solve nonlinear differential equations. The idea is to use the harmonic balance method (HBM) and the continuation algorithm (Asymptotic Numerical Method) to compute periodic solution of the systems described by means of smooth equations. The aim of this method is to quadratically recast the system in a quadratic arbitrary polynomial form before applying the harmonic balance.

Finally, the stiffness evaluation procedure has been validated against two examples available in bibliography: the simply supported plate [1] and the clamped-clamped beam [2] . In Chapter 8 a further investigation on the coupled modes of 3D FE beam model has been done to find out why a ROM using the linear modes as reduced basis is not enough to capture the dynamics of the geometrically nonlinear structure. A comparison between different techniques to proper select the reduced basis has been done to build a ROM able to predict the nonlinear behaviour of the structure including contact and geometric nonlinearities.

Formulation of Reduced Order Models (*CodeAster, Python*)	→	Validation of Reduced Order Models (*3D Beam & Plate*)	→	Harmonic Balance & Continuation Algorithm	→	Nonlinear Forced Response (*Matlab*)
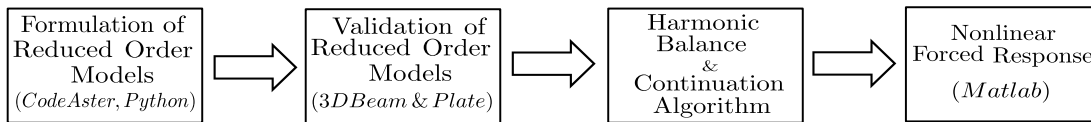
Figure 1.4: Procedure Description for Tracing the Nonlinear Forced Response

Chapter 2

The Finite Element Method

2.1 Introduction to FEM

The finite element method (FEM) is a discretizaion method for solving partial derivative differential equations. This method allows to solve a continuous problem in a discretized finite element problem, so that the linear algebraic system of equations can be solved in a closed form. In this project the FEM has been applied to structural static and dynamic analysis. In this chapter will be provided only the main features of the finite element method useful to understand how a finite element software works. The FEM is based on the subdivision of the continuous physical structure into a finite number of parts. In literature it is possible to find different element formulations such as: beam elements, shell elements, plate elements, 3D solid elements, and many others. Assembling all the structure's elements it has been possible to get the finite element formulation of the whole problem [3].

Overall, the finite element method steps to analyse an engineering problem are:

1. Discretize the physical structure into finite number of elements. The mesh is a grid that approximates the geometry of the problem's domain, this latter is formed by nodes and elements.

2. Select the shape function properly. The shape function is used to interpolate the domain variables over the elements and nodes. Usually, polynomials expressions are selected as shape (interpolation) functions. The degree of the polynomial is a function of the number of nodes element and if the problem is linear or nonlinear.

3. Evaluate the element properties. Establishing the finite element equation and writing it into a matrix relatives to the nodal value of the unknown.

4. Assemble the element equations. In order to evaluate the global matrices for the whole system it is necessary to assemble all the element equations. This means combining the equations of the local elements with all the discretization elements. Before solving the algebraic system, the boundary conditions have to be imposed. It means cancelling all the rows and columns corresponding to the degrees of freedom of nodes where the boundary conditions have been applied.

5. Solve the global system of algebraic equation. Usually, the linear algebraic system of equation of finite element method is written in sparse notation, and is symmetric and positive definite. To calculate the solution of the system iterative or direct methods can be used.

6. Evaluation other parameters of the system. It is possible to calculate additional parameters, for istance, in mechanical problems strains and stresses are of interest in addition to displacements, which can be obtained after solution of the global equation system.

2.1.1   Introduction to Geometrically Nonlinear FE

The finite element method can also be used to analyse nonlinear static, dynamic and transient problems. The application of nonlinear FEM to the solution of nonlinear static and dynamic problem is more complex than the linear and steady state problems within the commercial finite element software. They may involve a load step or time step integration (Newton–Raphson method), the majority of commercial finite element software programs include routines to optimaze the stepping, so that the solution can be reached in the minimum number of iterations during the computation.

A large displacement FE analysis is necessary when the structure's displacements become so large that the original stiffness matrix of the system doesn't represent the stucture. The finite element problems in terms of large displacement can be splitted into two types: those which result in a small (element) strains, and those resulting in large finite strains. Small strain behaviour means that the material remains elastic, and consequently that the structure returns to its original configuration when the loading is removed. The elements that show large strains, with the exception of hyperelastic materials (such as rubber), require non-linear material properties (such as nonlinear costitutive law), that in this project have not been taken into account.

In continuum mechanics a solid structure is mathematically treated as a continuum body constructed by a set of material particles. The position of all material particles comprising the body at a given time t is called the configuration of the body, and it is denoted by **C**. A sequence of body configurations for all times t defines the motion of the body. The motion of a body or structure starts from an initial position, usually undeformed, state at time t=0, called initial configuration, $\mathbf{C}_0$, to which displacements **u** are referred. Each point on the equilibrium path corresponds to a deformed configuration, $\mathbf{C}_n$, at time $t = t_n$.
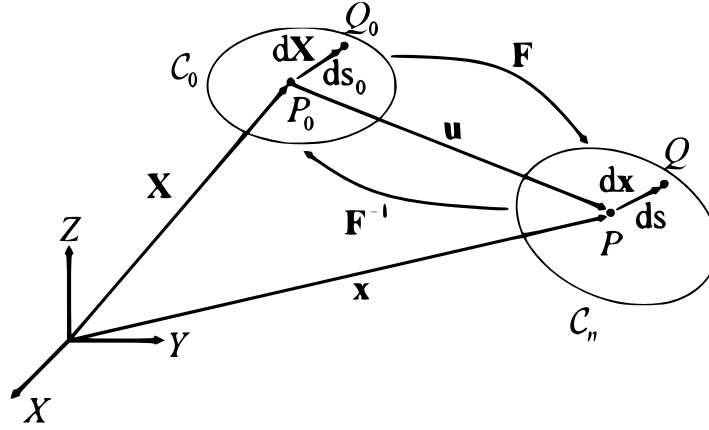
Figure 2.1: Fixed Global Cartesian Coordinates System (X,Y,Z)

The deformation of the body can be described by two set of coordinates:

1) Lagrangian Coordinates **X**

2) Eulerian Coordinates **x**=**x**(**X**, t)

In the Lagrangian approach, all physical quantities including displacements, strains and stresses are expressed as functions of time t and their initial position **X** , in the Eulerian approach they are functions of time and their current position. Nevertheless, both approaches can be used, even if the Lagrangian approach is the most used in solid and structural mechanics problems. The Lagrangian description of motion is referred to a fixed global reference frame, expressed in cartesian coordinates (X ,Y,Z).

In the Lagrangian description displacements of any material point in the solid is given by:

$$\boldsymbol{x}(\boldsymbol{X}, t) = \boldsymbol{X} - \boldsymbol{u}(\boldsymbol{X}, t) \tag{2.1}$$

$$\boldsymbol{u}(\boldsymbol{X}, t) = \boldsymbol{X} - \boldsymbol{x}(\boldsymbol{X}, t) \tag{2.2}$$

In order to define the strain we need to know the relative motion of two points on the body. Considering two points P and Q, where at time t=0 the relative position is $d\boldsymbol{X}$ and at time $t = t_n$ the relative position is $d\boldsymbol{x}$.

2.1.2 Green-Lagrange Strain Tensor

The deformation gradient $[\boldsymbol{F}]$, describes the point by point deformation of the infinitesimal body particles $d\boldsymbol{X}$, with length ds_0 , in $\mathbf{C}_0$ (the initial configuration) to its new position $d\boldsymbol{x}$, with length ds , in $\mathbf{C}_n$ (the current configuration):

$$d\boldsymbol{x} = \boldsymbol{F} d\boldsymbol{X} \tag{2.3}$$

$$[\boldsymbol{F}] = \left[\frac{\partial \boldsymbol{x}}{\partial \boldsymbol{X}} \right] = \left[\frac{\partial (\boldsymbol{X} + \boldsymbol{u})}{\partial \boldsymbol{X}} \right] = [\boldsymbol{I}] + \left[\frac{\partial \boldsymbol{u}}{\partial \boldsymbol{X}} \right] = [\boldsymbol{I}] + [\boldsymbol{G}] \tag{2.4}$$

$$[\boldsymbol{F}] = \begin{bmatrix} \frac{\partial x}{\partial X} & \frac{\partial x}{\partial Y} & \frac{\partial x}{\partial Z} \\ \frac{\partial y}{\partial X} & \frac{\partial y}{\partial Y} & \frac{\partial y}{\partial Z} \\ \frac{\partial z}{\partial X} & \frac{\partial z}{\partial Y} & \frac{\partial z}{\partial Z} \end{bmatrix} \tag{2.5}$$

$$[\boldsymbol{G}] = \begin{bmatrix} \frac{\partial u}{\partial X} & \frac{\partial u}{\partial Y} & \frac{\partial u}{\partial Z} \\ \frac{\partial v}{\partial X} & \frac{\partial v}{\partial Y} & \frac{\partial v}{\partial Z} \\ \frac{\partial w}{\partial X} & \frac{\partial w}{\partial Y} & \frac{\partial w}{\partial Z} \end{bmatrix} \tag{2.6}$$

where $[\boldsymbol{F}]$ is the deformation gradient; $[\boldsymbol{I}]$ is unit tensor; $[\boldsymbol{G}]$ is displacement gradient tensor.

The deformation gradient $\boldsymbol{F}$ describes how much the structure is stretched from $\mathbf{C}_0$ to $\mathbf{C}_n$. The nonlinear analysis has been considered in terms of large rigid body motion and large deformations. The Green-Lagrange strain tensor is reduced to the infinitesimal linear strains when the nonlinear terms are neglected.

One finite strain measure that has these desired properties is the Green strain tensor $[\boldsymbol{\varepsilon}]$, which is a symmetric tensor defining the relationship between the squares of the length vector $d\boldsymbol{X}$ with length ds_0 in $\boldsymbol{C}_0$ to its deformed vector $d\boldsymbol{x}$ with length ds in $\boldsymbol{C}_n$:

$$ds^2 - ds_0^2 = 2d\boldsymbol{X}^T[\varepsilon]d\boldsymbol{X} \tag{2.7}$$

Green strain tensor $[\boldsymbol{\varepsilon}]$ can also be expressed in terms of the deformation gradient $[\boldsymbol{F}]$ through:

$$[\boldsymbol{\varepsilon}] = \frac{1}{2}\left(\left[\boldsymbol{F}^T\right]\left[\boldsymbol{F}\right] - [\boldsymbol{I}]\right) \tag{2.8}$$

where:

$$[\boldsymbol{\varepsilon}] = \begin{bmatrix} \varepsilon_{xx} & \varepsilon_{xy} & \varepsilon_{xz} \\ \varepsilon_{yx} & \varepsilon_{yy} & \varepsilon_{yz} \\ \varepsilon_{zx} & \varepsilon_{zy} & \varepsilon_{zz} \end{bmatrix} \tag{2.9}$$

The six strain components of the Green strain tensor may be expressed in terms of the displacement gradients:

9

$$\varepsilon_{xx} = \frac{\partial u}{\partial X} + \frac{1}{2}\left[\left(\frac{\partial u}{\partial X}\right)^2 + \left(\frac{\partial v}{\partial X}\right)^2 + \left(\frac{\partial w}{\partial X}\right)^2\right]$$

$$\varepsilon_{yy} = \frac{\partial v}{\partial Y} + \frac{1}{2}\left[\left(\frac{\partial u}{\partial Y}\right)^2 + \left(\frac{\partial v}{\partial Y}\right)^2 + \left(\frac{\partial w}{\partial Y}\right)^2\right]$$

$$\varepsilon_{zz} = \frac{\partial w}{\partial Z} + \frac{1}{2}\left[\left(\frac{\partial u}{\partial Z}\right)^2 + \left(\frac{\partial v}{\partial Z}\right)^2 + \left(\frac{\partial w}{\partial Z}\right)^2\right]$$

$$\varepsilon_{xy} = \frac{1}{2}\left(\frac{\partial u}{\partial Y} + \frac{\partial v}{\partial X}\right) + \frac{1}{2}\left[\left(\frac{\partial u}{\partial X}\right)\left(\frac{\partial u}{\partial Y}\right) + \left(\frac{\partial v}{\partial X}\right)\left(\frac{\partial v}{\partial Y}\right) + \left(\frac{\partial w}{\partial X}\right)\left(\frac{\partial w}{\partial Y}\right)\right]$$

$$\varepsilon_{yz} = \frac{1}{2}\left(\frac{\partial v}{\partial Z} + \frac{\partial w}{\partial Y}\right) + \frac{1}{2}\left[\left(\frac{\partial u}{\partial Y}\right)\left(\frac{\partial u}{\partial Z}\right) + \left(\frac{\partial v}{\partial Y}\right)\left(\frac{\partial v}{\partial Z}\right) + \left(\frac{\partial w}{\partial Y}\right)\left(\frac{\partial w}{\partial Z}\right)\right]$$

$$\varepsilon_{zx} = \frac{1}{2}\left(\frac{\partial w}{\partial X} + \frac{\partial u}{\partial Z}\right) + \frac{1}{2}\left[\left(\frac{\partial u}{\partial Z}\right)\left(\frac{\partial u}{\partial X}\right) + \left(\frac{\partial v}{\partial Z}\right)\left(\frac{\partial v}{\partial X}\right) + \left(\frac{\partial w}{\partial Z}\right)\left(\frac{\partial w}{\partial X}\right)\right]$$

$$(2.10)$$

The Green strain tensor is symmetric and if the nonlinear portion (that enclosed in square brackets) is neglected, we obtain the infinitesimal strains:

$$(\varepsilon_{xx}, \ \varepsilon_{yy}, \ \varepsilon_{zz}, \ \gamma_{xy} = 2\varepsilon_{xy}, \ \gamma_{yz} = 2\varepsilon_{yz}, \ \gamma_{zx} = 2\varepsilon_{zx}) \tag{2.11}$$

Green strain tensor is often used for problems with large displacements, large rigid body motions but small strains. Several other finite strain measures are used in nonlinear continuum mechanics, however, they all have to satisfy the constraints of finite strain measures, in which they must predict zero strains for arbitrarily rigid-body motions, and reduce to the infinitesimal strains if the nonlinear terms are neglected.

2.1.3   PK1 and PK2 Stress Tensors

The force per unit of area is defined as:

$$\boldsymbol{t} = \frac{d\boldsymbol{f}}{dA} \tag{2.12}$$

where $d\boldsymbol{f}$ is the infinitesimal force vector that acts on the infinitesimal area element dA in deformed configuration.
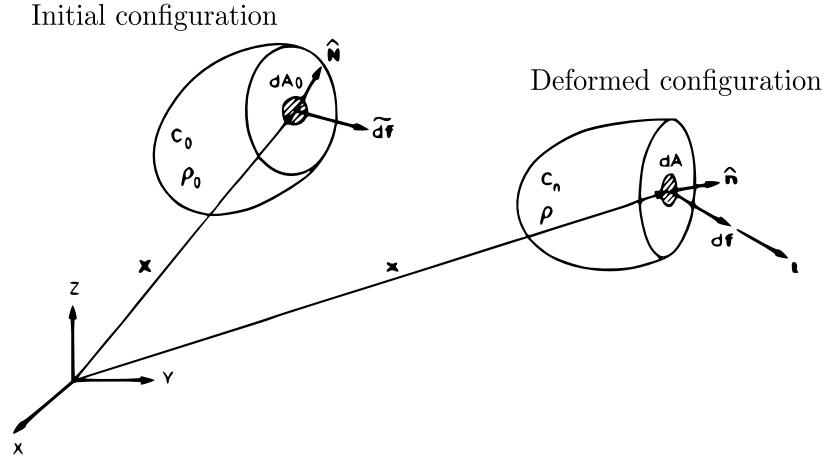
Figure 2.2: Body Configuration in Fixed Global Cartesian Coordinates System

The Cauchy or true stress tensor $\boldsymbol{\sigma}$, is conjugated to the strain tensor $\boldsymbol{\varepsilon}$. It gives the current force per unit area in deformed configuration:

$$\boldsymbol{t} = [\boldsymbol{\sigma}]\, \hat{\boldsymbol{n}} \tag{2.13}$$

where $\hat{\boldsymbol{n}}$ is the unit vector outward normal to the infinitesimal area element dA in deformed configuration. Multiplying $\boldsymbol{\sigma}$ by the determinant of $[\boldsymbol{F}]$ (J=$det([\boldsymbol{F}])$) gives the Piola-Kirchhoff stress tensor (PK1) $\boldsymbol{\tau}$:

$$[\boldsymbol{\tau}] = \boldsymbol{J}\ [\boldsymbol{\sigma}] = det\left([\boldsymbol{F}]\right)[\boldsymbol{\sigma}] \tag{2.14}$$

11

A stress tensor works conjugated to the Green-Lagrange strain tensor $[\boldsymbol{\varepsilon}]$, it has to be referred to the initial undeformed configuration as is the Green-Lagrange strain tensor. Nevertheless, it may be shown that the 2nd Piola-Kirchhoff stress tensor (PK2) $[\boldsymbol{S}]$ that gives the infinitesimal force $d\boldsymbol{f}$ acting on the undeformed area dA_0 is conjugated to $[\boldsymbol{\varepsilon}]$ and related to $[\boldsymbol{\sigma}]$ through:

$$[\boldsymbol{S}] = \boldsymbol{J}\,[\boldsymbol{F}]^{-1}\,[\boldsymbol{\sigma}]\,[\boldsymbol{F}]^{-T} = [\boldsymbol{F}]^{-1}\,[\boldsymbol{\tau}]\,[\boldsymbol{F}]^{-T} \tag{2.15}$$

The Piola-Kirchhoff stress tensors (PK1 and PK2) are used nonlinear finite element analysis (NFEA) involving large deformations and large rigid body motion, while the Cauchy stress tensor is a good approximation when the deformations are small (LFEA).

2.2   Isoparametric Solid Elements

The term "isoparametric" means that geometry and displacement field are specified in parametric form and are interpolated with the same shape functions $\boldsymbol{N}$ (polynomial). Shape functions used for interpolation are polynomials of the local coordinates (ξ, η, ζ) with $-1 \leq \xi, \eta, \zeta \leq 1$. Both coordinates and displacements are interpolated with the same shape functions. The hexahedral (or brick-type) linear 8-node (HEXA8) and quadratic 20-node (HEXA20) three-dimensional isoparametric elements are represented in Fig.2.3 [4].
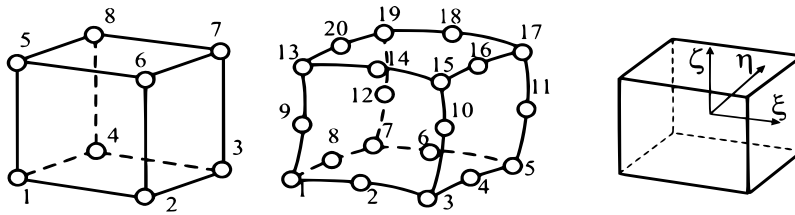
Figure 2.3: Linear and quadratic 3D finite elements and their representation in the local coordinate system

In global coordinates:

$${x} = [N] {x^e} \tag{2.16}$$

$${x} = {x \quad y \quad z} \tag{2.17}$$

$${x^e} = {x_1 \quad y_1 \quad z_1 \quad x_2 \quad y_2 \quad z_2 \ \ldots} \tag{2.18}$$

In local coordinates:

$${u} = [N] {q} \tag{2.19}$$

$${u} = {u \quad v \quad w} \tag{2.20}$$

$${\delta} = {u_1 \quad v_1 \quad w_1 \quad u_2 \quad v_2 \quad w_2 \ \ldots } \tag{2.21}$$

Here (u, v, w) are displacements at point with local coordinates (ξ, η, ζ); (u_i, v_i, w_i) are displacement values at nodes; (x, y, z) are point coordinates and (u_i, v_i, w_i) are coordinates of nodes. The shape functions of the linear element (HEXA8) are equal to:

$$N_i = \frac{1}{8} (1 + \xi_0) (1 + \eta_0) (1 + \zeta_0) \ , \qquad i = 1, \ \ldots, 8 \tag{2.22}$$

$$\xi_0 = \xi_i \hat{\boldsymbol{\xi}} \qquad \eta_0 = \eta_i \hat{\boldsymbol{\eta}} \qquad \zeta_0 = \zeta_i \hat{\boldsymbol{\zeta}} \tag{2.23}$$

where (ξ_i, η_i, ζ_i) are the values of local coordinates (ξ, η, ζ) at nodes.

For the quadratic element with 20 nodes (HEXA20) the shape functions can be written as the set of equations reported in 2.24.

$$N_i = \frac{1}{8} \left(1 + \xi_0\right) \left(1 + \eta_0\right) \left(1 + \zeta_0\right) \left(\xi_0 + \eta_0 + \zeta_0 - 2\right), \ \textit{vertices}$$

$$N_i = \frac{1}{4} \left(1 - \xi_0^2\right) \left(1 + \eta_0\right) \left(1 + \zeta_0\right) \ , \quad i = 2, \ 6, \ 14, \ 18$$

$$N_i = \frac{1}{4} \left(1 - \eta_0^2\right) \left(1 + \xi_0\right) \left(1 + \zeta_0\right) \ , \quad i = 4, \ 8, \ 16, \ 20 \tag{2.24}$$

$$N_i = \frac{1}{4} \left(1 - \zeta_0^2\right) \left(1 + \xi_0\right) \left(1 + \eta_0\right) \ , \quad i = 9, \ 10, \ 11, \ 12$$

Calculating all values of the shape function at each node is possible to assemble the matrix of shape function $\boldsymbol{N}$:

$$[N] = \begin{bmatrix} N_1 & 0 & 0 & N_2 & 0 & 0 & & N_i & 0 & 0 \\ 0 & N_1 & 0 & 0 & N_2 & 0 & \dots & 0 & N_i & 0 \\ 0 & 0 & N_1 & 0 & 0 & N_2 & & 0 & 0 & N_i \end{bmatrix} \tag{2.25}$$

The strain-displacement matrix $\boldsymbol{B}$ for three-dimensional elements has the following shape:

$$[B] = \begin{bmatrix} \partial N_i / \partial x & 0 & 0 \\ 0 & \partial N_i / \partial y & 0 \\ 0 & 0 & \partial N_i / \partial z \\ \partial N_i / \partial y & \partial N_i / \partial x & 0 \\ 0 & \partial N_i / \partial z & \partial N_i / \partial y \\ \partial N_i / \partial z & 0 & \partial N_i / \partial x \end{bmatrix} \tag{2.26}$$

Derivatives of shape functions with respect to the global coordinates are obtained as follows:

$$\begin{bmatrix} \partial N_i / \partial x \\ \partial N_i / \partial y \\ \partial N_i / \partial z \end{bmatrix} = [J]^{-1} \begin{bmatrix} \partial N_i / \partial \xi \\ \partial N_i / \partial \eta \\ \partial N_i / \partial \zeta \end{bmatrix} \tag{2.27}$$

where the Jacobian matrix $\boldsymbol{J}$ is:

$$[J] = \begin{bmatrix} \partial x/\partial \xi & \partial y/\partial \xi & \partial z/\partial \xi \\ \partial x/\partial \eta & \partial y/\partial \eta & \partial z/\partial \eta \\ \partial x/\partial \zeta & \partial y/\partial \zeta & \partial z/\partial \zeta \end{bmatrix} \tag{2.28}$$

The partial derivatives of (x, y, z) in respect to (ξ, η, ζ) are calculated by differentiation of displacements expressed with shape functions and nodal displacements:

$$\begin{aligned}
\frac{\partial x}{\partial \xi} &= \sum \frac{\partial N_i}{\partial \xi} x_i, & \frac{\partial y}{\partial \xi} &= \sum \frac{\partial N_i}{\partial \xi} y_i, & \frac{\partial z}{\partial \xi} &= \sum \frac{\partial N_i}{\partial \xi} z_i \\
\frac{\partial x}{\partial \eta} &= \sum \frac{\partial N_i}{\partial \eta} x_i, & \frac{\partial y}{\partial \eta} &= \sum \frac{\partial N_i}{\partial \eta} y_i, & \frac{\partial z}{\partial \eta} &= \sum \frac{\partial N_i}{\partial \eta} z_i \\
\frac{\partial x}{\partial \zeta} &= \sum \frac{\partial N_i}{\partial \zeta} x_i, & \frac{\partial y}{\partial \zeta} &= \sum \frac{\partial N_i}{\partial \zeta} y_i, & \frac{\partial z}{\partial \zeta} &= \sum \frac{\partial N_i}{\partial \zeta} z_i
\end{aligned} \tag{2.29}$$

The Jacobian allows to pass from global coordinates (x, y, z) to local coordinates (ξ, η, ζ):

$$dV = dxdydz = \det{(J)}d\xi d\eta d\zeta = |J| \, d\xi d\eta d\zeta \tag{2.30}$$

Equation of motion of a single element:

$$[m]\{\ddot{q}\} + [k]\{q\} = \{f\} \tag{2.31}$$

The element matrices have been calculated as follows [5]:

$$[m] = \int_V [N]^T \rho [N] dV = \int_{-1}^{1} \int_{-1}^{1} \int_{-1}^{1} [N]^T \rho [N] \, |J| \, d\xi d\eta d\zeta$$

$$[k] = \int_V [B]^T [E][B] dV = \int_{-1}^{1} \int_{-1}^{1} \int_{-1}^{1} [B]^T [E][B] \, |J| \, d\xi d\eta d\zeta \qquad (2.32)$$

$$\{f\} = \int_V [N]^T \left\{ f^V \right\} dV + \int_S [N]^T \left\{ f^S \right\} dS$$

where $[m]$ and $[k]$ are the mass, stiffness element matrices respectively; while $\{f\}$ is the force element vector.

After computing the matrices and vectors entries, the assembly process is used to build the global matrices of the system. Solving the algebraic system of equations it is possible to calculate the displacements at nodes of the finite element model. Stresses and strains inside the elements are determined with the use of the displacement differentiation matrix and elastic matrix:

$$\{\varepsilon\} = [B] \{q\}$$
$$\{\sigma\} = [E] \{\varepsilon\} \qquad (2.33)$$

where $[E]$ is the isotropic linear elastic matrix:

$$[E] = \begin{bmatrix} \lambda + 2\mu & \lambda & \lambda & 0 & 0 & 0 \\ \lambda & \lambda + 2\mu & \lambda & 0 & 0 & 0 \\ \lambda & \lambda & \lambda + 2\mu & 0 & 0 & 0 \\ 0 & 0 & 0 & \mu & 0 & 0 \\ 0 & 0 & 0 & 0 & \mu & 0 \\ 0 & 0 & 0 & 0 & 0 & \mu \end{bmatrix} \qquad (2.34)$$

16

the Lamé constants are:

$$\lambda = \frac{\nu E}{(1 + \nu)(1 - 2\nu)} \; , \quad \mu = \frac{E}{2(1 + \nu)} \tag{2.35}$$

2.2.1 Assembly Operations 3D Element

The assemble of the element equations into the system of linear algebraic equations consists to add each element stiffness and mass into the corresponding places of the global stiffness and mass matrices, and summing the force vector coefficients into the global force vector. These procedures are always the same regardless of type of problem and the number of elements used in the finite element analysis [5].

The matrices assembly operations are given by the following relations:

$$[K] = [A]^T [K_d] [A] \; , \quad \boldsymbol{Global\ Stiffness\ Matrix}$$

$$[M] = [A]^T [M_d] [A] \; , \quad \boldsymbol{Global\ Mass\ Matrix} \tag{2.36}$$

$$\{F\} = [A]^T \{F_d\} \; , \quad \boldsymbol{Global\ Force\ Vector}$$

where K_d, M_d, F_d are:

$$[K_d] = \begin{bmatrix} [k_1] & 0 & 0 \\ 0 & [k_2] & 0 \\ 0 & 0 & \ldots \end{bmatrix} \; , \quad [M_d] = \begin{bmatrix} [m_1] & 0 & 0 \\ 0 & [m_2] & 0 \\ 0 & 0 & \ldots \end{bmatrix} \; , \quad \{F_d\} = [\{F_1\} \; \{F_2\} \; \ldots \;] \tag{2.37}$$

$[A]$ is matrix of unit entries (usually never used in FEM codes) providing a connection between global and local numbers of nodes.

2.3 Plate Theory

Consider a rectangular flat plate element with constant thickness h. In this section has been treated the DKT and DKQ plate elements. The plate elements are particularly used to model structures where the relationship between dimensions (characteristic thickness/length) is almost 1/10 . The finite plate elements are most used in fields such as: civil and mechanical engineering in order to perform the modal analysis, the analysis of buckling of Euler, analysis of the elastic multi-layer composite material structures, etc.

In curved structures may be necessary to use a large number elements in order to approach the geometry of the structure correctly. The "Discrete Kirchhoff" (DKT and DKQ) kinematics formulation allows good performances in terms of static and modal analysis. The degrees of freedom of plate elements are the translations and rotations of the nodes [4].

2.3.1 Kirchhoff Plate Element

Plate elements are based on the theory of the plates in small displacements and small deformations. The displacement field changes linearly with the thickness $h(x, y)$ of the plate.
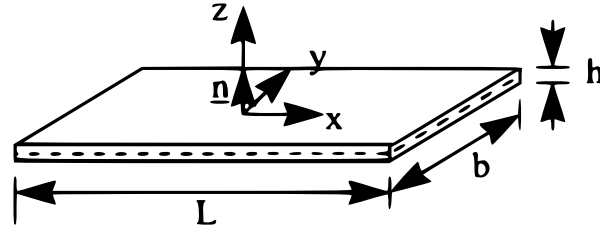
Figure 2.4: Geometry of the Plate Elements

According to Hencky-Mindlin kinematic theory has been possible to define the displacement of a single point on the plate:

$$
\begin{bmatrix} u_x\,(x, y, z) \\ u_y\,(x, y, z) \\ u_z\,(x, y, z) \end{bmatrix} = \begin{bmatrix} u(x, y) \\ v(x, y) \\ w(x, y) \end{bmatrix} + z \begin{bmatrix} \theta_y(x, y) \\ -\theta_x\,(x, y) \\ 0 \end{bmatrix} = \begin{bmatrix} u(x, y) \\ v(x, y) \\ w(x, y) \end{bmatrix} + z \begin{bmatrix} \beta_x(x, y) \\ \beta_y\,(x, y) \\ 0 \end{bmatrix} \tag{2.38}
$$

where (u, v, w) are the displacements of a single plate point with respect to the average surface and (θ_x, θ_y) the rotations along the x and y axes. Nevertheless, it has been useful to introduce β_x and β_y in order to symmetrize the formulation of the problem when the deformation will be defined.

$$\beta_x\left(x, y\right) = \theta_y\left(x, y\right) \qquad and \qquad \beta_y\left(x, y\right) = -\theta_x\left(x, y\right) \tag{2.39}$$

The three-dimensional deformations in a point of the plate are given by:

$$
\begin{aligned}
&\varepsilon_{xx} = e_{xx} + z\kappa_{xx}, &&\varepsilon_{yy} = e_{yy} + z\kappa_{yy} \\
&\gamma_{xy} = 2e_{xx} + 2z\kappa_{xy}, &&\gamma_{xz} = \beta_x + \frac{\partial w}{\partial x}, &&\gamma_{yz} = \beta_y + \frac{\partial w}{\partial y}
\end{aligned}
\tag{2.40}
$$

where e_{ij} represents the membrane deformation in correspondence of the average plate surface, while κ_{ij} is the curvature of the average surface.

The membrane deformations and the plate curvatures are:

$$
\begin{aligned}
&e_{xx} = \frac{\partial u}{\partial x} \ , &&e_{yy} = \frac{\partial v}{\partial y} \ , &&2e_{xy} = \frac{\partial v}{\partial x} + \frac{\partial u}{\partial y} \\
&\kappa_{xx} = \frac{\partial \beta_x}{\partial x} \ , &&\kappa_{yy} = \frac{\partial \beta_y}{\partial y} \ , &&2\kappa_{xy} = \frac{\partial \beta_x}{\partial y} + \frac{\partial \beta_y}{\partial x}
\end{aligned}
\tag{2.41}
$$

where the deformation ε_{zz}, as well as the stress σ_{zz}, along z-axis is negligible with respect the others two directions.

The stress tensor can be written as:

$$\begin{bmatrix} \sigma_{xx} \\ \sigma_{yy} \\ \sigma_{xy} \\ \sigma_{yz} \\ \sigma_{zx} \end{bmatrix} = \boldsymbol{C}\,(e,\alpha) \begin{bmatrix} \varepsilon_{xx} \\ \varepsilon_{yy} \\ \varepsilon_{xy} \\ \varepsilon_{yz} \\ \varepsilon_{zx} \end{bmatrix} = [C]\{e\} + z[C]\{\kappa\} + [C]\{\gamma\} \qquad (2.42)$$

$$[C] = \frac{E}{1-\nu^2} \begin{bmatrix} 1 & \nu & 0 & 0 & 0 \\ \nu & 1 & 0 & 0 & 0 \\ 0 & 0 & \frac{1-\nu}{2} & 0 & 0 \\ 0 & 0 & 0 & \frac{k}{2}(1-\nu) & 0 \\ 0 & 0 & 0 & 0 & \frac{k}{2}(1-\nu) \end{bmatrix} = \frac{E}{1-\nu^2} \begin{bmatrix} H_1 & 0 \\ 0 & H_2 \end{bmatrix} \qquad (2.43)$$

where $[C]$ is the local tangent rigidity for isotropic linear elastic behaviour, κ is a factor of transverse correction of sharing (κ=1 for DKT and DKQ), E is the Young's modulus and ν is the Poisson's ratio.

The finite plate elements DKT and DKQ are based on the Coils–Kirchhoff theory neglecting the transverse distortions γ_x and γ_y. The discretization of displacement field for isoparametric elements may be written as dot product between the kth shape function and the associated displacement u_k.

$$u = \sum_{k=1}^{N} N_k u_k \;, \quad v = \sum_{k=1}^{N} N_k v_k, \quad w = \sum_{k=1}^{N} N_k w_k \qquad (2.44)$$

The discretization has been maintained for β_x and β_y, so that β_s is the quadratic side while β_n is the linear one.
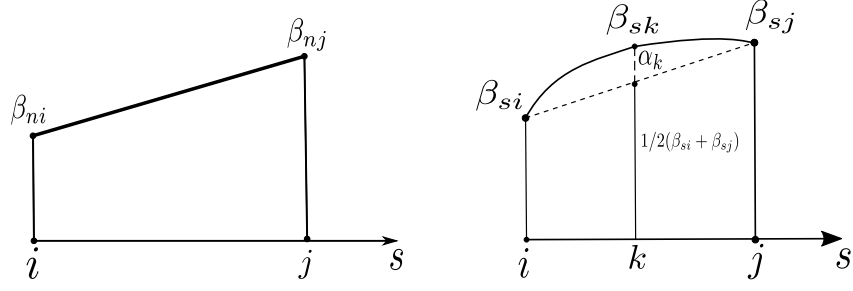
Figure 2.5: Linear and Quadratic Rotations

$$\beta_x = \sum_{k=1}^{N} N_k \beta_{x_k} + \sum_{k=N+1}^{2N} P_k C_k \alpha_k \ , \quad \beta_y = \sum_{k=1}^{N} N_k \beta_{y_k} + \sum_{k=N+1}^{2N} P_k S_k \alpha_k \qquad (2.45)$$

$$\begin{pmatrix} \beta_s \\ \beta_n \end{pmatrix} = \begin{pmatrix} C & S \\ S & -C \end{pmatrix} \begin{pmatrix} \beta_x \\ \beta_y \end{pmatrix} \qquad (2.46)$$

where C_i and S_i are the directional cosine and sine respectively, and (β_x, β_y) are:

$$\beta_x = -\frac{\partial w}{\partial x} \quad and \quad \beta_y = -\frac{\partial w}{\partial y} \qquad (2.47)$$

The shape functions $[N(\xi, \eta, \zeta); P(\xi, \eta, \zeta)]$ of DKT and DKQ plate elements are:

For DKT element:

$$
\begin{aligned}
&N_1(\xi, \eta) = 1 - \xi - \eta \quad &P_4(\xi, \eta) = 4\xi(1 - \xi - \eta) \\
&N_2(\xi, \eta) = \xi \quad &P_5(\xi, \eta) = 4\xi\eta \\
&N_3(\xi, \eta) = \eta \quad &P_6(\xi, \eta) = \frac{1}{2}(1 - \eta^2)(1 + \xi)
\end{aligned}
\qquad (2.48)
$$

21

For DKQ element:

$$N_1\left(\xi,\eta\right) = \frac{1}{4}(1-\xi)(1-\eta) \quad P_5\left(\xi,\eta\right) = \frac{1}{2}(1-\xi^2)(1-\eta)$$

$$N_2\left(\xi,\eta\right) = \frac{1}{4}(1+\xi)(1-\eta) \quad P_6\left(\xi,\eta\right) = 4\eta(1-\xi-\eta)$$

$$N_3\left(\xi,\eta\right) = \frac{1}{4}(1+\xi)(1+\eta) \quad P_7\left(\xi,\eta\right) = \frac{1}{2}(1-\xi^2)(1+\eta)$$

$$N_4\left(\xi,\eta\right) = \frac{1}{4}(1-\xi)(1+\eta) \quad P_8\left(\xi,\eta\right) = \frac{1}{2}(1-\eta^2)(1+\xi)$$

$$(2.49)$$
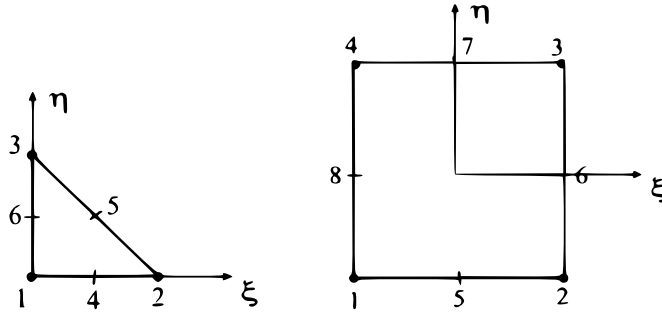
Figure 2.6: DKT and DKQ plate element representation

2.3.2 Assembly Operations Plate Element

The assembly operations for a plate element are the same of 3D element; the nodes of the plate element have 6 degrees of freedom $(u_x, u_y, u_z, \theta_x, \theta_y, \theta_z)$ or 5 if has been neglected the rotation along the z-axis $(\theta_z = 0)$.

Assembly of stiffness matrix:

$$K_{[5N\times5N]} = \begin{bmatrix} k_{m\ [2N\times2N]} & k_{mf\ [2N\times3N]} \\ k_{mf\ [3N\times2N]}^{T} & k_{f\ [3N\times3N]} \end{bmatrix} \ , \quad \boldsymbol{Element\ Stiffness\ Matrix}$$

(2.50)

$$k_{m} = \int_{S} B_{m}^{T} H_{m} B_{m} dS \ , \quad k_{mf} = \int_{S} B_{f}^{T} H_{mf} B_{m} dS \ , \quad k_{f} = \int_{S} B_{f}^{T} H_{f} B_{f} dS \quad (2.51)$$

$$H_{m} = \int_{-h/2}^{h/2} H \ dz \ , \quad H_{mf} = \int_{-h/2}^{h/2} H \ zdz \ , \quad H_{f} = \int_{-h/2}^{h/2} H \ z^{2} dz \quad (2.52)$$

$$with: \quad H = \frac{E}{1-\nu^{2}} \cdot H_{1} \quad and \quad H_{1} = \begin{bmatrix} 1 & \nu & 0 \\ \nu & 1 & 0 \\ 0 & 0 & (1-\nu)/2 \end{bmatrix} \quad (2.53)$$

All the previous equations are valid for an isotropic homogeneous elastic behavior of plate element, while the matrices k_{m}, k_{f}, k_{mf} are the stiffness matrices of membrane, flexural and of the coupling between the membrane and the out-of-plane inflection. The out-of-plane rigidity H_{mf} is equal to zero if there is a material symmetry with respect to the z-axis.

Assembly of mass matrix:

$$M = \begin{bmatrix} M_{m} & 0 & 0 & M_{mf} & 0 \\ 0 & M_{m} & 0 & 0 & M_{mf} \\ 0 & 0 & M_{m} & 0 & 0 \\ M_{mf}^{T} & 0 & 0 & M_{f} & 0 \\ 0 & M_{mf}^{T} & 0 & 0 & M_{f} \end{bmatrix} \ , \quad \boldsymbol{Element\ Mass\ Matrix} \quad (2.54)$$

$$M_m = \int_S \rho_m \ N^T N dS \ , \qquad M_{mf} = \int_S \rho_{mf} \ N^T N dS \ , \ \ M_f = \int_S \rho_f \ N^T N dS$$

(2.55)

$$\rho_m = \int_{-h/2}^{h/2} \rho \ dz \ , \ \ \rho_{mf} = \int_{-h/2}^{h/2} \rho \ z dz \ , \ \ \rho_f = \int_{-h/2}^{h/2} \rho \ z^2 dz$$

(2.56)

Once again, if the plate is homogeneous or symmetrical with respect to the z-axis, then ρ_{mf} can be considered nil; ρ_m, ρ_f, ρ_{mf} are the densities of membrane, flexural and of the coupling between the membrane and the out-of-plane inflection.

Chapter 3

Model Order Reduction (MOR)

3.1   Introduction to MOR

During the last decades the size of finite element models, used in industrial and research applications, is constantly growing. The increased of computational power and the accuracy of FEM software are leading an interest in nonlinear behaviour of nonlinear structure. However, the solution of large set of nonlinear equations is still computationally expensive. The idea of any Model Order Reduction (MOR) is reducing the number of degrees of freedom of a given structure, so that it is possible to reduce the number of unknowns of a large model into a subset of equations faster to solve.

The aircraft industry is very interested in model order reduction (MOR) for non-linear mechanical system as thin-walled structures. This latter structure is characterized by geometric nonlinearities where the coupling between the bending (out-of-plane) displacement couples with the axial (in-plane) one. The material is assumed to remain linear so that the Hook's law is still applicable.

In literature many MOR for linear mechanical system are widely explained, such as modal superposition, Guyan reduction, dynamic substructuring, Craig-Bampton method, Rubin's method etc. For nonlinear system, it has been possible to identify two reduction techniques. The first is Proper Orthogonal Decomposition (POD) where the full solution is necessary to compute a ROM of the structure, it is a tool to proper select the reduced order basis that will be used during the Galerkin projection. The second is the reduced order basis (ROB) without computing the solution of full model; all the equation will be projected on ROB able to capture the nonlinearity of the system.

In this project have been used the non-intrusive Reduced Order Models (ROMs) where, projecting a large system of equations in a smaller subspace has been possible to create a lower dimensional space of reduced unknowns.

3.2   MOR in Linear Structural Dynamics

The finite element method was developed for linear elastic systems first and then extended to nonlinear mechanical system. Because of limited resources in terms of computational power in 1960s and 1970s have been invented reduction and substructuring methods to decrease the computational time of structural dynamics systems. The scope of this thesis in not to discuss all the reduced order models founded in literature, so only few methods have been analysed [6].

In linear structural dynamics, the idea is to linearize the internal forces around an equilibrium point $x = 0$, so that the governing equation can be written as:

$$\boldsymbol{M\ddot{x}} + \boldsymbol{C\dot{x}} + \boldsymbol{Kx} = \boldsymbol{f} \tag{3.1}$$

where $\boldsymbol{M}$ is the mass matrix, $\boldsymbol{C}$ the damping matrix, $\boldsymbol{K}$ the Jacobian of the internal forces $\partial \boldsymbol{f}/\partial \boldsymbol{x}|_{x=0}$ and $\boldsymbol{f}$ is the external force vector. Introducing a subspace $\boldsymbol{V}$, it has been possible to project the linear operators onto the previous subspace. Applying the modal transformation $\boldsymbol{x} = \boldsymbol{Vq}$ and pre-multiply by the transpose of subspace $\boldsymbol{V}$ the governing equation become [7]:

$$\boldsymbol{V^T M V \ddot{q}} + \boldsymbol{V^T C V \dot{q}} + \boldsymbol{V^T K V q} = \boldsymbol{V^T f} \tag{3.2}$$

$$\widetilde{\boldsymbol{M}} \boldsymbol{\ddot{q}} + \widetilde{\boldsymbol{C}} \boldsymbol{\dot{q}} + \widetilde{\boldsymbol{K}} \boldsymbol{q} = \tilde{\boldsymbol{f}} \tag{3.3}$$

with $\widetilde{\boldsymbol{M}}$, $\widetilde{\boldsymbol{C}}$, $\widetilde{\boldsymbol{K}}$, $\tilde{\boldsymbol{f}}$ are the reduced mass, damping, stiffness and external force respectively.

The reduced matrices may be considered as a projection of linear basis onto the subspace $\boldsymbol{V}$. This latter, if correctly selected, should be able to catch all the dynamics of the system.

3.2.1 Modal Truncation

The simplest model order reduction is the modal truncation. The idea is to study a dynamical system as superposition of modal displacements calculating the free motion of the undamped homogeneous system:

$$\boldsymbol{M}\ddot{\boldsymbol{x}} + \boldsymbol{K}\boldsymbol{x} = \boldsymbol{f} \tag{3.4}$$

with the analytical solution equal to:

$$\boldsymbol{x}(t) = \boldsymbol{\Phi}cos(\omega t + \varphi) \tag{3.5}$$

substituting the (3.5) in (3.4) and cancelling the time dependence, the eigenproblem has been formulated as:

$$\omega^2\boldsymbol{M}\boldsymbol{\Phi} = \boldsymbol{K}\boldsymbol{\Phi} \tag{3.6}$$

solving the eigenproblem the solutions ω_i are the eigenvalues (undamped eigenfrequencies) and $\boldsymbol{\Phi}_i$ the corresponding eigenvectors (mode shapes). The eigenvectors represent the spatial solutions of the homogeneous undamped system oscillating around its equilibrium position with the associated natural frequencies. Since the solution of the eigenproblem is not unique, it is useful normalised the eigenvectors with respect the mass.

$$\boldsymbol{\Phi}^T\boldsymbol{M}\boldsymbol{\Phi} = \boldsymbol{I} \tag{3.7}$$

The mass is $\boldsymbol{M}$-orthogonal as well as the stiffness is $\boldsymbol{K}$-orthogonal, so that the modes are orthogonal one to each other. Selecting the eigenvectors $\boldsymbol{\Phi}$, as subspace

27

V, it has been possible to write the system as following:

$$\boldsymbol{\Phi}^T \boldsymbol{M} \boldsymbol{\Phi} \ddot{\boldsymbol{q}} + \boldsymbol{\Phi}^T \boldsymbol{C} \boldsymbol{\Phi} \dot{\boldsymbol{q}} + \boldsymbol{\Phi}^T \boldsymbol{K} \boldsymbol{\Phi} \boldsymbol{q} = \boldsymbol{\Phi}^T \boldsymbol{f} \qquad (3.8)$$

only in case of proportional damping $\boldsymbol{C} = \alpha \boldsymbol{K} + \beta \boldsymbol{M}$ (Rayleigh damping) is possible to write the equation of motion as:

$$\boldsymbol{I} \ddot{\boldsymbol{q}} + 2 \cdot \mathbf{diag}(\boldsymbol{\zeta}\boldsymbol{\omega}) \dot{\boldsymbol{q}} + \mathbf{diag}(\boldsymbol{\omega^2}) \boldsymbol{q} = \boldsymbol{\Phi}^T \boldsymbol{f} \qquad (3.9)$$

$$
\begin{bmatrix} \ddot{q}_1 \\ \vdots \\ \ddot{q}_N \end{bmatrix} + 2 \begin{bmatrix} \zeta_1\omega_1 & \cdots & 0 \\ \vdots & \ddots & \vdots \\ 0 & \cdots & \zeta_N\omega_N \end{bmatrix} \begin{bmatrix} \dot{q}_1 \\ \vdots \\ \dot{q}_N \end{bmatrix} + \begin{bmatrix} \omega_1^2 & \cdots & 0 \\ \vdots & \ddots & \vdots \\ 0 & \cdots & \omega_N^2 \end{bmatrix} \begin{bmatrix} q_1 \\ \vdots \\ q_N \end{bmatrix} = \begin{bmatrix} \phi_1^T \\ \vdots \\ \phi_N^T \end{bmatrix} f \qquad (3.10)
$$

Using the eigenvectors $\boldsymbol{\Phi}$ as modal basis the system has been decoupled into N independent equations, where N is equal to the number of degrees of freedom of the full system. It has been obtained a system of N independent ordinary differential equations ($ODEs$). In order to create a reduced order model of the system the full basis $\boldsymbol{\Phi}$ has been truncated selecting only the vibration modes of interest. Since all the equations are independent, the truncation does not affect the other modes.

$$\boldsymbol{V} = (\Phi_1, ..., \Phi_n) , \qquad with \quad n < N \qquad (3.11)$$

where n is the number of independent equations selected into the reduced basis $\boldsymbol{V}$.

3.2.2 Guyan Reduction

The idea of Guyan reduction is to eliminate all the internal degrees of freedom of the system by statically forcing the internal nodes of the structure to follow the boundary nodes. Neglecting the external forces acting on the internal dofs and all the inertia terms, the equation of the system can be written as:

$$\begin{bmatrix} \boldsymbol{K}_{II} & \boldsymbol{K}_{IB} \\ \boldsymbol{K}_{BI} & \boldsymbol{K}_{BB} \end{bmatrix} \begin{bmatrix} \boldsymbol{x}_I \\ \boldsymbol{x}_B \end{bmatrix} = \begin{bmatrix} 0 \\ \boldsymbol{f}_B \end{bmatrix} \tag{3.12}$$

where:

$$\boldsymbol{K}_{II}\boldsymbol{x}_I + \boldsymbol{K}_{IB}\boldsymbol{x}_B = 0 \tag{3.13a}$$

$$\boldsymbol{K}_{BI}\boldsymbol{x}_I + \boldsymbol{K}_{BB}\boldsymbol{x}_B = \boldsymbol{f}_B \tag{3.13b}$$

from (3.13*a*):

$$\boldsymbol{x}_I = -\boldsymbol{K}_{II}^{-1}\boldsymbol{K}_{IB}\boldsymbol{x}_B \tag{3.14}$$

substituting (3.14) in (3.13*b*):

$$(\boldsymbol{K}_{BB} - \boldsymbol{K}_{BI}\boldsymbol{K}_{II}^{-1}\boldsymbol{K}_{IB})\boldsymbol{x}_B = \boldsymbol{f}_B \tag{3.15}$$

and so the Guyan basis is:

$$\boldsymbol{V}_{guyan} = \begin{bmatrix} \boldsymbol{V}_B \\ \boldsymbol{V}_I \end{bmatrix} = \begin{bmatrix} \boldsymbol{I} \\ \boldsymbol{K}_{II}^{-1}\boldsymbol{K}_{IB} \end{bmatrix} \tag{3.16}$$

Using the Guyan reduction (static condensation) is not possible to catch the dynamics of the internal nodes.

3.2.3   Craig and Bampton Method

The substructuring method invented by Craig and Bampton (CBM) was formulated so that also the dynamics of the internal nodes was considered in the reduced model of the full system [8]. This method allows to catch all the dynamics of internal nodes, that was not possible using the static condensation. The internal modes are computed solving the eigenproblem of the system where the boundary nodes are fixed. The eigenproblem can be formulated as:

$$\boldsymbol{K}_{II}\boldsymbol{x}_I = \omega_I^2\boldsymbol{M}_{II}\boldsymbol{x}_I \qquad \rightarrow \qquad \boldsymbol{\textit{Internal Modes}} \; (\boldsymbol{\Phi}_I) \tag{3.17}$$

The equation of the system can be written as:

$$\begin{bmatrix} \boldsymbol{K}_{II} & \boldsymbol{K}_{IB} \\ \boldsymbol{K}_{BI} & \boldsymbol{K}_{BB} \end{bmatrix} \begin{bmatrix} \boldsymbol{x}_I \\ \boldsymbol{x}_B \end{bmatrix} - \omega^2 \begin{bmatrix} \boldsymbol{M}_{II} & \boldsymbol{M}_{IB} \\ \boldsymbol{M}_{BI} & \boldsymbol{M}_{BB} \end{bmatrix} \begin{bmatrix} \boldsymbol{x}_I \\ \boldsymbol{x}_B \end{bmatrix} = \begin{bmatrix} 0 \\ \boldsymbol{f}_B \end{bmatrix} \tag{3.18}$$

Where the internal degrees of freedom can be calculated by static condensation:

$$\boldsymbol{x}_I = -\boldsymbol{K}_{II}^{-1}\boldsymbol{K}_{IB}\boldsymbol{x}_B \tag{3.19}$$

and so, the reduction matrix of the internal modes of the structure is:

$$\boldsymbol{V}_I = \begin{bmatrix} \boldsymbol{\Phi}_I \\ 0 \end{bmatrix} \tag{3.20}$$

where x_B and x_I are the boundary and internal dofs of the structure. From the static condensation it is possible to get the reduction matrix of the static modes on the boundary nodes. The idea is to select only the first $m < n_I$ internal modes keeping all the static modes at the boundary.

$$\boldsymbol{V}_B = \begin{bmatrix} \boldsymbol{\Psi} \\ \boldsymbol{I} \end{bmatrix} \tag{3.21}$$

Assembling the reduction matrix of the system:

$$\boldsymbol{V}_{CB} = \begin{bmatrix} \boldsymbol{\Phi}_I & \boldsymbol{\Psi} \\ \boldsymbol{0} & \boldsymbol{I} \end{bmatrix} \tag{3.22}$$

$$\boldsymbol{x} = \begin{bmatrix} \boldsymbol{\Phi}_I & \boldsymbol{\Psi} \\ \boldsymbol{0} & \boldsymbol{I} \end{bmatrix} \begin{bmatrix} \boldsymbol{q} \\ \boldsymbol{x}_B \end{bmatrix} \tag{3.23}$$

where $\boldsymbol{q}$ are the intensity parameters of the structure internal modes $[size(\boldsymbol{q}) = size(\boldsymbol{x}_I)]$.

The Craig-Bampton method is used to re-shape a large finite element model into a subset of smaller matrices containing mass, stiffness and mode shape information of the structure.

$$\boldsymbol{K}_R = \boldsymbol{V}_{CB}^T \boldsymbol{K} \boldsymbol{V}_{CB}$$
$$\boldsymbol{M}_R = \boldsymbol{V}_{CB}^T \boldsymbol{M} \boldsymbol{V}_{CB} \tag{3.24}$$

with $\boldsymbol{M}_R$ and $\boldsymbol{K}_R$ the reduced mass and stiffness of the structure. The reduced mass and stiffness have the following size:

$$size\left(\boldsymbol{M}_R\right) = size\left(\boldsymbol{K}_R\right) = (n_B + m) \cdot (n_B + m) \tag{3.25}$$

3.3 Determination of ROM parameters for Geometric Nonlinearities

The aim of this section is to give an overview on the techniques useful to evaluate the nonlinear stiffness coefficients from a structural finite element model. It is possible to identify two different approaches; the first is an intrusive method (*direct*) because the nonlinear coefficients are determined within the finite element formulation. The second method is named non-intrusive (*indirect*) and it can be used within any finite element software such as Nastran, Abaqus, Code Aster, Ansys, etc. where a nonlinear static analysis may be performed. There are two class of non-intrusive method: displacement-base and force-base indirect method. The first consists in imposing a series of static displacements field to determine the nodal forces field prescribing the nodal displacements. In the second one, the idea is to prescribe a force field instead of imposing a static displacement field at each node. The stiffness parameters are computed solving the resulting set of equations.

During the computation of the reduced order parameters, only the quadratic and cubic nonlinearities have been considered. This hypothesis is widely verified because the Green-Lagrange strain tensor is used within the finite element software as strain measure. Green strain tensor $[\boldsymbol{\varepsilon}]$ can also be expressed in terms of the deformation gradient $[\boldsymbol{F}]$ and it is function of the nodal displacement $\mathbf{u}$ [9]. ($\mathbf{F} = \frac{\partial \mathbf{u}}{\partial \mathbf{X}} + \mathbf{I} \implies \mathbf{F} = \mathcal{O}(\mathbf{u})$)

$$[\boldsymbol{\varepsilon}] = \frac{1}{2}\left(\left[\boldsymbol{F}^T\right][\boldsymbol{F}] - [\boldsymbol{I}]\right) \implies \boldsymbol{\varepsilon} = \mathcal{O}(\mathbf{u}^2) \tag{3.26}$$

The potential energy $\boldsymbol{\Pi}$ of a deformable body in the domain Ω_0 is linked to the Green-Lagrange tensor by the fourth order material tensor $\mathbf{C}$.

$$\boldsymbol{\Pi} = \int_{\Omega_0} \boldsymbol{\varepsilon} : \mathbf{C} : \boldsymbol{\varepsilon} \; d\Omega_0 \implies \boldsymbol{\Pi} = \mathcal{O}(\mathbf{u}^4) \tag{3.27}$$

The nodal displacement is a quartic function of the potential energy. Under the assumption of conservative system, the internal forces are equal to the negative gradient of the potential energy with respect to the displacement $\mathbf{u}$.

$$\boldsymbol{f}(\boldsymbol{u}) = -\frac{\partial \boldsymbol{\Pi}}{\partial \mathbf{u}} \implies \boldsymbol{f} = \mathcal{O}(\mathbf{u}^3) \tag{3.28}$$

Consequently, the internal forces of any elastic system characterized by a forth order material tensor exhibits cubic nonlinearities with respect to the nodal displacement **u**.

3.3.1 Intrusive: Direct Method

The idea of direct method is to project the finite element tensors on their modal counterparts; the main problem is that the quadratic and cubic nonlinear tensors are not available within the finite element software, so a non-intrusive method, instead of the intrusive one, is needed to compute them.

Writing the equation of the full finite element model:

$$M_{ij}\ddot{x}_j + C_{ij}\dot{x}_j + K_{ij}^{(1)}x_j + K_{ijk}^{(2)}x_jx_k + K_{ijkl}^{(3)}x_jx_kx_l = f_i \tag{3.29}$$

applying the modal expansion:

$$\boldsymbol{x}(t) = \sum_{n=1}^{N} q_n(t)\boldsymbol{\phi}^{(n)} \tag{3.30}$$

where $\boldsymbol{\phi}^{(n)}$ is the basis function and $q_n(t)$ are the generalised coordinates. Substituting (3.30) in (3.29) and neglecting the damping C_{ij}:

$$\tilde{M}_{ij}\ddot{q}_j + \tilde{K}_{ij}^{(1)}q_j + \tilde{K}_{ijk}^{(2)}q_jq_k + \tilde{K}_{ijkl}^{(3)}q_jq_kq_l = \tilde{f}_i \tag{3.31}$$

where:

$$\tilde{M}_{ij} = \phi_p^{(i)} M_{pr} \phi_r^{(j)}$$

$$\tilde{K}_{ij}^{(1)} = \phi_p^{(i)} K_{pr}^{(1)} \phi_r^{(j)}$$

$$\tilde{K}_{ijk}^{(2)} = K_{prs}^{(2)} \phi_p^{(i)} \phi_r^{(j)} \phi_s^{(k)} \tag{3.32}$$

$$\tilde{K}_{ijkl}^{(3)} = K_{rsuv}^{(3)} \phi_r^{(i)} \phi_s^{(j)} \phi_u^{(k)} \phi_v^{(l)}$$

As already explained the quadratic and cubic coefficients $\tilde{K}_{ijk}^{(2)}$ and $\tilde{K}_{ijkl}^{(3)}$ can not be computed within any commercial finite element software.

3.3.2 Non-Intrusive: Force-based Indirect Method

The nonlinear reduced order model is built prescribing a set of static loading at each node of the finite element model, it can be written as [10]:

$$\boldsymbol{f}^{(s)} = a_r^{(s)} \boldsymbol{\phi}_r^{(s)} \tag{3.33}$$

Per each imposed static load a displacement vertor $\boldsymbol{x}^{(s)}$ has been calculated.

$$\boldsymbol{x}^{(s)} = q_i^{(s)} \boldsymbol{\phi}^{(i)} \tag{3.34}$$

Substituting (3.34) in (3.29):

$$\tilde{K}_{ij}^{(1)} q_j^{(s)} + \tilde{K}_{ijk}^{(2)} q_j^{(s)} q_k^{(s)} + \tilde{K}_{ijkl}^{(3)} q_j^{(s)} q_k^{(s)} q_l^{(s)} = \phi_j^{(i)} f_j^{(s)} \tag{3.35}$$

The load scale factor $a_r^{(s)}$ must be selected in such a way the displacement fields are the same order of magnitude of the panel thickness to be sure that the structure will be excited in nonlinear range. The load scale factor may be estimated from the linear analysis:

$$a_r^{(s)} = \frac{\omega_r^2}{\boldsymbol{\phi}^{(r)T}\boldsymbol{\phi}^{(r)}} \cdot \frac{W_c}{\phi_c^{(r)}} \tag{3.36}$$

Where ω_r is the natural frequency of the system associated to $\boldsymbol{\phi^{(r)}}$, W_c the desidered displacement at point C on the structure with the associated displacement $\phi_c^{(r)}$. The ratio between the linear and nonlinear displacements may be considered a degree of structure's nonlinearities.

3.3.3   Non-Intrusive: Displacement-based Indirect Method

The indirect methods are useful when the quadratic and cubic nonlinear stiffness tensors are not available within the finite element software. The equation of motion of geometrically nonlinear mechanical system can be written as:

$$\boldsymbol{M}\ddot{\boldsymbol{X}}\left(t\right) + \boldsymbol{C}\dot{\boldsymbol{X}}\left(t\right) + \boldsymbol{K}\boldsymbol{X}\left(t\right) + \boldsymbol{\Gamma}\left(\boldsymbol{X}\left(t\right)\right) = \boldsymbol{F}\left(t\right) \tag{3.37}$$

where $\boldsymbol{M}$, $\boldsymbol{K}$, $\boldsymbol{C}$ are the mass, linear stiffness and proportional viscous damping ($\boldsymbol{C} = \alpha\boldsymbol{M} + \beta\boldsymbol{K}$), respectively. While $\boldsymbol{X}(t)$ is the displacement response vector and $\boldsymbol{F}(t)$ the external harmonic force acting on the system. The nonlinear stiffness force vector $\boldsymbol{\Gamma}\left(\boldsymbol{X}\left(t\right)\right)$ represents how much the linear stiffness force diverges from the nonlinear one. In case of small deformation the nonlinear quadratic and cubic terms are negligible, therefore the system behaves as the linear one. The mass, stiffness and proportional damping have been calculated within the finite element commercial software while the nonlinear quadratic and cubic terms have been evaluated with STEP (*Stiffness Evaluation Procedure*) [1].

Applying the modal transformation has been possible to reduce the size of the system using the modal truncation, as explained in Chapter 3.2.1, where the system

of N physical degrees of freedom has been reduced in a subset of L-dofs.

$$\boldsymbol{X} = \boldsymbol{\Phi}\boldsymbol{q} \tag{3.38}$$

where $\boldsymbol{\Phi}$ is the modal matrix containing the eigenvectors (with $L \leq N$) of the MDOF system (Eq. 3.37) neglecting the nonlinear stiffness force vector. Equation of motion in modal coordinates:

$$\boldsymbol{M}\boldsymbol{\Phi}\ddot{\boldsymbol{q}} + \boldsymbol{C}\boldsymbol{\Phi}\dot{\boldsymbol{q}} + \boldsymbol{K}\boldsymbol{\Phi}\boldsymbol{q} + \boldsymbol{\Gamma}(\boldsymbol{\Phi}\boldsymbol{q}) = \boldsymbol{F}(t) \tag{3.39}$$

pre-multiplying the equation (3.39) by the transposed of modal matrix $\boldsymbol{\Phi}$:

$$\boldsymbol{\Phi}^T\boldsymbol{M}\boldsymbol{\Phi}\ddot{\boldsymbol{q}} + \boldsymbol{\Phi}^T\boldsymbol{C}\boldsymbol{\Phi}\dot{\boldsymbol{q}} + \boldsymbol{\Phi}^T\boldsymbol{K}\boldsymbol{\Phi}\boldsymbol{q} + \boldsymbol{\Phi}^T\boldsymbol{\Gamma}(\boldsymbol{\Phi}\boldsymbol{q}) = \boldsymbol{\Phi}^T\boldsymbol{F}(t) \tag{3.40}$$

where:

$$
\begin{aligned}
\widetilde{\boldsymbol{M}} &= \boldsymbol{\Phi}^T\boldsymbol{M}\boldsymbol{\Phi} = [\boldsymbol{I}] \\
\widetilde{\boldsymbol{C}} &= \boldsymbol{\Phi}^T\boldsymbol{C}\boldsymbol{\Phi} = [2\zeta_r\omega_r] \\
\widetilde{\boldsymbol{K}} &= \boldsymbol{\Phi}^T\boldsymbol{K}\boldsymbol{\Phi} = [\omega_r^2] \\
\widetilde{\boldsymbol{\gamma}} &= \boldsymbol{\Phi}^T\boldsymbol{\Gamma} \\
\widetilde{\boldsymbol{F}} &= \boldsymbol{\Phi}^T\boldsymbol{F}
\end{aligned}
\tag{3.41}
$$

$\widetilde{\boldsymbol{M}}$, $\widetilde{\boldsymbol{C}}$, $\widetilde{\boldsymbol{K}}$ are the modal mass, damping and stiffness, respectively. While $\boldsymbol{q}$ is the vector containing the modal amplitude associated to each mode-shape, ω_r are the natural frequency of the undamped system and ζ_r is the modal damping ratio. The modal mass is equal to the identity matrix $\boldsymbol{I}$ since the eigenvectors are mass normalised.

$$\widetilde{\boldsymbol{M}}\ddot{\boldsymbol{q}} + \widetilde{\boldsymbol{C}}\dot{\boldsymbol{q}} + \widetilde{\boldsymbol{K}}\boldsymbol{q} + \widetilde{\boldsymbol{\gamma}}\,(q_1,\ q_2,\ \ldots,\ q_L) = \widetilde{\boldsymbol{F}} \tag{3.42}$$

The nonlinear stiffness force vector contains the quadratic and cubic terms in $\boldsymbol{X}(t)$ and therefore it has been expressed in modal coordinates as:

$$\gamma_r\left(q_1,\ q_2,\ \ldots,\ q_L\right) = \sum_{j=1}^{L}\sum_{k=j}^{L} a_{jk}^r q_j q_k + \sum_{j=1}^{L}\sum_{k=j}^{L}\sum_{l=k}^{L} b_{jkl}^r q_j q_k q_l\ ,\quad r = 1,\ldots,L \quad (3.43)$$

The nonlinear system has been reduced to a simple set of algebraic equation that can be easily solved with any software having a solver for linear and nonlinear static analysis. It is important to point out that to study the coupling between the membrane and bending mode-shapes the geometrically nonlinear mechanical systems are well represented by quadratic and cubic nonlinearities within the nonlinear stiffness force vector $\boldsymbol{\Gamma}(\boldsymbol{\Phi q})$.

The nonlinear quadratic and cubic terms α_{jk}^r and β_{jkl}^r have been calculated prescribing a nodal displacement (physical coordinates) in linear and nonlinear static solution. The nonlinear forces have been computed imposing a displacements field associated to the first L^{th} mode-shapes solving the eigenproblem of the undamped linear system $(\boldsymbol{\Gamma}(\boldsymbol{X}(t)) = 0\ \&\ \boldsymbol{C} = 0)$.

This means applying a nodal displacement vector to evaluate the nodal force vector necessary to achieve the desired displacements field of the structure. The total force vector $\boldsymbol{F}_T$ acting on the structure can be written as the sum between the linear and nonlinear force vectors in physical coordinates. The linear nodal force vector $\boldsymbol{F}_L$ and total nodal force vector $\boldsymbol{F}_T$ have been calculated solving the linear and nonlinear static problem, respectively.

$$\boldsymbol{F}_T = \boldsymbol{F}_L + \boldsymbol{F}_{NL} = \boldsymbol{K}\boldsymbol{X}_c + \boldsymbol{\Gamma}\left(\boldsymbol{X}_c\right) \quad (3.44)$$

and so, the nonlinear force vector $\boldsymbol{F}_{NL}$ can be obtained by subtracting the linear force vector $\boldsymbol{F}_L$ from the total one $\boldsymbol{F}_T$:

$$\boldsymbol{F}_{NL} = \boldsymbol{\Gamma}\left(\boldsymbol{X}_c\right) = \boldsymbol{F}_T - \boldsymbol{F}_L \quad (3.45)$$

It has been possible to notice that for small displacement field the nonlinear forces acting on the system are negligible; therefore it has been fundamental to properly select the modal amplitude during the computation of nonlinear quadratic and cubic stiffness terms.

The number of nonlinear static solutions $\mathbf{\Xi}_{NL}$, in Eq. 3.46, is strongly dependent on how many modes have been considered when the modal truncation has been applied.

$$\mathbf{\Xi}_{NL} = 3 \cdot \left(\frac{M!}{1! \, (M-1)!} + \frac{M!}{2! \, (M-2)!} + \frac{M!}{3! \, (M-3)!} \right), \qquad M = 1, \ldots, r \quad (3.46)$$

Therefore, it has been possible to evaluate the number of linear, quadratic and cubic coefficients calculated with the displacement-based indirect method. At the same time, the number of nonlinear static solutions represents the efficiency of the reduced order model in terms of computational time to perform all the static analysis with respect to the simulated time response of the full model.

Once solved the linear and nonlinear static analysis to evaluate the nonlinear force vector $\boldsymbol{F}_{NL}$, the quadratic and cubic entries of nonlinear tensors are calculated within three loops.

1st loop

The first loop has been used to calculate the quadratic and cubic entries with three equal lower indices ($j = k = l$), while the nonlinear force vector $\boldsymbol{F}_{NL} = \boldsymbol{\Gamma}(\boldsymbol{X}_c)$ has been evaluated using the equation 3.45 prescribing the following displacement fields:

$$
\begin{aligned}
\boldsymbol{X}_c &= +\phi_1 q_1 \\
\boldsymbol{X}_c &= -\phi_1 q_1
\end{aligned}
\tag{3.47}
$$

Projecting the nonlinear forces on the basis $\boldsymbol{\Phi}$, the modal nonlinear force vector can be written as:

$$
\begin{aligned}
\widetilde{\boldsymbol{F}_{NL_1}} &= \boldsymbol{\Phi}^T \boldsymbol{F}_{NL_1} = \boldsymbol{\Phi}^T \boldsymbol{\Gamma}\left(+\phi_1 q_1\right) = \left[a_{11}^r\right] q_1 q_1 + \left[b_{111}^r\right] q_1 q_1 q_1 \\
\widetilde{\boldsymbol{F}_{NL_2}} &= \boldsymbol{\Phi}^T \boldsymbol{F}_{NL_2} = \boldsymbol{\Phi}^T \boldsymbol{\Gamma}\left(-\phi_1 q_1\right) = \left[a_{11}^r\right] q_1 q_1 - \left[b_{111}^r\right] q_1 q_1 q_1
\end{aligned}
\tag{3.48}
$$

The nonlinear stiffness coefficients $\left[a_{jj}^r\right]$ and $\left[b_{jjj}^r\right]$ have been determined by solving the algebraic system of $2 \times L$ linear equations with $j = 1, 2, \ldots, L$.

2nd loop

Following the same approach of the first loop, the entries of nonlinear stiffness tensors with two unequal lower indices ($j = k \ \wedge \ k \neq l \ \ or \ j = l \ \wedge \ j \neq k \ or \ k = l \ \wedge \ j \neq l$) have been calculated prescribing the displacement fields:

$$
\begin{aligned}
\boldsymbol{X}_c &= +\phi_1 q_1 + \phi_2 q_2 \\
\boldsymbol{X}_c &= -\phi_1 q_1 - \phi_2 q_2 \\
\boldsymbol{X}_c &= +\phi_1 q_1 - \phi_2 q_2
\end{aligned}
\tag{3.49}
$$

and so, the nonlinear modal force vector can be written as [1]:

$$
\begin{aligned}
\widetilde{\boldsymbol{F}}_{\boldsymbol{NL}_1} = \boldsymbol{\Phi}^T \boldsymbol{F_{NL_1}} = \boldsymbol{\Phi}^T \boldsymbol{\Gamma}(+\phi_1 q_1 + \phi_2 q_2) =\ & [a^r_{11}]\, q_1 q_1 + [b^r_{111}]\, q_1 q_1 q_1 + [a^r_{22}] q_2 q_2 \\
& + [b^r_{222}] q_2 q_2 q_2 + [a^r_{12}] q_1 q_2 + [b^r_{112}] q_1 q_1 q_2 \\
& + [b^r_{122}] q_1 q_2 q_2
\end{aligned}
$$

$$
\begin{aligned}
\widetilde{\boldsymbol{F}}_{\boldsymbol{NL}_2} = \boldsymbol{\Phi}^T \boldsymbol{F_{NL_2}} = \boldsymbol{\Phi}^T \boldsymbol{\Gamma}(-\phi_1 q_1 - \phi_2 q_2) =\ & [a^r_{11}]\, q_1 q_1 - [b^r_{111}]\, q_1 q_1 q_1 + [a^r_{22}] q_2 q_2 \\
& - [b^r_{222}] q_2 q_2 q_2 + [a^r_{12}] q_1 q_2 - [b^r_{112}] q_1 q_1 q_2 \\
& - [b^r_{122}] q_1 q_2 q_2
\end{aligned}
$$

$$
\begin{aligned}
\widetilde{\boldsymbol{F}}_{\boldsymbol{NL}_3} = \boldsymbol{\Phi}^T \boldsymbol{F_{NL_3}} = \boldsymbol{\Phi}^T \boldsymbol{\Gamma}(+\phi_1 q_1 - \phi_2 q_2) =\ & [a^r_{11}]\, q_1 q_1 + [b^r_{111}]\, q_1 q_1 q_1 + [a^r_{22}] q_2 q_2 \\
& - [b^r_{222}] q_2 q_2 q_2 - [a^r_{12}] q_1 q_2 - [b^r_{112}] q_1 q_1 q_2 \\
& + [b^r_{122}] q_1 q_2 q_2
\end{aligned}
$$

$$(3.50)$$

Solving the linear algebraic system of equations, the nonlinear stiffness coefficients $\left[a^r_{jk}\right]$, $\left[b^r_{jjk}\right]$ and $\left[b^r_{kkj}\right]$ for $j, k = 1,2, ..., L$ have been determined. In order to clarify what are the unknowns of the system, the linear algebraic equations have been written in matrix form:

$$
\begin{bmatrix}
q_1 q_2 & q_1^2 q_2 & q_1 q_2^2 \\
q_1 q_2 & -q_1^2 q_2 & -q_1 q_2^2 \\
-q_1 q_2 & -q_1^2 q_2 & q_1 q_2^2
\end{bmatrix}
\begin{bmatrix}
a^r_{12} \\
b^r_{112} \\
b^r_{122}
\end{bmatrix}
=
\begin{bmatrix}
\widetilde{F}_{NL_1} \\
\widetilde{F}_{NL_2} \\
\widetilde{F}_{NL_3}
\end{bmatrix}
-
\begin{bmatrix}
q_1^2 & q_1^3 & q_2^2 & q_2^3 \\
q_1^2 & q_2^2 & -q_1^3 & -q_2^3 \\
q_1^2 & q_1^3 & q_2^2 & -q_2^3
\end{bmatrix}
\begin{bmatrix}
a^r_{11} \\
a^r_{22} \\
b^r_{111} \\
b^r_{222}
\end{bmatrix}
\quad (3.51)
$$

for instance, imposing the modal amplitudes equal to one ($q_1 = q_2 = 1$):

$$
\begin{bmatrix}
1 & 1 & 1 \\
1 & -1 & -1 \\
-1 & -1 & 1
\end{bmatrix}
\begin{bmatrix}
a^r_{12} \\
b^r_{112} \\
b^r_{122}
\end{bmatrix}
=
\begin{bmatrix}
\widetilde{F}_{NL_1} \\
\widetilde{F}_{NL_2} \\
\widetilde{F}_{NL_3}
\end{bmatrix}
-
\begin{bmatrix}
1 & 1 & 1 & 1 \\
1 & 1 & -1 & -1 \\
1 & 1 & 1 & -1
\end{bmatrix}
\begin{bmatrix}
a^r_{11} \\
a^r_{22} \\
b^r_{111} \\
b^r_{222}
\end{bmatrix}
\quad (3.52)
$$

The procedure is the same followed to implement the stiffness evaluation procedure ($STEP$) using the Python language. The system has the following form:

$$\boldsymbol{A}\boldsymbol{x} = \boldsymbol{F} - \boldsymbol{C}\boldsymbol{d} \tag{3.53}$$

where $\boldsymbol{A}$ and $\boldsymbol{C}$ are the matrix of modal amplitude $\boldsymbol{q}$, $\boldsymbol{x}$ is the vector of the unknowns of quadratic and cubic entries of the tensors while $\boldsymbol{d}$ contains all the coefficients calculated in the first loop.

3rd loop

Finally, the nonlinear stiffness coefficients $[b^r_{jkl}]$ with three unequal lower indices ($j \neq k \neq l$) have been determined by imposing the displacement field:

$$\boldsymbol{X}_c = +\phi_1 q_1 + \phi_2 q_2 + \phi_3 q_3 \tag{3.54}$$

then:

$$
\begin{aligned}
\widetilde{\boldsymbol{F}_{NL}} = \boldsymbol{\Phi}^T \boldsymbol{\Gamma}(+\phi_1 q_1 + \phi_2 q_2 + \phi_3 q_3) = {}& [a^r_{11}] \, q_1 q_1 + [a^r_{22}] \, q_2 q_2 + [a^r_{33}] \, q_3 q_3 \\
& + [a^r_{12}] \, q_1 q_2 + [a^r_{13}] \, q_1 q_3 + [a^r_{23}] \, q_2 q_3 \\
& + [b^r_{111}] \, q_1 q_1 q_1 + [b^r_{222}] \, q_2 q_2 q_2 \\
& + [b^r_{333}] \, q_3 q_3 q_3 + [b^r_{112}] \, q_1 q_1 q_2 \\
& + [b^r_{221}] q_2 q_2 q_1 + [b^r_{113}] \, q_1 q_1 q_3 \\
& + [b^r_{331}] \, q_3 q_3 q_1 + [b^r_{223}] \, q_2 q_2 q_3 \\
& + [b^r_{332}] \, q_3 q_3 q_2 + [b^r_{123}] \, q_1 q_2 q_3
\end{aligned} \tag{3.55}
$$

The linear algebraic equation of the third loop may be solved once calculated all the coefficients of the previous loops. An alternative procedure to STEP algorithm may be used with the finite element software which utilize the tangent stiffness matrix evaluated on the full finite element model of the structure.

Chapter 4

Harmonic Balance Method

4.1   HBM applied to Nonlinear Vibration

The Harmonic Balance Method (HBM) is a numerical method for the computation of nonlinear ordinary differential equations (ODEs). The harmonic balance may be used to solve problems formulated in differential form comes from different engineering fields such as: fluid-dynamics, structures, micro-mechanics (MEMS), nano-mechanics (NEMS) and dynamics of mechanical systems. HBM is used to compute periodic solution of ODEs; for this reason, it is adopted to solve differential equations with periodic time dependence as in case of the dynamics of rotating machinery.

The idea of harmonic balance method is to develop the periodic oscillation in Fourier series and then, to determine its coefficients an algebraic system of equations has to be solved. The number of unknows is strongly related to the low or high truncation order of Fourier series. To better understand the basics of HBM it has been decided to start from the nonlinear mechanical system with one degree of freedom (Duffing Oscillator). The idea is to solve the nonlinear second order differential equation using the harmonic balance method.

4.1.1   Duffing Oscillator

The Duffing oscillator is the simplest case to model a nonlinear mechanical system with geometric nonlinearities. It is described by a nonlinear second order differential equation representing a single degree of freedom oscillator with cubic spring (Fig. 4.1) [11].
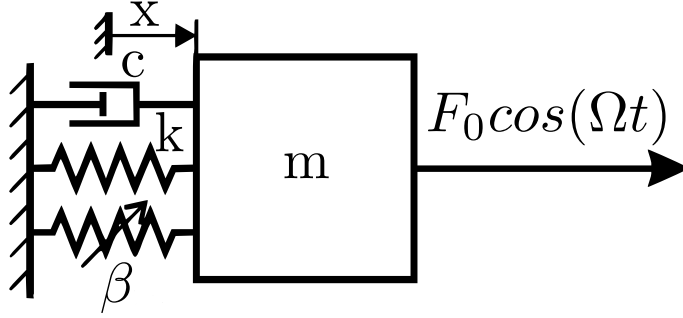
Figure 4.1: Duffing Oscillator

The equation of motion of nonlinear oscillator may be written as:

$$m\ddot{x} + c\dot{x} + kx + \beta x^3 = F_0 cos(\Omega t) \qquad (4.1)$$

where m, k, c are the mass, stiffness and viscous damping, respectively; while β is the nonlinear cubic stiffness, F_0 the amplitude of the external force and Ω is the forcing frequency. If β is equal to zero the system behaves as linear and so, the response of the system is the sum of the "particular" and "homogeneous" solution. In case of linear second ODE the response is independent of the initial state of the system in terms of position $x(0)$ and velocity $\dot{x}(0)$. Whereas the system is nonlinear ($\beta \neq 0$) the superposition principle is no valid anymore; for the nonzero external force ($F \neq 0$) the steady state force response may be periodic, quasi-periodic or chaotic with a strong dependence on the initial state of the system [11].

The idea of the harmonic balance is to approximate the periodic solution $x(t + T) = x(t)$ with $T = 2\pi/\Omega$ as Fourier series:

$$x_h(t) = a_0 + \sum_{k=1}^{\infty} \left[a_k \cos(k\Omega t) + b_k \sin(k\Omega t) \right] \qquad (4.2)$$

Assuming $x_h(t) \simeq x(t)$ and considering only the 1st harmonic (with the zero harmonic equal to zero):

$$
\begin{aligned}
x_h(t) &= a_1 cos(\Omega t) + b_1 sin(\Omega t) \\
\dot{x}_h(t) &= -a_1 sin(\Omega t) + b_1 cos(\Omega t) \\
\ddot{x}_h(t) &= -a_1 \Omega^2 cos(\Omega t) - b_1 \Omega^2 sin(\Omega t)
\end{aligned}
\tag{4.3}
$$

while the nonlinear term x^3 may be written as:

$$
\begin{aligned}
x_h^3(t) &= (a_1 cos(\Omega t) + b_1 sin(\Omega t))^3 \\
&= a_1^3 cos^3(\Omega t) + 3a_1^2 b_1 cos^2(\Omega t) sin(\Omega t) \\
&+ 3a_1 b_1^2 cos(\Omega t) sin^2(\Omega t) + b_1^3 sin^3(\Omega t)
\end{aligned}
\tag{4.4}
$$

The trigonometric identities to linearize the nonlinear stiffness force are:

$$
\begin{aligned}
cos^3(\Omega t) &= \frac{3}{4} cos(\Omega t) + \frac{1}{4} cos(3\Omega t) \\
sin^3(\Omega t) &= \frac{3}{4} sin(\Omega t) - \frac{1}{4} sin(3\Omega t) \\
cos^2(\Omega t) sin(\Omega t) &= \frac{1}{4} sin(\Omega t) + \frac{1}{4} sin(3\Omega t) \\
cos(\Omega t) sin^2(\Omega t) &= \frac{1}{4} cos(\Omega t) - \frac{1}{4} cos(3\Omega t)
\end{aligned}
\tag{4.5}
$$

substituting 4.5 in 4.4:

$$x_h^3(t) = a_1^3 \left[\frac{3}{4}cos(\Omega t) + \frac{1}{4}cos(3\Omega t) \right] + 3a_1^3 b_1 \left[\frac{1}{4}sin(\Omega t) + \frac{1}{4}sin(3\Omega t) \right]$$
$$+ 3a_1 b_1^2 \left[\frac{1}{4}cos(\Omega t) - \frac{1}{4}cos(3\Omega t) \right] + b_1^3 \left[\frac{3}{4}sin(\Omega t) - \frac{1}{4}sin(3\Omega t) \right] \tag{4.6}$$

Sorting the equation with respect sine and cosine:

$$x_h^3(t) = \frac{3}{4}\left(a_1^3 + a_1 b_1^2 \right)cos(\Omega t) + \frac{3}{4}\left(b_1^3 + a_1^2 b_1 \right)sin(\Omega t)$$
$$+ \frac{1}{4}\left(a_1^3 - 3a_1 b_1^2 \right)cos(3\Omega t) - \frac{1}{4}\left(b_1^3 - 3a_1^2 b_1 \right)sin(3\Omega t) \tag{4.7}$$

Neglecting the high-order harmonics $cos(3\Omega t)$ and $sin(3\Omega t)$ and substituting the terms $\ddot{x}_h$, $\dot{x}_h$, x_h and x_h^3 in the eq. 4.1:

$$m\left(- a_1 \Omega^2 cos(\Omega t) - b_1 \Omega^2 sin(\Omega t) \right) + c\left(- a_1 sin(\Omega t) + b_1 cos(\Omega t) \right)$$
$$+ k\left(a_1 cos(\Omega t) + b_1 sin(\Omega t) \right) + \beta\left[\frac{3}{4}\left(a_1^3 + a_1 b_1^2 \right)cos(\Omega t) \right.$$
$$\left. + \frac{3}{4}\left(b_1^3 + a_1^2 b_1 \right)sin(\Omega t) \right] = F_0 cos(\Omega t) \tag{4.8}$$

Balancing the sine and cosine terms $(R_c(a_1, b_1), R_s(a_1, b_1)) = (0,0)$:

$$R_c = (k - m\Omega^2)a_1 + c\Omega b_1 + \frac{3}{4}\beta(a_1^3 + a_1 b_1^2) - F_0 = 0$$

$$R_s = (k - m\Omega^2)b_1 - c\Omega a_1 + \frac{3}{4}\beta(b_1^3 + a_1^2 b_1) = 0$$

$$(4.9)$$

It has been obtained a system of two linear algebraic equations in two unknowns (a_1, b_1) representing the coefficients of Fourier series. Assuming the mass and the linear stiffness equal to one, in such a way that the natural frequency of the linear system is equal to the unit, yields:

$$R_c = (1 - \Omega^2)a_1 + c\Omega b_1 + \frac{3}{4}\beta(a_1^3 + a_1 b_1^2) - F_0 = 0$$

$$R_s = (1 - \Omega^2)b_1 - c\Omega a_1 + \frac{3}{4}\beta(b_1^3 + a_1^2 b_1) = 0$$

$$(4.10)$$

For this simple example of Duffing oscillator, the solution can be derived analytically for a fixed set of parameters Ω, F, c, β, while for systems with more degrees of freedom and harmonics, the numerical solutions and continuation methods are needed to calculate the steady state response of the nonlinear system:

$$R(X) = \begin{bmatrix} R_c & R_s \end{bmatrix}^T = 0, \quad with: \quad X = \begin{bmatrix} a_k & b_k \end{bmatrix}^T \qquad (4.11)$$

The MDOF nonlinear systems may show features such as modal interactions, this latter can be catch only considering higher harmonics within the Taylor series. Only the first harmonic is not enough to capture the entire dynamics of the system. Even for mechanical systems with only one degree of freedom, such as Duffing oscillator, the number of harmonics plays an important rule. Nevertheless, considering only one harmonic (H=1) the super and sub-harmonic can not be evaluated in the FRF of the system.

4.1.2   MDOF Nonlinear Mechanical System

The idea is to generalise what it has been explained for a SDOF nonlinear system to a MDOF nonlinear mechanical system with multiple harmonics. The equation of motion of multi degrees of freedom nonlinear system with periodic forcing may be written, in generalised coordinates, as [12]:

$$M\ddot{q} + C\dot{q} + Kq + f_{nl}\left(q, \dot{q}\right) = f_{ext}\left(t\right) \tag{4.12}$$

The vectors $\boldsymbol{F}_{nl}$ and $\boldsymbol{F}_{ext}$ gathered the nonlinear and external forces, respectively, while the mass matrix $\boldsymbol{M}$ is symmetric and positive definite. Since the solution is periodic, it has been possible to use the Fourier series to calculate the response of the system $q(t) = q(t + T) \simeq q_h(t)$.

$$\boldsymbol{q}_h\left(t\right) = a_0 + \sum_{k=1}^{\infty} \left[a_k \cos\left(k\Omega t\right) + b_k \sin\left(k\Omega t\right)\right] = \mathbb{R}\left\{\sum_{k=0}^{+\infty} c_k e^{ik\Omega t}\right\} \tag{4.13}$$

Considering the real valued formulation of Fourier series and calculating the first and second derivatives of $q_h(t)$, yields:

$$
\begin{aligned}
\boldsymbol{q}_h &= \mathbb{R}\left\{\sum_{k=0}^{\infty} c_k e^{ik\Omega t}\right\} \\
\dot{\boldsymbol{q}}_h &= \mathbb{R}\left\{\sum_{k=0}^{\infty} ik\Omega c_k e^{ik\Omega t}\right\} \\
\ddot{\boldsymbol{q}}_h &= \mathbb{R}\left\{\sum_{k=0}^{\infty} -\left(k\Omega\right)^2 c_k e^{ik\Omega t}\right\}
\end{aligned}
\tag{4.14}
$$

Substituting the Eq. 4.14 in Eq. 4.12:

$$\boldsymbol{M}\mathbb{R}\left\{\sum_{k=0}^{\infty} -(k\Omega)^2 c_k e^{ik\Omega t}\right\} + \boldsymbol{C}\mathbb{R}\left\{\sum_{k=0}^{\infty} ik\Omega c_k e^{ik\Omega t}\right\}$$
$$+ \boldsymbol{K}\mathbb{R}\left\{\sum_{k=0}^{\infty} c_k e^{ik\Omega t}\right\} + \boldsymbol{f_{nl}} - \boldsymbol{f_{ext}} = \boldsymbol{r} \tag{4.15}$$

$$\mathbb{R}\left\{\sum_{k=0}^{\infty} \left(\left[-(k\Omega)^2 \boldsymbol{M} + ik\Omega \boldsymbol{D} + \boldsymbol{K}\right] c_k + \boldsymbol{F_{nl,k}} + \boldsymbol{f_{ext,k}}\right) e^{ik\Omega t}\right\} = \boldsymbol{r} \tag{4.16}$$

$$\mathbb{R}\left\{\sum_{k=0}^{\infty} \boldsymbol{R}_k e^{ik\Omega t}\right\} = \boldsymbol{r} \tag{4.17}$$

The periodic solution $\boldsymbol{q}_h(t)$ is only an approximation of the exact solution $\boldsymbol{q}(t)$; even if the Fourier series is not truncated, with k ranges between zero and infinity, the error or residue $\boldsymbol{r}$ is nonzero. Assuming the nonlinear forces as smooth in $\boldsymbol{q}_h(t)$ and $\dot{\boldsymbol{q}}_h(t)$, yields [12]:

$$\frac{1}{\pi}\int_0^{2\pi} \boldsymbol{f}_{nl}\left(\boldsymbol{q}, \dot{\boldsymbol{q}}\right) e^{-ik\Omega t} d(\Omega t) = \begin{cases} 2Fnl,0 & k = 0 \\ Fnl,k & k \neq 0 \end{cases} \tag{4.18}$$

The idea is to balance the harmonics imposing the residue $\boldsymbol{R}_k$ equal to zero:

$$\begin{cases} \boldsymbol{R}_0\left(\boldsymbol{c}_0,\ \boldsymbol{c}_1,\ \ldots,\ \boldsymbol{c}_H\right) = 0 \\ \boldsymbol{R}_1\left(\boldsymbol{c}_0,\ \boldsymbol{c}_1,\ \ldots,\ \boldsymbol{c}_H\right) = 0 \\ \quad\vdots \\ \boldsymbol{R}_H\left(\boldsymbol{c}_0,\ \boldsymbol{c}_1,\ \ldots,\ \boldsymbol{c}_H\right) = 0 \end{cases} \tag{4.19}$$

The Fourier series is truncated to the order H and so, the number of unknowns are equal to the number of equations governing the algebraic system of the harmonic balance method, where the residues have been imposed equal to zero. The $n(2H+1)$ system of algebraic equation in $n(2H+1)$ unknowns has to be solved, where n is the number of degrees of freedom of the system. The equation 4.16 represents the mechanical interpretation of the governing algebraic equation 4.19 where $\boldsymbol{R}_k$ may be seen as the dynamic force equilibrium in frequency domain.

$$\boldsymbol{R}_k = \left[-(k\Omega)^2 \boldsymbol{M} + ik\Omega\boldsymbol{D} + \boldsymbol{K}\right]\boldsymbol{c}_k + \boldsymbol{F}_{nl,k} - \boldsymbol{F}_{ext,k} = \boldsymbol{0} \qquad (4.20)$$

with:

$$\boldsymbol{K}_{dyn} = \left[-(k\Omega)^2 \boldsymbol{M} + ik\Omega\boldsymbol{D} + \boldsymbol{K}\right] \qquad (4.21)$$

where $\boldsymbol{K}_{dyn}$ is the dynamic linear stiffness matrix of the system, $\boldsymbol{F}_{ext,k}$ is the external force vector and $\boldsymbol{F}_{nl,k}$ the nonlinear internal force vector.

The efficiency of the HBM is strictly related to the number of harmonics considered in the Taylor series ($k = 1, 2, \ldots, H$). The number of harmonics H must be selected in such a way to capture the higher order harmonics caused by the nonlinear forces acting on the system. The higher order harmonics of interest are all the harmonics multiple of the fundamental frequency of the system. The physical meaning of the previous sentence is that a nonlinear system, if excited at its first natural frequency, does not respond with only the imposed frequency; also higher frequencies participate in the periodic response of the system. Therefore, the response of nonlinear mechanical system is magnified due to the interaction between the low and high-resonances (*superharmonic resonance*).

The convergence of HBM is related to the number of harmonics, especially in case of non-smooth systems where $q(t)$ and $\dot{q}$ are not infinitely differentiable. In this case to achieve the convergence of the HBM a large number of harmonics may be required.

One of the costs of HBM is the calculation of nonlinear force $\boldsymbol{F}_{nl}(c_0, \ldots, c_H)$ in the equation 4.18. Usually, the Alternating-Frequency-Time (AFT) scheme is used

for determining the nonlinear forces, replacing the continuous Fourier transform 4.18 with the discrete Fourier transform computed with the FFT (Fast Fourier Transform) algorithm.

$$\boldsymbol{F}_{nl,k} = FFT\Big[\boldsymbol{f}_{nl}(iFFT[c_k], \ iFFT[ik\Omega c_k])\Big] \tag{4.22}$$
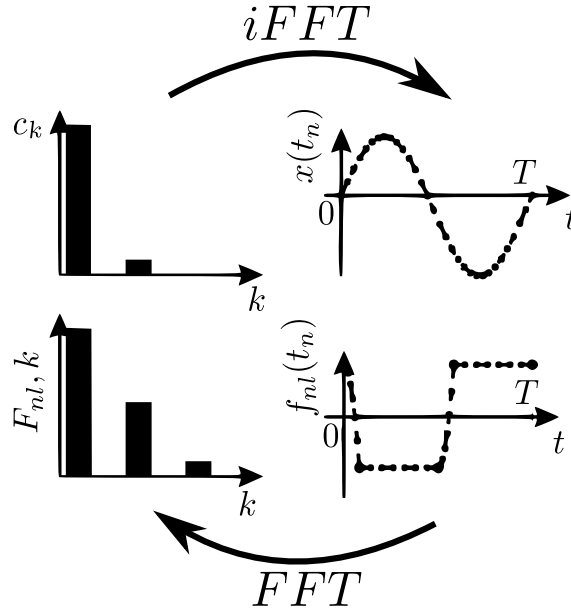
Figure 4.2: Alternating Frequency Time (AFT) scheme

The fast Fourier transform (FFT) has been used to convert the signal from the time domain to the frequency domain; and viceversa using the inverse Fourier transform (iFFT). According to the Nyquist-Shannon theorem, the number of samples per period must be large to solve the highest harmonics in the spectrum guaranteeing the convergence of HBM.

In structural dynamics field, the most common method to solve the algebraic equations is the Newton method; the idea is to linearize the residues in a Taylor series at $x^{(j)}$ in order to calculate the next step $x^{(j+1)}$ as a solution of the linearized problem [12].

$$\boldsymbol{R}\left(\boldsymbol{x}^{j+1}\right) = \boldsymbol{R}\left(\boldsymbol{x}^{j}\right) + \frac{\partial \boldsymbol{R}}{\partial \boldsymbol{x}}\Big|_{\boldsymbol{x}^{j}}\left(\boldsymbol{x}^{j+1} - \boldsymbol{x}^{j}\right) = 0 \tag{4.23}$$

51

In the proposed work, the Alternating Frequency Time (AFT) as well as the Newton method have not been used to solve the nonlinear system, since the all procedure has been performed in the frequency domain. Nevertheless, the algebraic system has been solved adopting the Asymptotic Numerical Method (ANM) continuation algorithm where no iterations are needed.

Chapter 5

Asymptotic Numerical Method

5.1 Numerical Bifurcation

The Asymptotic Numerical Method (ANM) is a continuation algorithm based on Taylor series using a quadratic recast of smooth nonlinear systems. The solution of single branch is computed step by step following the same logic of predictor-corrector algorithm. The idea is to develop in Taylor series the arc-length parameter, so that the corrector is not needed due to the accuracy of high order Taylor Series prediction. To better understand the ANM, the general rules of a generic continuation method has been explained. Usually, the continuation algorithm consists to have: predictor, parametrization strategy, corrector and step-length control [13].

The predictor-corrector method provides an initial guess for the next iterations of the corrector. Starting from the continuation step (x_{j+1}, λ_j), where λ is the continuation parameter, the continuation methods allow to calculate the next solution $(x_{j+1}, \lambda_j + 1)$ solving the equation $F(x, \lambda) = 0$. To solve the previous equation, a relation that identifies the location of the solution on the branch is needed. This identification is strictly related to the type of parametrization strategy chosen to trace the curve. The singularity of the Jacobian matrix necessary to evaluate the solution is a problem during the prediction and correction process; the idea is to parametrize the curve by arc-length in order to avoid singularity. The continuation method starts from a known solution and uses the predictor-corrector scheme to find the forward solutions at different values of λ [14].
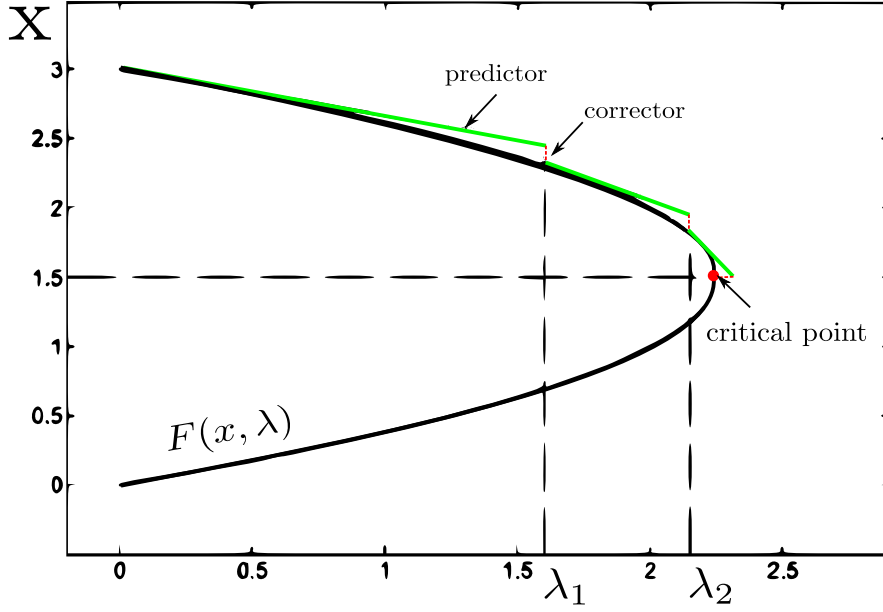
Figure 5.1: Predictor-Corrector continuation method

The continuation method is also used to identify the nature of various bifurcation points. Analysing the eigenvalues of the Jacobian matrix, it is possible to study the stability of nonlinear systems. To explain the basic concept of nonlinear dynamics of mechanical system, two coupled 1st ODEs have been considered.

$$\dot{x}_1 = \frac{dx_1}{dt} = f_1(x_1, x_2)$$
$$\dot{x}_2 = \frac{dx_2}{dt} = f_2(x_1, x_2)$$

$$(5.1)$$

Perturbing the system around its equilibrium points $(f_1, f_2) = (0,0)$ by Δx_1 and Δx_2, respectively; expanding the equations in Taylor series and linearizing the equations near the equilibrium point, yields [14]:

$$\Delta x_1 = C_1 e^{\lambda_1 t} + C_2 e^{\lambda_2 t}$$
$$\Delta x_1 = C_3 e^{\lambda_1 t} + C_4 e^{\lambda_2 t}$$

$$(5.2)$$

54

The coefficients (C_1, C_2, C_3, C_4) are determined imposing the initial conditions, while (λ_1, λ_2) are the eigenvalues of the Jacobian matrix $\boldsymbol{J}$.

$$\boldsymbol{J} = \begin{bmatrix} \frac{\partial f_1}{\partial x_1} & \frac{\partial f_1}{\partial x_2} \\ \frac{\partial f_2}{\partial x_1} & \frac{\partial f_2}{\partial x_2} \end{bmatrix} \tag{5.3}$$

The eigenvalues are calculated by solving the determinant of $(\boldsymbol{J} - \lambda \boldsymbol{I})$ equal to zero.

$$\left| \boldsymbol{J} - \lambda \boldsymbol{I} \right| = 0 \quad \rightarrow \quad (\lambda_1, \lambda_2) \tag{5.4}$$

$$\lambda_{1,2} = \frac{1}{2}\left[Tr(\boldsymbol{J}) + \sqrt{Tr(\boldsymbol{J})^2 - 4\ det(\boldsymbol{J})} \right] = \frac{1}{2}\left[Tr(\boldsymbol{J}) + \sqrt{\Delta} \right] \tag{5.5}$$

where Tr is the trace of the Jacobian matrix:

$$Tr(\boldsymbol{J}) = \frac{\partial f_1}{\partial x_1} + \frac{\partial f_2}{\partial x_2} \tag{5.6}$$

The stability of the system depends on the magnitude of $det(\boldsymbol{J})$ and $Tr(\boldsymbol{J})$; it is possible to identify the following cases [14]:

$1^{st}\ CASE$: $Tr(\boldsymbol{J}) < 0$, $det(\boldsymbol{J}) > 0$, $\Delta > 0$

The eigenvalues are real and negative and so, the stationary state is stable belonging to a stable node. The perturbations decay.

2nd CASE: $Tr(\boldsymbol{J}) > 0$, $det(\boldsymbol{J}) > 0$, $\Delta > 0$

The eigenvalues (λ_1, λ_2) are both real and positive; the exponential term e^{λ_i} in the equation 5.2 increased monotonically in time belonging to an unstable node where the perturbation grows exponentially.

3rd CASE: $Tr(\boldsymbol{J}) < 0$, $det(\boldsymbol{J}) > 0$, $\Delta < 0$

In this case the eigenvalues (λ_1, λ_2) are complex with the negative real part of λ_1 and λ_2. The perturbations may be written as:

$$
\begin{aligned}
\Delta x &= c_1 e^{\mathbb{R}(\lambda t)} cos(\mathbb{I}(\lambda t) + \theta_1) \\
\Delta y &= c_2 e^{\mathbb{R}(\lambda t)} cos(\mathbb{I}(\lambda t) + \theta_2)
\end{aligned}
\tag{5.7}
$$

This represents a damped oscillatory motion and due to the decay term, the system returns to its original stationary state belonging to a stable focus.

4th CASE: $Tr(\boldsymbol{J}) > 0$, $det(\boldsymbol{J}) > 0$, $\Delta < 0$

The eigenvalues are complex while the real part of (λ_1, λ_2) is positive. The result is that the perturbations grow diverging with an oscillation motion. It belongs to an unstable focus.

5th CASE: $Tr(\boldsymbol{J}) > 0$ or $Tr(\boldsymbol{J}) < 0$, $det(\boldsymbol{J}) < 0$, $\Delta > 0$

The eigenvalues of the system are real, one positive and one negative; the eigenvalue with positive root increase in time, while the negative decrease exponentially. The exponential term dominates the system that moves away to the stationary state leading the system to a saddle point.

6th CASE: $det(\boldsymbol{J}) = 0$

If the determinant of the Jacobian matrix is equal to zero, the eigenvalues (λ_1, λ_2) are both real leading the system to a saddle node bifurcation. In order to describe the correct behaviour of the system it is important to consider also the nonlinear terms.

7th $CASE$: $Tr(\boldsymbol{J}) = 0$, $det(\boldsymbol{J}) > 0$, $\Delta < 0$

The eigenvalues are both complex with the real part equal to zero; this condition may lead the system to a critical point (Hopf bifurcation) where the system's stability changes. The stability of equilibrium points has been summarized in Fig. 5.2.
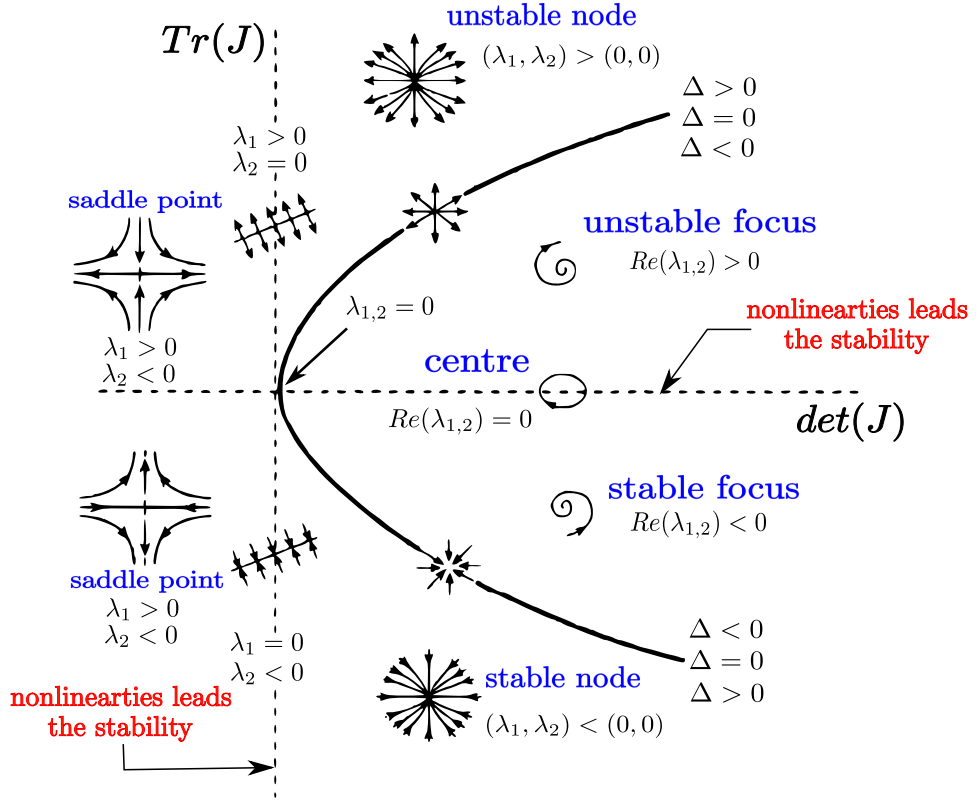
Figure 5.2: Phase Diagram

The discussion about the stability of the dynamical system can be easily extended to a nth order autonomous differential equation:

$$\dot{\boldsymbol{x}} = F(\boldsymbol{x}, \lambda), \quad \boldsymbol{x} \in \mathbb{R}^n, \quad \lambda \in \mathbb{R}^k \tag{5.8}$$

When the system is in equilibrium (x_0, λ_0) the left hand-side of the equation is nil. The idea is to find the set of state variables $\boldsymbol{x}$ and the continuation parameters

57

that satisfy the following equation $F(\boldsymbol{x}, \lambda) = 0$.

One of the challenge in the scientific world is to determine the root of nonlinear differential equation, that depends not only on the state variables of the system, but also on the continuation parameter λ. Assuming that $F(x, \lambda)$ is a smooth function in $\mathbb{R}^n$ it is possible to calculate the state variable x by Newton's method [15].

$$x_{n+1} = x_n - J_F(x_n)^{-1} F(x_n) \tag{5.9}$$

where J_F is the Jacobian of F:

$$F_x(x,0) = \frac{\partial F(x,0)}{\partial x} \tag{5.10}$$

The main issue of Newton's method is the initial guess for the iterations; for instance, the homotopy method may be used to get the first initial point on the curve and then using the continuation method to trace the original curve $F(x, \lambda)$. Solving the nonlinear equation with Newton's algorithm the singularity of Jacobian $F_x(x, \lambda_k)$ may be occur in correspondence of a turning point.

5.1.1   Stability Computation with Hill's Method

Consider a periodically non-autonomous dynamical system governed by the Nth order differential equation [16]:

$$\dot{\boldsymbol{X}}(t) = F(t, \boldsymbol{X}(t), \lambda) \tag{5.11}$$

The stability of periodic solution $\boldsymbol{X}(t)$ has been studied by superimposing a small disturbance $\boldsymbol{x}(t)$, yields:

$$\boldsymbol{X}(t) = \boldsymbol{X}_0(t) + \boldsymbol{x}(t) \tag{5.12}$$

Assuming that the disturbance is linear and expanding the response $\boldsymbol{X}(t)$ in Taylor series with respect to $\boldsymbol{X}_0$, so that:

$$\dot{\boldsymbol{x}}(t) = \boldsymbol{J}(t)\boldsymbol{x}(t) = \frac{\partial \boldsymbol{F}}{\partial \boldsymbol{X}}(t, \boldsymbol{X}_0(t), \lambda_0) \tag{5.13}$$

where $\boldsymbol{J}(t)$ is the Jacobian matrix at $(\boldsymbol{X}_0, \lambda_0)$.

$$\dot{\boldsymbol{x}}(t) = \boldsymbol{J}(t)\boldsymbol{x}(t) = \frac{\partial \boldsymbol{F}}{\partial \boldsymbol{X}}(t, \boldsymbol{X}_0(t), \lambda_0) \tag{5.14}$$

Consider a linear dynamical system with N-dofs having N linearly independent solutions $q_n(t)$ so that the response $\boldsymbol{x}(t)$ may be written as follows:

$$\boldsymbol{x}(t) = \sum_{n=1}^{N} c_n \boldsymbol{q}_n(t) \tag{5.15}$$

where c_n is a constant vector having N constants depending on the boundary conditions of the system. The linearly independent solutions $\boldsymbol{q}_n(t)$ of the system may be expressed, according to the Floquet theory [16], as:

$$\boldsymbol{q}_n(t) = \boldsymbol{p}_n(t)e^{\alpha_n t} \tag{5.16}$$

Where $\boldsymbol{p}_n(t+T) = \boldsymbol{p}_n(t)$ is a periodic vector and α_n are complex numbers called Floquet exponents; it has been imposed that the function $\boldsymbol{p}_n(t)$ has T-periodicity, so that:

$$\boldsymbol{q}_n(t + T) = \boldsymbol{p}_n(t + T)e^{\alpha_n(t+T)} = \boldsymbol{q}_n(t)e^{\alpha_n t} \tag{5.17}$$

The Floquet exponents are used within the Hill's method to determine the stability of the periodic response. In case of non-autonomous systems: if the real part of the Floquet exponent is real and negative the periodic solution is asymptotically

stable; while if real and positive the solution tends to increase exponentially driving the system to an unstable periodic solution. The periodic function $\boldsymbol{p}_n(t)$ may be expressed by Fourier series, yields:

$$\boldsymbol{p}_n(t) = \sum_{k=-\infty}^{+\infty} \boldsymbol{p}_n^k e^{ik\Omega t}, \quad \Omega = \frac{2\pi}{T} \tag{5.18}$$

where Ω is the fundamental frequency and combining the Eq.s 5.18 and 5.16, it has been possible to get the fundamental solution $\boldsymbol{q}_n(t)$ as an infinite sum of harmonics.

$$\boldsymbol{q}_n(t) = \sum_{k=-\infty}^{+\infty} \boldsymbol{p}_n^k e^{(ik\Omega+\alpha_n)t} \tag{5.19}$$

also the Jacobian is T-periodic, and so it can be written in Fouries series as:

$$\boldsymbol{J}(t) = \sum_{h=-\infty}^{+\infty} \boldsymbol{J}^h e^{ih\Omega t} \tag{5.20}$$

it yields:

$$\begin{aligned} \dot{\boldsymbol{q}}(t) = \boldsymbol{J}(t)\boldsymbol{q}_n(t) &= \sum_{h=-\infty}^{+\infty} \boldsymbol{J}^h e^{ih\Omega t} \sum_{k=-\infty}^{+\infty} \boldsymbol{p}_n^k e^{(ik\Omega+\alpha_n)t} \\ &= \sum_{k=-\infty}^{+\infty}\sum_{h=-\infty}^{+\infty} \boldsymbol{J}^h \boldsymbol{p}_n^k e^{[i(k+h)\Omega+\alpha_n]t} \end{aligned} \tag{5.21}$$

that is equal to the first time derivative of the perturbation function:

$$\sum_{k=-\infty}^{+\infty} \boldsymbol{p}_n^k (ik\Omega + \alpha_n) e^{(ik\Omega+\alpha_n)t} = \sum_{k=-\infty}^{+\infty}\sum_{h=-\infty}^{+\infty} \boldsymbol{J}^h \boldsymbol{p}_n^k e^{[i(k+h)\Omega+\alpha_n]t} \tag{5.22}$$

since the sums range between minus and plus infinity it is possible to replace $k = k - h$ in the right-hand side, as follows:

$$\sum_{k=-\infty}^{+\infty} \left[\sum_{h=-\infty}^{+\infty} \boldsymbol{J}^h \boldsymbol{p}_n^{k-h} - \boldsymbol{p}_n^k (ik\Omega + \alpha_n) \right] e^{(ik\Omega + \alpha_n)t} = 0 \qquad (5.23)$$

the Eq. 5.23 may be written as an eigenproblem:

$$(\boldsymbol{H} - s\boldsymbol{I})\boldsymbol{u} = 0 \qquad (5.24)$$

where $\boldsymbol{H}$ is the Hill matrix, $\boldsymbol{I}$ is the identity matrix and $\boldsymbol{u}$ is an infinite-dimensional vector, where $s_n^k = ik\Omega + \alpha_n$ and $\boldsymbol{u}_n^k = \boldsymbol{p}_n^k$. The idea is to calculate the set of s_n^k solving the eigenproblem, so that it is possible to evaluate α_n determining the set of stability solutions [16]. The Fourier series has been truncated to the H order so that a system of $N(2H + 1)$ unknowns has to be solved.

5.1.2 Hill's Method applied to ANM

The stability analysis in case of nonlinear smooth systems can be performed combining the Hill's method with the HBM and ANM. When the system is nonlinear the most expensive operation in terms of computational time is the assembly of the Jacobian matrix; nevertheless, this operation can be efficiently implemented using the ANM since the system is quadratically recast before the computation of the Jacobian [16]. A generic quadratic system may be written as:

$$m(\dot{\boldsymbol{Z}}) = c(t, \lambda) + l(t, \boldsymbol{Z}, \lambda) + q(t, \boldsymbol{Z}, \boldsymbol{Z}, \lambda) \qquad (5.25)$$

where c, l, q are the constant, linear and quadratic operators in $\boldsymbol{Z}$, respectively.

Even in this case the periodic solution can be extended in Fourier series:

$$\boldsymbol{Z}(t) = \sum_{k=-H}^{H} \boldsymbol{Z}_0 e^{ik\Omega t} \tag{5.26}$$

Also the Jacobian can be quadratically recast as follows:

$$\boldsymbol{J}(t) = \boldsymbol{J}_C(t, \lambda_0) + \boldsymbol{J}_L(t, \boldsymbol{Z}_0, \lambda_0) + \boldsymbol{J}_Q(t, \boldsymbol{Z}_0, \boldsymbol{Z}_0, \lambda_0) \tag{5.27}$$

where $\boldsymbol{J}_C$, $\boldsymbol{J}_L$, $\boldsymbol{J}_Q$ are the constant, linear and quadratic Jacobian matrices. Once calculated the Jacobian matrix, the same procedure explained in Section 5.1.1 has been followed to determine the stability of periodic solutions.

In the next chapter has been explained how to solve a nonlinear differential equation using an alternative method for the frequency-based HBM, where no FFT and Newton's method are needed to compute the response of the system in the frequency domain. In addition, the ANM, instead of corrector-predictor scheme, has been used as continuation algorithm to trace the curve $F(x, \lambda)$ while the stability of bifurcation points have been computed using the Hill's method combined with HBM and ANM.

5.2   Frequency-Based HBM for Continuation Method

In the world of nonlinear dynamics, it is common to deal with numerical method to solve nonlinear differential equations. The idea is to use the harmonic balance method (HBM) and the continuation method (ANM) to compute periodic solution of dynamical systems described by means of smooth equations. The aim of this method is to recast the system in a quadratic arbitrary polynomial form before applying the harmonic balance. Using the proposed HBM with ANM, it has been possible to avoid the Fast Fourier Transform within the AFT method. The aim of the Asymptotic Numerical Method is to write the equation of motion of a nonlinear system in quadratic form. The quadratic recast does not represent a limitation because a mechanical system with quadratic and cubic geometric nonlinearities may be easily recast in quadratic form introducing auxiliary variables [17].

5.2.1   Quadratic Recast of an Autonomous System

The idea is to consider an autonomous system of differential equations:

$$\dot{X} = F(X, \lambda) \tag{5.28}$$

where X is the state vector of unknowns, F the smooth nonlinear vector and λ the continuation parameter. The quadratic recast of non-autonomous (forced) system has been treated separately. All the nonlinearities of the system, Eq. 5.28, have been recast in a quadratic polynomials as follows:

$$m(\dot{Z}) = c + l(Z) + q(Z, Z) \tag{5.29}$$

The Eq. 5.29 is a hybrid equation because contains differential al algebraic equations; the vector Z has the original components of Y plus some new variables introduced to get the quadratic form. The operators c, $l(\cdot)$, $q(\cdot, \cdot)$ are the contant, linear and quadratic vectors with respect to the unknown vector Z; while $m(\cdot)$ is the linear vector operator with respect to the entry vector $\dot{Z}$. Also a nonlinear system with a quadratic polynomial nonlinearities can be solved using the HBM with ANM continuation method [17].

5.2.2   Quadratic Recast of a Periodically Forced System

Consider a periodically forced (non-autonomous) system (Eq. 5.30):

$$\dot{X} = F(t, X, \lambda) \tag{5.30}$$

where F is a periodic smooth function in t with a forcing period equal to T. The idea is to recast the system in a quadratic form as in the case of autonomous systems and then to calculate the periodic solution with a period pT or T/p (p is an integer). An example of periodically forced system is the Duffing Oscillator presented in Chapter 4.

$$m\ddot{x} + c\dot{x} + kx + \beta x^3 = F_0 cos(\lambda t) \tag{5.31}$$

Assume the damping c and the force amplitude F_0 constant while the linear stiffness and the mass are equal to one so that the first natual frequency of the linear system is $\omega_n = 1$; use the forcing frequency λ as continuation parameter. Introducing the auxiliary variable $r(t) = x^2(t)$ and writing the equation of motion in state space, yields:

$$
\begin{aligned}
y &= \dot{x} \\
0 &= r - x^2 \\
\dot{y} &= F_0 cos(\lambda t) - cy - x - \beta xr
\end{aligned}
\tag{5.32}
$$

The Eq. 5.32 may be recast as:

$$m(\dot{Z}) = c(t, \lambda) + l(Z) + q(Z, Z) \tag{5.33}$$

where $Z = [x, y, r]^T$, while the continuation parameter λ has been included within the constant operator. The forcing frequency is strictly related to the frequency response of the system as:

$$\lambda = j\omega, \quad j = 0,1,2,...,p \tag{5.34}$$

The constant term $c(t)$ is then expanded in Fourier series with respect to ω. The continuation parameter λ is not an unkown, since it has been chosen as multiple of ω. This assumption is valid only if the response is synchronous with respect to the forcing frequency, that means considering the phase equal to zero.

Introducing the auxiliary variables (arbitrary choice) the unknowns are splitted in U and U_{aux}:

$$U = (x, \lambda)$$
$$U_{aux} = (r)$$
$$U_{tot} = (U, \ U_{aux}) = (x, \lambda, r)$$
(5.35)

where U_{aux} is the vector of the auxiliary variables and U_{tot} is the full vector of unknowns. The residue function of the full vector of unknowns may be written as:

$$R_{tot}\left(U_{tot}\right) = \begin{bmatrix} R \\ R_{aux} \end{bmatrix} = R_{quad}(U_{tot}) + R_{fun}\left(U_{tot}\right)$$
(5.36)

The total residue function can be splitted in the function that are quadratic R_{quad} and the elementary transcendental function quadratically recast R_{fun}. The residue of an elementary function has to be differentiated (dR_{fun}) and since it is an elementary trascendental function, its differentiated form is quadratic. Therefore, the residue $R(X, \lambda)$ may be written as follows [18]:

$$R_{tot}\left(U_{tot}\right) = \left[C + L\left(U_{tot}\right) + Q\left(U_{tot}, U_{tot}\right)\right] + \left[L_d\left(U_{tot}\right) - f\left(U_{tot}\right)\right]$$
(5.37)

where $C(\cdot)$, $L(\cdot)$, $Q(\cdot, \cdot)$ are the constant, linear and quadratic operators, respectively; while $f(U_{tot})$ is a non-quadratic trascendental function that has to be differentiated to become quadratic.

$$\frac{\partial R_{tot}}{\partial U_{tot}} = L + Q\left(U_{tot}, \cdot\right) + Q\left(\cdot, \ U_{tot}\right) + L_d - \frac{\partial f}{\partial U_{tot}}\left(\cdot\right)$$
$$= L + Q\left(U_{tot}, \cdot\right) + Q\left(\cdot, \ U_{tot}\right) + L_d - Q_d(U_{tot}, \cdot)$$
(5.38)

where the operator Q_d is the bi-linear operator of the differentiated form of $f(U_{tot})$. In order to decrease the computational time the system quadratically recast may be written in sparse tensorial formalism.

$$R_i = C_i + \sum_{j=1}^{M} L_{ij} X_j + \sum_{j,k=1}^{M} Q_{ijk} X_j X_k, \quad 1 \le i \le N \tag{5.39}$$

where C_i, L_{ij} and Q_{ijk} are the constant, linear and quadratic sparse tensors, respectively.

5.2.3 The HBM applied to a Quadratic System

The harmonic balance method has been applied to the system of equations 5.33, where the unknown vector Z has been decomposed into Fourier series considering H harmonics [17].

$$Z(t) = Z_0 + \sum_{k=1}^{H} [Z_{c,k} \cos(k\omega t) + Z_{s,k} \sin(k\omega t)] \tag{5.40}$$

All the coefficient of the Fourier series have been collected into a column vector U having the size of $(2H + 1) \times N_e$, where N_e represents the number of equations quadratically recast.

$$U = \left[Z_0^T, Z_{c,1}^T, Z_{s,1}^T, Z_{c,2}^T, Z_{s,2}^T, \ ... \ , Z_{c,H}^T, Z_{s,H}^T \right]^T \tag{5.41}$$

Substituting the eq. 5.40 in 5.33 and collecting the terms with the same harmonics, yields:

$$\omega M(U) = C + L(U) + Q(U,U) \tag{5.42}$$

The system 5.42 contains $(2H + 1) \times N_e$ algebraic equations in $(2H + 1) \times N_e$ unknowns plus the continuation parameter λ and the angular frequency ω.

Once applied the HBM, the algebraic system $\boldsymbol{R}(\boldsymbol{U}) = 0 \in \mathbb{R}^N$ with $\boldsymbol{U} = \left[U^T, \lambda, \omega\right]^T$ has to be solved. $(N = (2H + 1) \times N_e + 1)$.

5.2.4 The Continuation Method applied to a Quadratic System

The output of the harmonic balance method is an algebraic system of equation that may be written as follows:

$$\boldsymbol{R}(\boldsymbol{U}) = 0 \tag{5.43}$$

Within the continuation method the parameter λ becomes an unknow; the arc-length parametrization has been used to plot the curve when the continuation parameter is changing. The continuation step has been computed from the starting point $U_0 = (x_0, \lambda_0)$ of the analytic function $R(x, \lambda)$ while $U_1 = (x_1, \lambda_1)$ is the unitary tangent vector at U_0. The idea is to compute the Taylor series, truncated at p^{th} order, of the arch-length parameter $a = (u - u_0) \cdot u_1 + (\lambda - \lambda_0) \cdot \lambda_1 = (U - U_0) \cdot U_1$ [18].

$$U(a) = U_0 + aU_1 + a^2 U_2 + a^3 U_3 + \ldots + a^p U_p \tag{5.44}$$

Substituting the Eq. 5.44 in Eq. 5.43:

$$R(U(a)) = R(U(0)) + aR_1 + a^2 R_2 + a^3 R_3 + \ldots + a^p R_p \tag{5.45}$$

where:

$$R_1 = \left.\frac{dR}{da}\right|_{a=0} = \frac{\partial R}{\partial U}U_1$$

$$R_2 = \left.\frac{1}{2}\frac{d^2 R}{da^2}\right|_{a=0} = \frac{\partial R}{\partial U}U_2 - F_2(U_1)$$

$$R_3 = \left.\frac{1}{3!}\frac{d^3 R}{da^3}\right|_{a=0} = \frac{\partial R}{\partial U}U_3 - F_3(U_1, U_2) \tag{5.46}$$

$$\vdots$$

$$R_p = \left.\frac{1}{p!}\frac{d^p R}{da^p}\right|_{a=0} = \frac{\partial R}{\partial U}U_p - F_p(U_1, \ldots, U_{p-1})$$

The function F_K with $k = 1,2,...,p$ depends only on the parameters already computed in the series. All the residue R_k share the same Jacobian matrix $\frac{\partial R}{\partial U} = \left[\frac{\partial R}{\partial x}, \frac{\partial R}{\partial \lambda}\right]$ at U_0. The arc-length parameter has been computed inside the domain $[0, a_{max}]$ setting the residue less than ϵ_r, reasonably small, the maximum admissible value of a can be written as:

$$|R(U(a)) - R(U(0))| < \epsilon_r, \quad a \in [0, a_{max}] \tag{5.47}$$

assuming that $R(U(a)) - R(U(0)) = a^{p+1}R_{p+1}$:

$$a_{max} = \left(\frac{\epsilon_r}{||R_{p+1}||}\right)^{\frac{1}{p+1}} \tag{5.48}$$

The series has been computed by imposing all the coefficients a^k of the series equal to zero as follows:

$$0 = C + L\sum_{k=0}^{N} a^k U_k + Q\left(\sum_{k=0}^{N} a^k U_k, \sum_{k=0}^{N} a^k U_k\right), \quad k = 1,2,...,p \tag{5.49}$$

The original nonlinear problem has been written as a series of linear algebraic equations. The series expansion represents only one section of the entire branch of solutions, to determine the full path of the curve, the calculation of the series must be repeated taking the forward U_0 as starting point. Since it has been used the ANM continuation method, the solution branch can be calculated section by section solving a linear algebraic system of equations. The bifurcation points may be easily traced with a small perturbation thanks to the high-order Taylor series expansion [17].

Overall, the entire procedure has been performed in frequency domain where an arbitrary number of harmonics may be used to solve the analytical system, therefore there is no need to discretize the system in time. Since the ANM works in frequency domain, the FFT and IFFT are not needed anymore, the consequence is a gain in terms of computational time with respect the AFT. As already explained, the Jacobian has been calculated analytically since the system has been quadratically recast.

5.2.5   Numerical Results of Duffing Oscillator

The nonlinear frequency response of a system governed by Duffing's equation has been traced using the frequency-based HBM and ANM as continuation method. The equation of motion of a damped forced Duffing oscillator for hardening system $(\beta > 0)$ may be written as follows:

$$\ddot{x} + 2\zeta\omega_n\dot{x} + \omega_n^2 x + \frac{\beta}{m}x^3 = \frac{F_0}{m}cos(\lambda t) \tag{5.50}$$

assuming the mass m, the linear stiffness k and cubic nonlinear stiffness β equal to one, so that:

$$\ddot{x} + 2\zeta\dot{x} + x + x^3 = F_0 cos(\lambda t) \tag{5.51}$$

The amplitude of the system can be obtained by summing the individual amplitude $X_i = \sqrt{x_{c,i} + x_{s,i}}$ of the odd harmonics, while the even harmonics are all zero

69

because of the quadratic term in the Duffing's equation has been neglected. The plot of the sine and cosine coefficients has been reported in Fig.5.3.
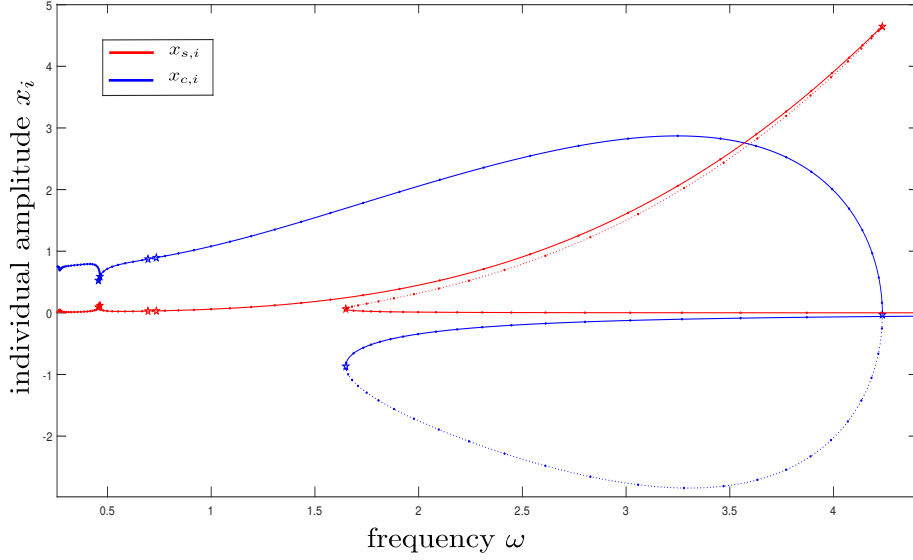

Figure 5.3: Individual Amplitude of Duffing Oscillator (H=25, F_0=1, 2ζ=0.05, ω_n=1, β=1)

In Fig.5.3 have been plotted the individual amplitudes sine ($x_{s,i}$) and cosine ($x_{c,i}$) contribution in the frequency response of Duffing oscillator. It has been possible to notice that, in correspondence of the resonance peak, the sine component is maximum while the cosine is nil. The dots-lines represent the unstable branch of the nonlinear frequency response. The stability analysis has been done within MAN-LAB 4.0 according to the Hill's method.

The nonlinear frequency response of Duffing oscillator has been plotted in Fig.5.4 using 25 harmonics (H=25) during the harmonic balance procedure. The typical nonlinear response of a hardening system as well as the super-harmonic resonances may be observed.
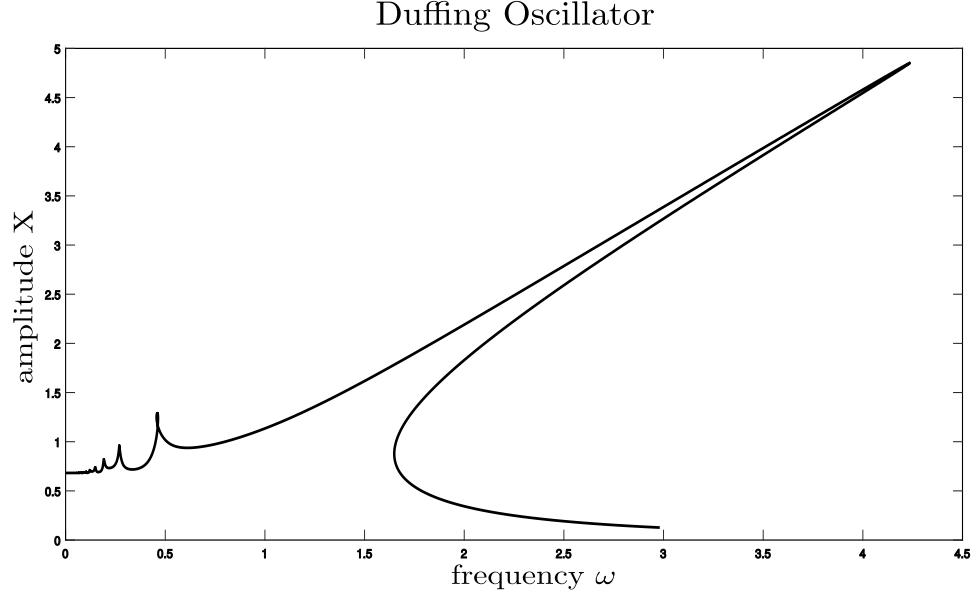
Duffing Oscillator

Figure 5.4: Nonlinear Frequency Response of Duffing Oscillator (H=25, F_0=1, 2ζ=0.05, ω_n=1, β=1)

The super-harmonic resonances comprising all the frequencies multiple of the forcing frequency ω. Although the amplitude of the super-harmonics is much smaller than the main resonance peak, in case of contact's study, it plays an important rule. In case of periodic forcing function $F_0 cos(\omega t)$, the response of the system may be written as:

$$x\left(t\right) = x_0 + \sum_{i=1}^{H} \left[x_{c,i}\cos\left(k_i\omega t\right) + x_{s,i}\sin\left(k_i\omega t\right)\right] \tag{5.52}$$

Where H is the number of harmonics considered to compute the harmonic balance, for instance considering only the odd harmonics, the response of the system is equal to:

$$\begin{aligned} x\left(t\right) &= x_{c,1}\cos\left(\omega t\right) + x_{s,1}\sin\left(\omega t\right) + x_{c,2}\cos\left(3\omega t\right) + x_{s,2}\sin\left(3\omega t\right) \\ &\quad + x_{c,3}\cos\left(5\omega t\right) + x_{s,3}\sin\left(5\omega t\right) + \dots \end{aligned} \tag{5.53}$$

where the third harmonic is the first super-harmonic of the system represented by the Duffing equation. In the contrary, all the harmonics submultiple of the fundamental frequency $(\omega/3, \omega/5, \omega/7, \dots)$ are called sub-harmonics. The response of the system can be written as:

$$x\left(t\right) = x_0 + \sum_{i=1}^{H} \left[x_{c,i} \cos\left(\frac{\omega}{k_i} t\right) + x_{s,i} \sin\left(\frac{\omega}{k_i} t\right) \right] \tag{5.54}$$

considering only the odd harmonics:

$$x\left(t\right) = x_{c,1} \cos\left(\omega t\right) + x_{s,1} \sin\left(\omega t\right) + x_{c,2} \cos\left(\frac{\omega}{3} t\right) + x_{s,2} \sin\left(\frac{\omega}{3} t\right)$$
$$+ x_{c,3} \cos\left(\frac{\omega}{5} t\right) + x_{s,3} \sin\left(\frac{\omega}{5} t\right) + \dots \tag{5.55}$$

The Duffing Oscillator described by the Eq.5.51 may show a chaotic motion within a certain range of parameters. It has been possible to notice a strong nonlinear behaviour of the system in correspondence of the super-harmonics resonances, as shown in Fig.5.5. In order to better understand the chaotic behaviour of the Duffing oscillator the phase diagram have been plotted in Fig.5.5 at the points $(P1, P2, P3, P4)$. Even if the forcing term is harmonic in time, the system may responde as a random motion (Fig.5.8) with a strong sensitivity with respect to the initial conditions.

At the primary resonance peak the corresponding phase diagram has the shape of an ellipse, while at point $P4$ the system behaves as a chaotic motion having four bases of attraction (attractors). The time spectrum at the super-harmonic resonance $P4$ shows a chaotic motion similar to a random vibration.
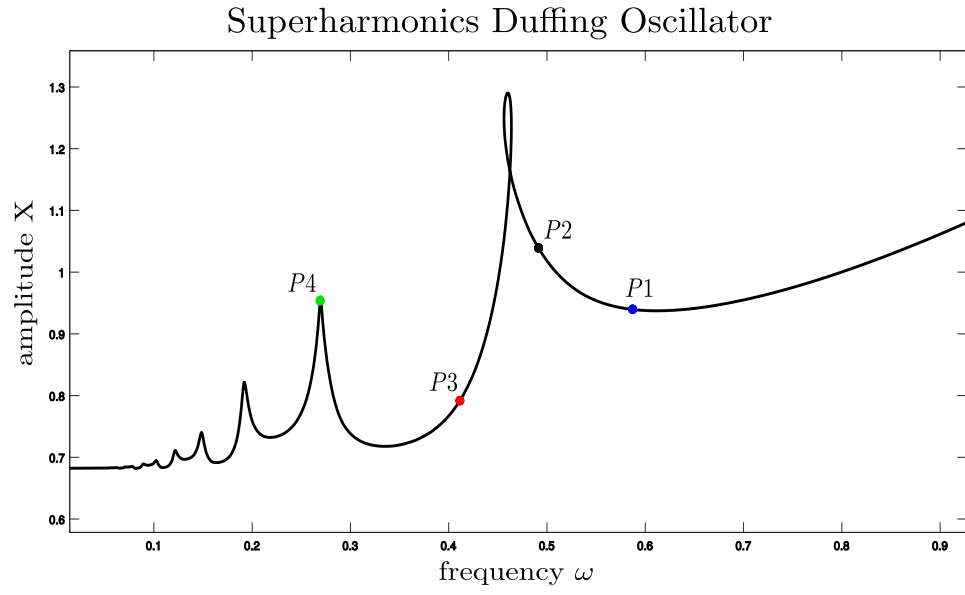
Superharmonics Duffing Oscillator

Figure 5.5: Superharmonics of Duffing Oscillator (H=25, F_0=1, 2ζ=0.05, ω_n=1, β=1)
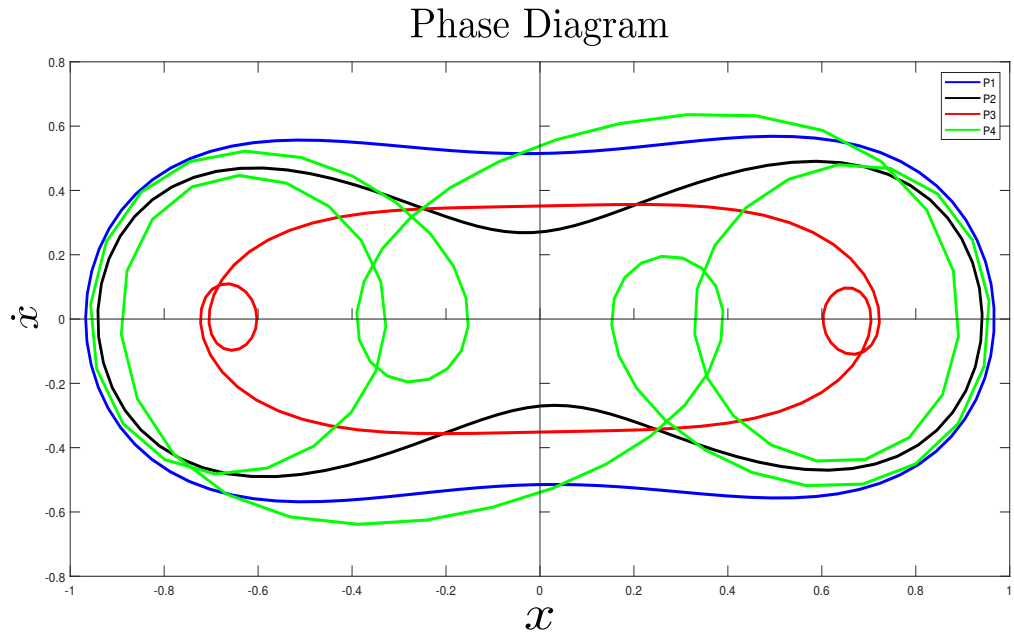
Phase Diagram

Figure 5.6: Phase Diagram of Duffing Oscillator (H=25, F_0=1, 2ζ=0.05, ω_n=1, β=1)
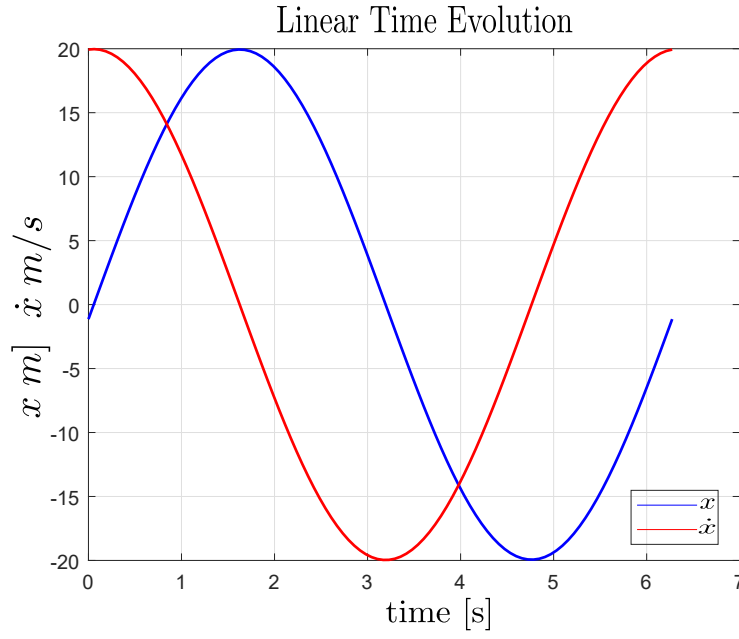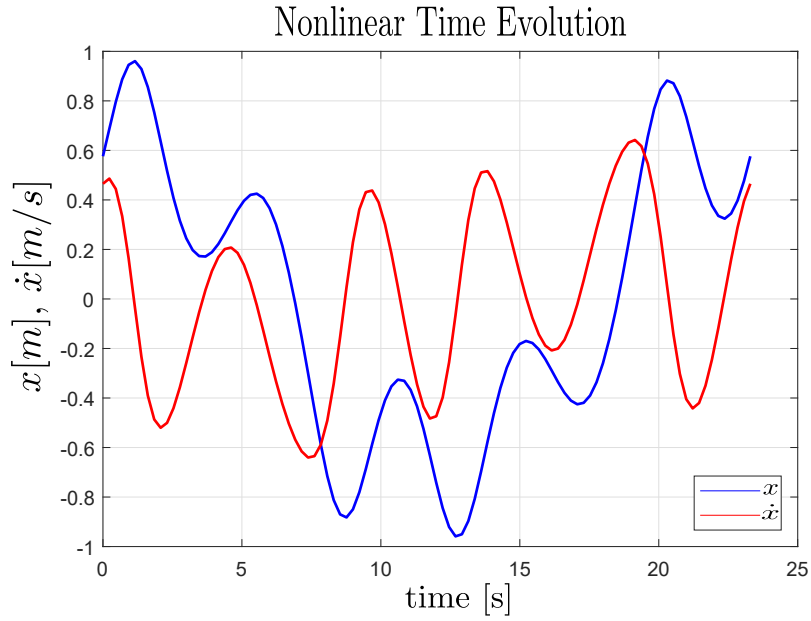
Figure 5.7: Linear Time Evolution of Duffing Oscillator (β=0)

Figure 5.8: Nonlinear Time Evolution of Duffing Oscillator

In Figure 5.7 has been showed the time evolution of periodically forced Duffing oscillator with vanished nonlinear cubic stiffness (β=0). As expected, the response

74

of the system, as well as the time evolution of the velocity, are periodic. Neverthe-less, the in Fig.5.8 the system has a chaotic behaviour, as already explained above, in correspondence of the second super-harmonic resonance.
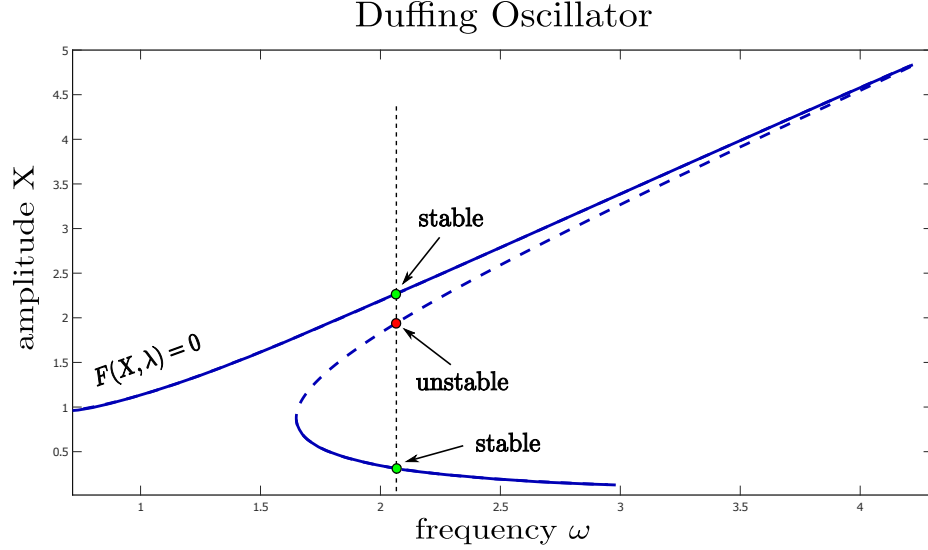
Duffing Oscillator

Figure 5.9: Primary Resonance of Duffing Oscillator

The primary resonance of Duffing oscillator with positive cubic stiffness ($\beta > 0$) has been plotted in Fig. 5.9; it shows the typical bend shape of hardening system where two stable points and one unstable have been identified. Nevertheless, at low frequency the system is dominated by the nonlinear stiffness while, the force amplitude F_0 is responsible of the magnification and the bend shape of the pri-mary resonance peak. At high frequency the inertia of the mass dominates the system that tends to have a behaviour like the linear one. The Duffing oscillator is characterized by the jump phenomenon and it is typical of all the nonlinear sys-tems governed by the Duffing's equation [19]. Starting from the high-frequencies and going backward in the spectrum the system with an upward jump reaches a different domain of attraction due to the presence of the unstable branch; quite the opposite, following the path from lower to higher frequencies the system with a downward jump gets the stable branch. The dashed line represents the unstable branch of the frequency response computed using the asymptotic numerical method.

Chapter 6

Validation of Stiffness Evaluation Procedure

The stiffness evaluation procedure (STEP) is a non-intrusive displacement-based indirect method to evaluate the nonlinear modal stiffness coefficients starting from an arbitrary finite element model. The aim of this chapter is to validate the displacement-base indirect method in case of 3D and shell elements, comparing the results of nonlinear quadratic and cubic coefficients with the following two papers:

1st Test Case: Clamped-Clamped 3D Beam

"Dynamique non-lineaire des structures mecaniques : application aux systemesa symetrie cyclique" - Aurélien Grolet, PhD Thesis - [2]

2nd Test Case: Simply Supported Plate

"Dertermination of nonlinear stiffness with application to random vibration of geometrically nonlinear structures" - Alexander A. Muravyov, Stephen A. Rizzi , NASA Langley Research Center - [1]

The entire procedure to evaluate the nonlinear stiffness of the quadratic and cubic tensors has been widely explained in Section 3.3.3. Nevertheless, the stiffness evaluation procedure has been coded within the Code Aster environment using the Python language. Considering the nonlinear dynamical system governed by the following equation:

$$\boldsymbol{M}\ddot{\boldsymbol{X}}\left(t\right) + \boldsymbol{C}\dot{\boldsymbol{X}}\left(t\right) + \boldsymbol{K}\boldsymbol{X}\left(t\right) + \boldsymbol{\Gamma}\left(\boldsymbol{X}\left(t\right)\right) = \boldsymbol{F}\left(t\right) \tag{6.1}$$

The tensor entries a_{jk}^r and b_{jkl}^r have been calculated prescribing the nodal displacement in linear and nonlinear static solutions; the nonlinear modal stiffness force vector may be expressed as:

$$\gamma_r\left(q_1,\ q_2,\ \ldots,\ q_L\right) = \sum_{j=1}^{L}\ \sum_{k=j}^{L} a_{jk}^r q_j q_k + \sum_{j=1}^{L}\ \sum_{k=j}^{L}\ \sum_{l=k}^{L} b_{jkl}^r q_j q_k q_l \qquad (6.2)$$

An example of Python script to evaluate the nonlinear stiffness, using operators available in Code Aster, has been reported in Fig. 6.1.

```
for j in range(L):
    for k in range(j+1,L):
        for l in range(k+1,L):

            # displacement Phi1*q1 + Phi2*q2 + Phi3*q3

            DU = CREA_CHAMP(COMB=(_F(CHAM_GD=MODE[j],
                        COEF_R=Ampl_q[j]*q[5,0]),
                        _F(CHAM_GD=MODE[k],
                        COEF_R=Ampl_q[k]*q[5,1]),
                        _F(CHAM_GD=MODE[l],
                        COEF_R=Ampl_q[l]*q[5,2])),
                    OPERATION='COMB',
                    TYPE_CHAM='NOEU_DEPL_R')

            # linear static analysis

            SMALL = CALCUL (CHAM_MATER=fieldmat,
                        COMPORTEMENT=_F(DEFORMATION= 'PETIT',
                        RELATION='ELAS'),
                        DEPL=U,
                        EXCIT=_F(CHARGE=BC),
                        INCREMENT=_F(LIST_INST=LIST,NUME_ORDRE=1),
                        INCR_DEPL=DU,
                        MODELE=model,
                        OPTION=('COMPORTEMENT','MATR_TANG_ELEM'),)

            # nonlinear static analysis

            LARGE = CALCUL (CHAM_MATER=fieldmat,
                        COMPORTEMENT=_F(DEFORMATION= 'GROT_GDEP',
                        RELATION='ELAS'),
                        DEPL=U,
                        EXCIT=_F(CHARGE=BC),
                        INCREMENT=_F(LIST_INST=LIST,NUME_ORDRE=1),
                        INCR_DEPL=DU,
                        MODELE=model,
                        OPTION=('COMPORTEMENT','MATR_TANG_ELEM',),)
```

Figure 6.1: Example of Python Script in Code Aster (2nd Loop)

The operator CREA_CHAMP has been used to create a field of nodal displacement associated to the first L-mode shapes. The nonlinear forces have been computed with the operator CALCUL prescribing the field of nodal displacements DU. Within the operator CALCUL has been possible to perform the linear (PETIT) and nonlinear (GROT_GDEP) static analysis to evaluate the entries of nonlinear

quadratic and cubic tensors. The Code Aster script has been validated against the NASTRAN script, written by NASA, comparing the nonlinear stiffness terms for a simply supported plate.

6.1   Clamped-Clamped 3D Beam

The verification studies have been done using a finite element model of 3D beam, shown in Fig.6.2, having the following material properties:

$$E = 210\ GPa, \quad \nu = 0.3, \quad \rho = 7800\ \frac{kg}{m^3} \tag{6.3}$$

where E is the Young's modulus (or elastic modulus), ν is Poisson's ratio and ρ the mass density. The proportional viscous damping ($\boldsymbol{C} = 3\boldsymbol{M}$) has been used for the computation of the nonlinear forced response of the beam. The dimensions have been reported in Tab. 6.1, where L is the length of the beam and S the measure of its cross section.

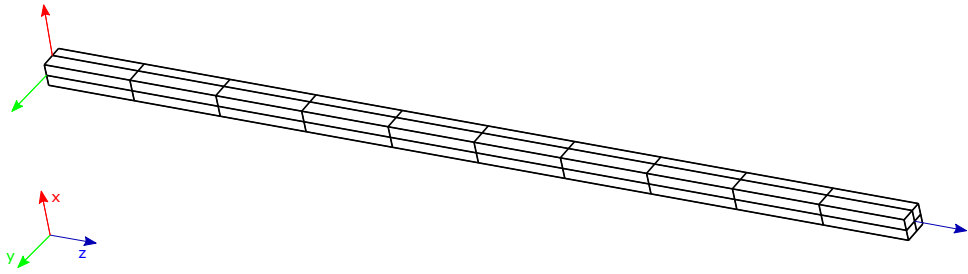|	
L	1 m
S	$(0.03{\times}0.03)\text{m}^2$

Table 6.1: Dimensions of 3D Beam

Figure 6.2: Finite Element Model of 3D Beam

The mesh has been done using the isoparametric solid element HEXA20, that means to have 20 nodes per each brick element. To build the FEM, 10 elements along the length and 2×2 elements on the cross section have been used. The clamped-clamped beam has 297 active nodes and 891 total degrees of freedom.

Before using the STEP, it is important to proper select the modes to consider within the modal basis $\mathbf{\Phi}$. The idea is to check the modal forces, calculated during the STEP, prescribing the nodal displacements of the first mode-shape in linear and nonlinear static solution.

$$\boldsymbol{F}_T = \boldsymbol{F}_L + \boldsymbol{F}_{NL} = \boldsymbol{K}\boldsymbol{X}_c + \boldsymbol{\Gamma}\left(\boldsymbol{X}_c\right)$$

$$\boldsymbol{F}_{NL} = \boldsymbol{\Gamma}\left(\boldsymbol{X}_c\right) = \boldsymbol{F}_T - \boldsymbol{F}_L \qquad (6.4)$$

$$\widetilde{\boldsymbol{F}}_{NL} = \boldsymbol{\Phi}^T \boldsymbol{F}_{NL}$$

The modal forces of the first 34 modes have been reported in Fig. 6.3, where it seems reasonable to consider only the first bending (1B) and the fourth axial (4A) eigenvector as modal basis.
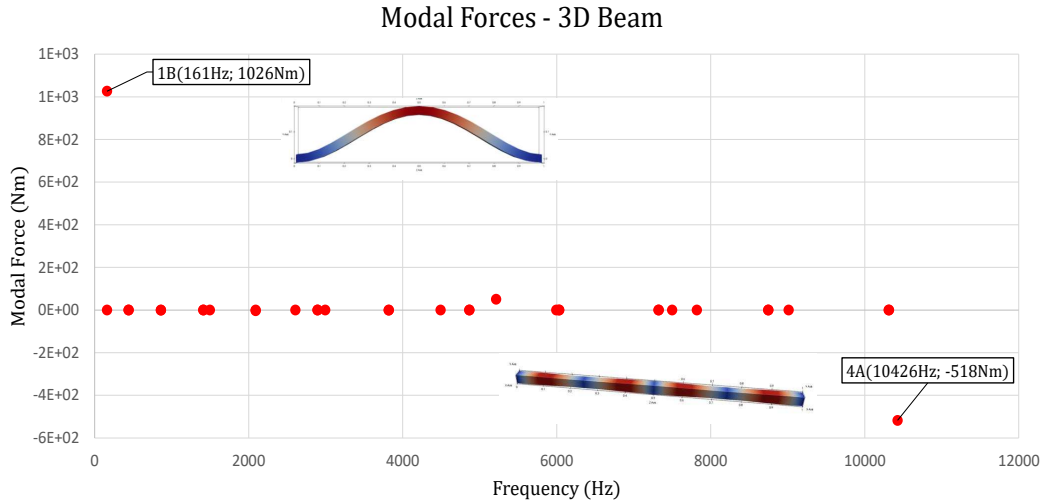

Figure 6.3: Modal Forces 3D Beam prescribing 1B

Mode	Frequency	Modal Force
1B	160 Hz	1026 Nm
4A	10426 Hz	-518 Nm

Table 6.2: Selected Modes 3D Beam

In Tab. 6.3 have been reported the nonlinear quadratic and cubic terms of non-linear modal stiffness evaluated taking the 1st transversal mode (bending) and the 4th longitudinal mode (axial) as selected modes in the modal basis used to formulate the reduced order model of the 3D beam.

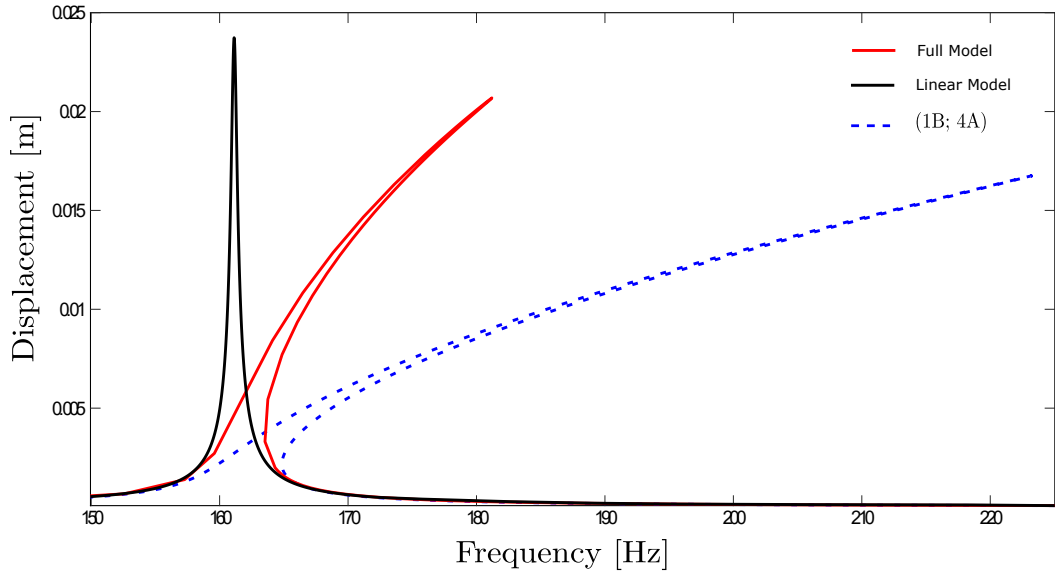|	a_{11}^2	a_{21}^1	b_{111}^1	b_{222}^2	b_{211}^2
EF 3D SAMCEF	-5.1664e8	-1.033e9	1.6308e9	1.15e11	1.3040e10
CODE ASTER	-5.2497e8	-1.0499e9	1.6734e09	1.13e11	1.3395e10

Table 6.3: 3D Beam Quadratic and Cubic Tensor's entries

Figure 6.4: Nonlinear Forced Response of 3D Beam (center beam node y-axis) using H=3 with a forcing amplitude F_0=200 N

Even if the quadratic and cubic entries of the stiffness tensors have been calculated, within Code Aster, with a maximum relative error less than 3%, the nonlinear

81

frequency response of the 3D beam model, traced with ANM continuation, doesn't fit the full response of the structure evaluated with an in-house HBFEM (using libMesh and LOCA). Computing the nonlinear modal forces as $\widetilde{\boldsymbol{F}}_{NL} = \boldsymbol{\Phi}^T(\boldsymbol{F}_T - \boldsymbol{F}_L)$ seemed reasonable to consider only the 1B and 4A, since they had the greater modal contribution, while the others modal forces associated to the remaining modes, were almost nil.

Due to the fact that the nonlinear response computed solving the ROM of 3D beam is far from the response of the full model, further investigations have been done in Chapter 8.

6.2   Simply Supported Plate

The same procedure to compute the nonlinear stiffness coefficients has been used for a simply supported plate having the following material properties:

$$E = 73\ GPa, \quad \nu = 0.3, \quad \rho = 2763\ \frac{kg}{m^3} \tag{6.5}$$

The finite element model has been built using the DKT plate element element available in Code Aster, since no others shell elements compatible with the large deformation assumption are implemented within the software. The rectangular plate has the dimensions reported in Table 6.4.

b	254 mm
l	355.6 mm
s	1.02 mm

Table 6.4: Dimensions of Rectangular Plate

where b, l, s are the base, length and the thickness, respectively. The mesh has been built in such a way to have 56 elements along the length and 40 elements along the base with a total of 2145 active nodes. The rectangular plate has 12870 active degrees of freedom because the DKT elements have 6 dofs per each node of the mesh.

The modal nonlinear forces $\widetilde{\boldsymbol{F}}_{NL}$, shown in Fig. 6.5, have been calculated prescribing the nodal displacement field associated to the first mode-shape (1M) on the first 25 modes within the 1st loop of the STEP method.
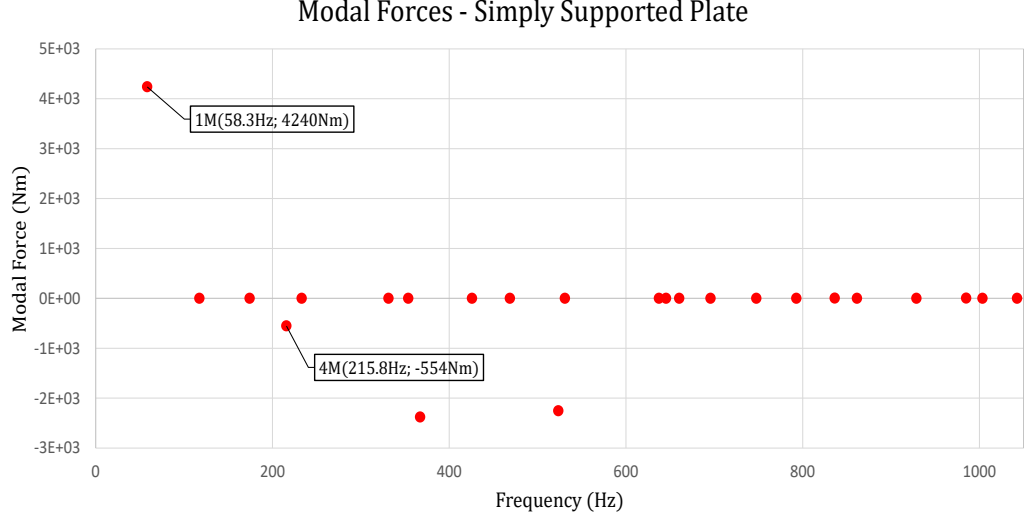

Figure 6.5: Modal Forces Simply Supported Plate prescribing 1B

Following the Nasa paper [1], only the first (1M) and fourth (4M) mode-shape have been considered to compute the reduced order model (ROM).
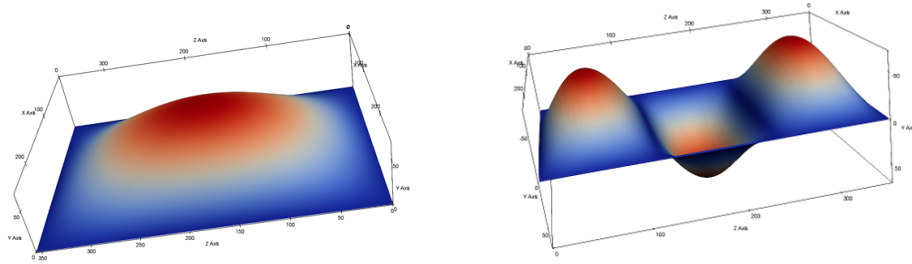

Figure 6.6: 1st and 4th Mode-shape of the Simply Supported Plate

Nevertheless, also the eighth (8M) and eleventh (11M) eigenvector give a non-negligible contribution in the nonlinear response of the system, as shown in Tab. 6.5.

83

Mode	Frequency	Modal Force
1M	58.3 Hz	4240 Nm
4M	215.8 Hz	-554 Nm
8M	367.2 Hz	-2380 Nm
11M	523.55 Hz	-2254 Nm

Table 6.5: Selected Modes Simply Supported Plate

The quadratic and cubic entries of the stiffness tensors, considering only 1M and 4M as selected modes within the stiffness evaluation procedure, have been reported in Tab. 6.6. The maximum relative error is less than 4%.

	b^1_{111}	b^1_{112}	b^1_{122}	b^2_{111}	b^2_{222}
NASA	4.109e12	1.722e12	2.273e13	5.550e11	6.818e13
CODE ASTER	4.077e12	1.744e12	2.181e13	5.459e11	6.599e13

Table 6.6: Simply Supported Plate Cubic Tensor's entries

More in detail, the QUAD4 instead of DKT element has been used in the Nasa reference paper; nevertheless, the nonlinear stiffness coefficients fit the tensors entries calculated by the Nasa. The cross section of DKT shell elements remains perpendicular to its neutral axis, and so no rotations of the cross section are allowed in this model. The simply supported plate means that the structure is clamped at its edges where only the rotations DRX, DRY, DRZ are allowed.

Chapter 7

Nonlinear Frequency Response of an Inclined Plate

In this chapter has been explained how to model the contact as smooth function to simulate the tip-rubbing phenomenon. Since the contact has been modelled as smooth function, it has been possible to apply the ANM continuation method to trace the nonlinear response of the structure. In order to better understand all the phenomena linked to the contact and geometric nonlinearities, an inclined straight plate has been used as case study. The idea is to test if the ANM is also effective to solve regularized non-smooth dynamics problems like vibrating systems with contact conditions and friction laws. Instead of using the modal truncation, the Craig-Bampton method has been adopted to formulate the reduced order model of the structure where the RITZ basis has been used as reduction matrix of the system. Finally, a comparison between the 3D isoparametric solid element and shell element has been done to find out the more suitable element type to adopt within the computation of nonlinear frequency response (NFR) including contact and large deformations.

7.1 Smooth Function for Tip-Rubbing

The idea is to regularize non-smooth function to study the tip-rubbing using the ANM continuation method to solve the nonlinear system. Consider a 1 DOF mechanical system in Fig.7.1 governed by the Duffing's equation:

$$m\ddot{x} + c\dot{x} + kx + \beta x^3 = F_{ext}(t) + F_N(x) \tag{7.1}$$

where $\ddot{x}$ and $\dot{x}$ are the first and second time derivatives of the displacement x; β is the nonlinear cubic stiffness while F_{ext} and F_N are the external periodic force and the normal contact force acting on the system, respectively.
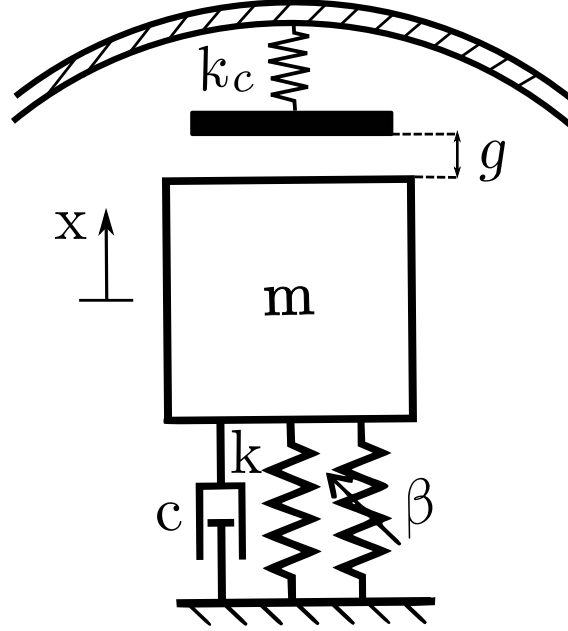

Figure 7.1: Duffing Oscillator with External Contact Force

The contact phenomenon is a non-smooth problem where the normal contact force may be written as follows [20]:

$$F_N = \begin{cases} -k_c(x - g) & \text{if } g = 0 \\ 0 & \text{if } g > 0 \end{cases} \tag{7.2}$$

where k_c is the contact stiffness $(k_c >> k)$ and g is the gap between the mass m and the casing. If the gap is greater than zero means that there is no contact phenomenon, and so the system is governed by the classical Duffing's equation; otherwise, if the gap is nil an additional external contact force must be considered during the computation of the nonlinear forced response.

In case of contact-friction a 2 DOFs model in Fig.7.2 must be introduced due to the presence of the tangential component of the force. The system has been modelled as a belt representing the casing that rotates with the tangential velocity v_t, while the mass may oscillate along the normal and tangential direction.
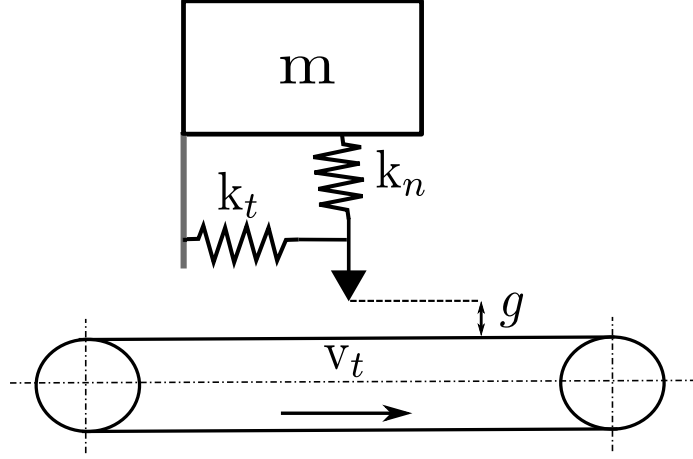

Figure 7.2: 2 DOFs System to Model the Contact-Friction Phenomenon

where k_t and k_n are the tangential and normal contact stiffness, respectively. The normal force F_n may be written as [21]:

$$F_n = \begin{cases} k_n(x_n - g) & \text{if } g = 0 \\ 0 & \text{if } g > 0 \end{cases} \tag{7.3}$$

while the tangential force F_t is equal to:

$$F_t = \begin{cases} k_t(\dot{x}_t - v_t) & \text{if } g = 0 \\ \mu F_n \; \text{sign}(\dot{x}_t - v_t) & \text{if } g = 0 \\ 0 & \text{if } g > 0 \end{cases} \tag{7.4}$$

The Coulomb model of friction has been used to state the tangential contact force F_t, where μ is the coefficient of friction.

To regularize the non-smooth function that describes the contact law of the structure, the Eq.7.5 must be introduced.

$$F_n^2 - k_n(x-g)F_n - \epsilon_n^2 = 0 \tag{7.5}$$

Solving the Eq.7.5 two distinct real solutions may be found, nevertheless, only the positive one is suitable to model the contact force function shown in Fig.7.3.

$$F_n = \frac{k_n(x-g)}{2} + \sqrt{\left[\frac{k_n(x-g)}{2}\right]^2 + \epsilon_n^2} \tag{7.6}$$

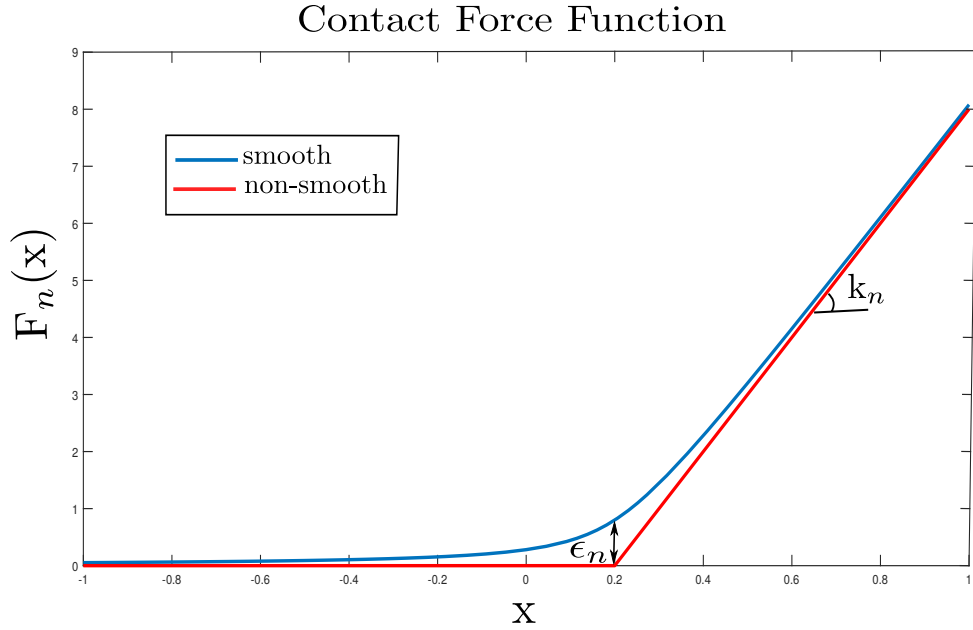Figure 7.3: Contact Force Function

The parameter ϵ_n defines the smoothness of the contact force function; decreasing ϵ_n, less smooth the system will be.

88

7.2   Clamped-Free Inclined Plate

The clamped-free straight plate has been modelled to study the nonlinear frequency response including the contact and geometric nonlinearities. The plate has a slope of 15 degrees with respect to the z-axis to simulate the inclination of a real HP compressor blade, guaranteeing the perpendicularity between the tip-face and the casing of the turbo-engine. The cantilever plate has been adopted to study the tip-rubbing phenomenon, where the plate-root is clamped, and one contact tip node has been considered. The material properties are stated below:

$$E = 210 \ GPa, \quad \nu = 0.3, \quad \rho = 7800 \ \frac{kg}{m^3} \tag{7.7}$$

The HEXA20 isoparametric solid element has been used to build the finite element model of the structure where an uniform mesh of 15×15 with 4 elements along the thickness has been used, so that the FEM has 4484 active nodes and 13452 degrees of freedom. The dimensions of the plate have been reported in Tab. 7.1.
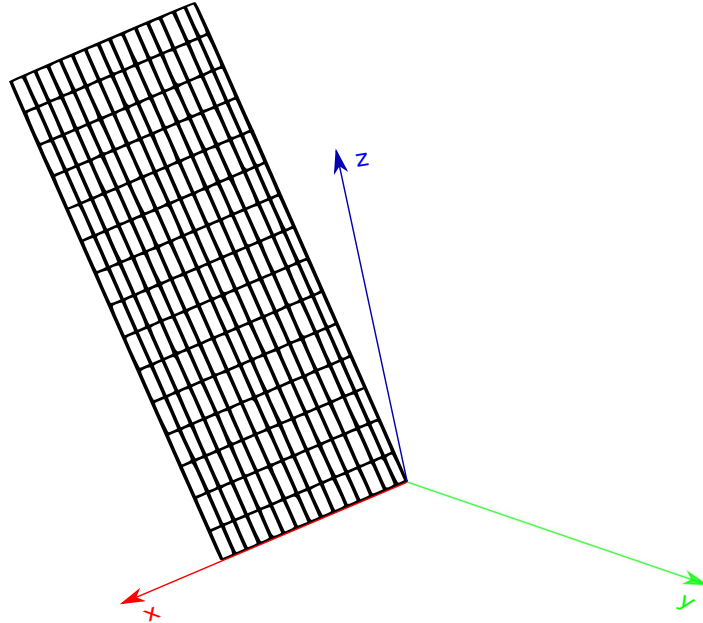

Figure 7.4: Finite Element Model of 3D Inclined Plate

b	300 mm
l	800 mm
s	15 mm

Table 7.1: Dimensions of Inclined Plate

The computation of the nonlinear forced response has been done assuming the proportional viscous damping (Rayleigh damping) equal to $3\boldsymbol{M}$.

7.2.1 RITZ basis as Reduction Matrix in STEP

The STEP method explained in Section 3.3.3 works in modal coordinates where the modal truncation has been applied to reduced the size of the full system. Considering only the geometric nonlinearities the STEP method, using the modal truncation is still valid. Nevertheless, in case of a structure including geometric and contact nonlinearities, a new concept of STEP method must be introduced. Since the contact problem has been formulated in real coordinate, it is important to have the contact nodes of the structure in real coordinates.

The idea is to formulate the reduction problem no more in modal coordinate but using the Craig-Bampton method, so that also the boundary nodes may be considered. Within the STEP, instead of imposing the nodal displacement field associated to the internal modes $\boldsymbol{\Phi}_{int}$, the RITZ basis has been used as reduction matrix $\mathbf{R}$. A comparison between the internal modes and the RITZ basis has been presented below.

Internal Modes as Basis

The equation of motion of the system is in modal coordinates with $\mathbf{q}$ as set of modal equations with reduced dofs:

$$\widetilde{\boldsymbol{M}}\ddot{\boldsymbol{q}} + \widetilde{\boldsymbol{C}}\dot{\boldsymbol{q}} + \widetilde{\boldsymbol{K}}\boldsymbol{q} + \widetilde{\boldsymbol{\gamma}}\left(q_1,\ q_2,\ \ldots,\ q_L\right) = \widetilde{\boldsymbol{F}}, \quad L \leq N \tag{7.8}$$

where:

$$\widetilde{\boldsymbol{M}} = \boldsymbol{\Phi}_{int}^{T}\boldsymbol{M}\boldsymbol{\Phi}_{int} = [\boldsymbol{I}]$$

$$\widetilde{\boldsymbol{C}} = \boldsymbol{\Phi}_{int}^{T}\boldsymbol{C}\boldsymbol{\Phi}_{int} = [2\zeta_r\omega_r]$$

$$\widetilde{\boldsymbol{K}} = \boldsymbol{\Phi}_{int}^{T}\boldsymbol{K}\boldsymbol{\Phi}_{int} = [\omega_r^2] \qquad (7.9)$$

$$\widetilde{\boldsymbol{\gamma}} = \boldsymbol{\Phi}_{int}^{T}\boldsymbol{\Gamma}$$

$$\widetilde{\boldsymbol{F}} = \boldsymbol{\Phi}_{int}^{T}\boldsymbol{F}$$

The eigenvalue problem has been solved considering the root and tip both clamped, because to impose the contact, the real coordinates of the tip must be preserved within the reduced order model. Prescribing the nodal displacement field of the first bending on the first 100 modes of the system, it has been possible to find out the coupled modes of the structure.
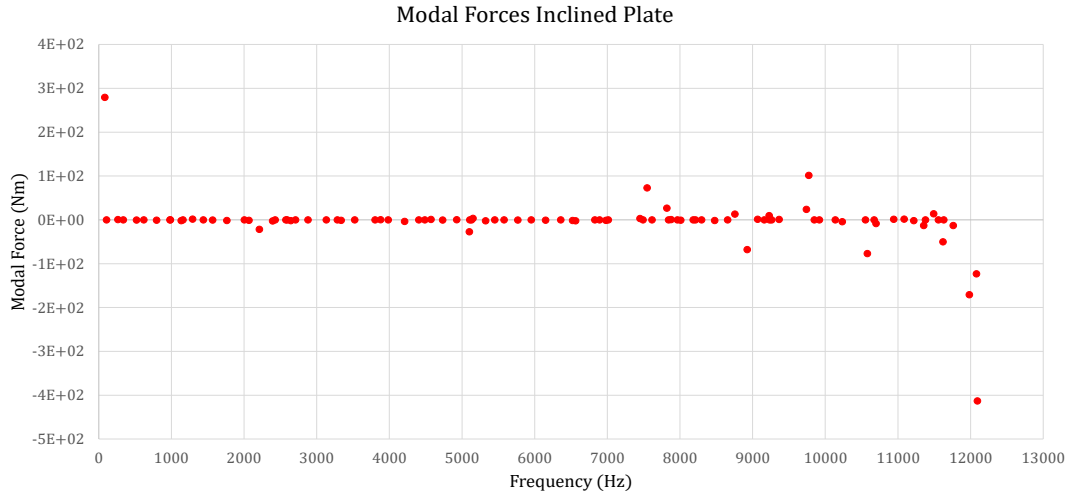

Figure 7.5: Modal Forces Inclined Plate prescribing 1B on 100 modes

In Fig.7.5 has been plotted the nonlinear modal forces $\tilde{\boldsymbol{F}}_{NL} = \boldsymbol{\Phi}^{T}(\boldsymbol{F}_{T} - \boldsymbol{F}_{L})$, while the non-negligible modal forces are shown in Fig.7.6.
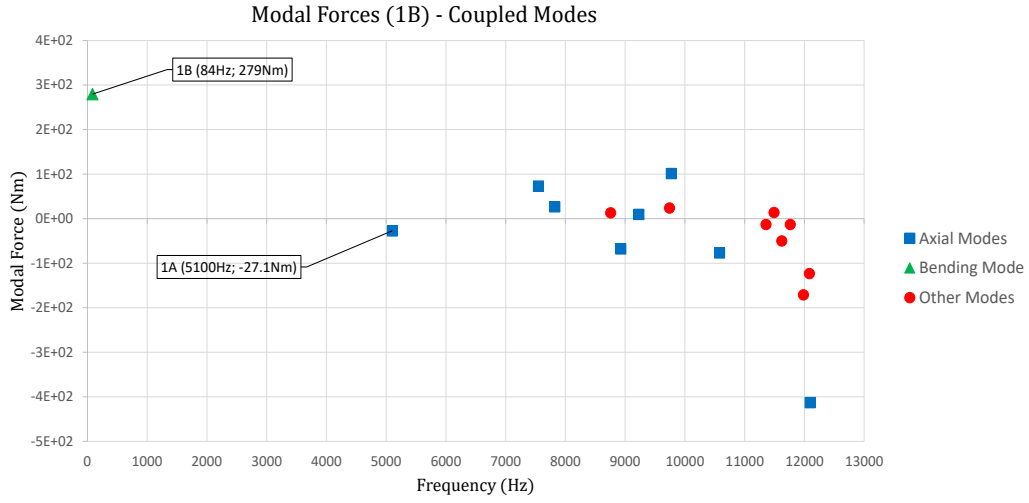
Figure 7.6: Coupled Modes in terms of Modal Forces of the Inclined Plate prescribing 1B

Mode	Frequency	Modal Force
1B	84 Hz	279 Nm
1A	5100 Hz	-27.1 Nm

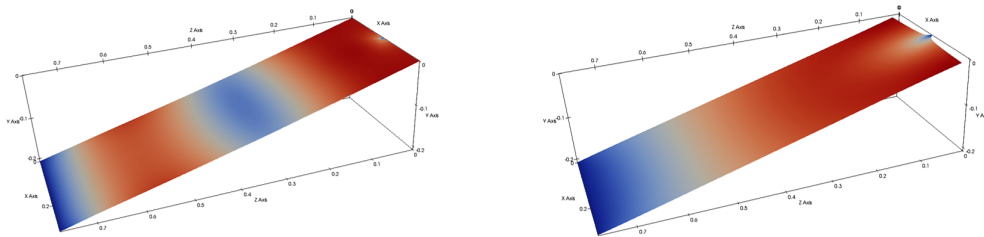Table 7.2: Selected Modes Inclined Plate

Figure 7.7: 1st Bending and 1st Axial Mode-shape of the Inclined Plate

Using the internal modes listed in Tab.7.3 the nonlinear frequency response of the tip-node along z-axis has been plotted in Fig.7.8.
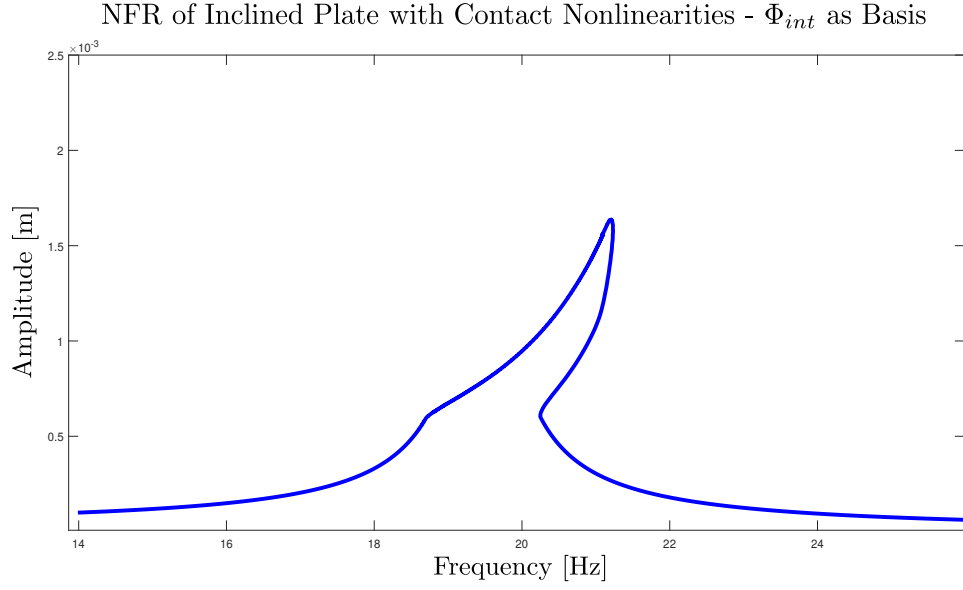
Figure 7.8: NFR of Tip Contact Node along z-axis - H=50, F_0=20 N, gap=0.6 mm, ϵ_n=1.5, μ=0.1, k_c=10^6 N/m.
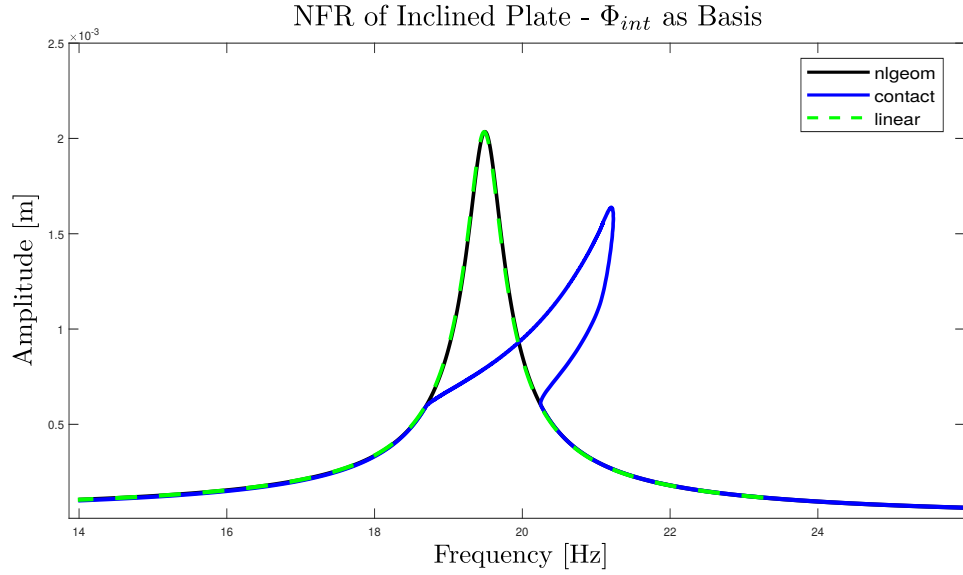

Figure 7.9: Frequency Response of Tip Contact Node along z-axis, comparison between Contact and Geometric Nonlinearities using the internal modes as basis - H=50, F_0=20 N, gap=0.6 mm, ϵ_n=1.5, μ=0.1, k_c=10^6 N/m.

93

It has been possible to notice that the contact-node is not affected by the geometric nonlinearities since the plate has been clamped for the computation of quadratic and cubic stiffness tensors during the stiffness evaluation procedure. Therefore, using the internal modes as reduction basis, only the contact nonlinearities can be caught, and the hypothesis of large deformation is not valid anymore. As shown in Fig.7.9, the structure in absence of contact behaves as a linear system because the geometric nonlinearities act only on the internal nodes.

To demonstrate that the system behaves as linear in absence of contact, the nonlinear forced response has been plotted (Fig.7.10) increasing the amplitude of the external periodic force and the gap between the tip-plate and the casing.
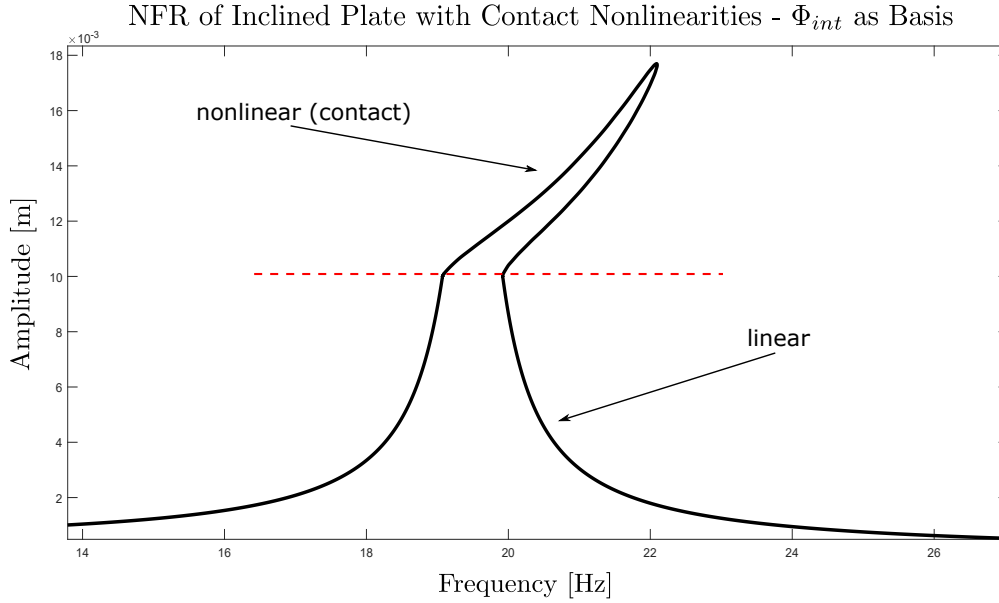

Figure 7.10: Nonlinear Frequency Response of Tip Contact Node along z-axis using the internal modes as basis - H=50, F_0=200 N, gap=10 mm, ϵ_n=0.5, μ=0.1, k_c=10^6 N/m.

Reduction Matrix as Basis

The Ritz basis has been used as reduction matrix to build the reduced order model of the structure. The Craig-Bampton method, explained in Section 3.2.3, has been useful to capture the dynamics of the full system taking into account the internal modes and the static modes on the boundary. The equation of motion of the system may be written as:

$$\begin{bmatrix} \boldsymbol{K}_{II} & \boldsymbol{K}_{IB} \\ \boldsymbol{K}_{BI} & \boldsymbol{K}_{BB} \end{bmatrix} \begin{bmatrix} \boldsymbol{x}_I \\ \boldsymbol{x}_B \end{bmatrix} - \omega^2 \begin{bmatrix} \boldsymbol{M}_{II} & \boldsymbol{M}_{IB} \\ \boldsymbol{M}_{BI} & \boldsymbol{M}_{BB} \end{bmatrix} \begin{bmatrix} \boldsymbol{x}_I \\ \boldsymbol{x}_B \end{bmatrix} = \begin{bmatrix} 0 \\ \boldsymbol{f}_B \end{bmatrix} \tag{7.10}$$

where x_B and x_I are the boundary and internal degrees of freedom of the structure, respectively.

Following the same procedure adopted in CBM, it has been possible to assemble the RITZ basis used as reduction matrix within the stiffness evaluation procedure.

$$\boldsymbol{R} = \begin{bmatrix} \boldsymbol{\Phi}_I & \boldsymbol{\Psi} \\ \boldsymbol{0} & \boldsymbol{I} \end{bmatrix} \tag{7.11}$$

Where $\boldsymbol{\Phi}_I$ is the matrix containing all the internal modes of the structure that has been calculated solving the eigenvalue problem associated to the internal degrees of freedom of the structure considering the tip-nodes clamped; $\boldsymbol{\Psi}$ is the matrix of the static modes at the boundary of the structure. The idea is to select only the coupled internal modes keeping all the static modes on the boundary. Imposing the reduction matrix $\boldsymbol{R}$ as basis into the STEP, it has been possible to include also the contribution comes from the static modes at boundary (tip). The equation of motion of the reduced nonlinear structure may be written as:

$$\boldsymbol{M}_R \ddot{\boldsymbol{x}} + \boldsymbol{C}_R \dot{\boldsymbol{x}} + \boldsymbol{K}_R \boldsymbol{x} + \boldsymbol{\gamma} \left(x_{L_1}, x_{L_2}, \ldots, x_{L_L}, x_{B_1}, x_{B_2}, \ldots, x_{B_N} \right) = \boldsymbol{F}_R \tag{7.12}$$

$$\boldsymbol{M}_R = \boldsymbol{R}^T \boldsymbol{M} \boldsymbol{R}$$

$$\boldsymbol{C}_R = \boldsymbol{R}^T \boldsymbol{C} \boldsymbol{R}$$

$$\boldsymbol{K}_R = \boldsymbol{R}^T \boldsymbol{K} \boldsymbol{R} \tag{7.13}$$

$$\boldsymbol{\gamma} = \boldsymbol{R}^T \boldsymbol{\Gamma}$$

$$\boldsymbol{F}_R = \boldsymbol{R}^T \boldsymbol{F}$$

where $\boldsymbol{x}_L$ holds the amplitude of the internal modes, it ranges between one and the number of selected internal modes, while $\boldsymbol{x}_B$ is the vector of amplitude of the tip-nodes having the size of the degrees of freedom of boundary nodes. Instead of prescribing only the nodal displacement field of the internal modes, also the static displacement at the tip has been considered in the ROM, playing an important role in the nonlinear frequency response of the system.

As in the first case, the nodal displacement field calculated prescribing a unitary static force along the y-axis, has been prescribed to evaluate the nonlinear quadratic and cubic stiffness tensor of the inclined plate.
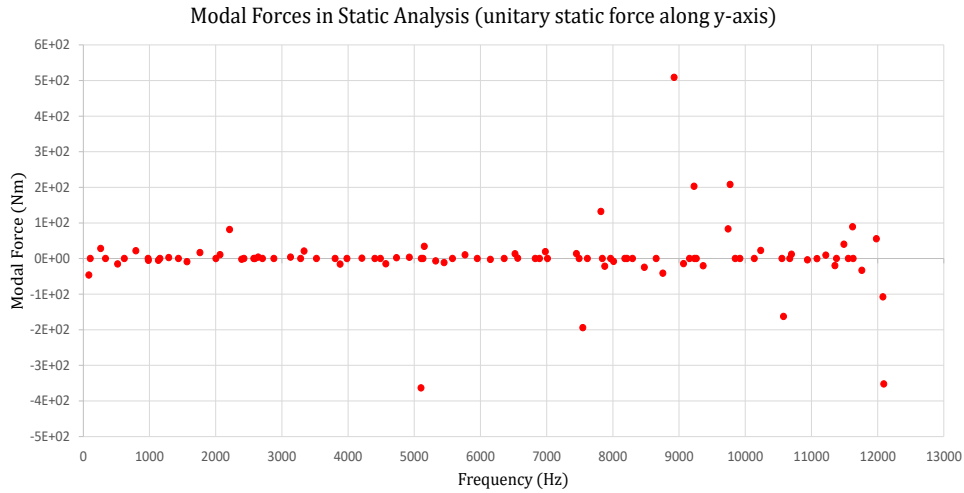

Figure 7.11: Modal Forces Inclined Plate prescribing prescribing a Unitary Static Force along y on the first 100 modes
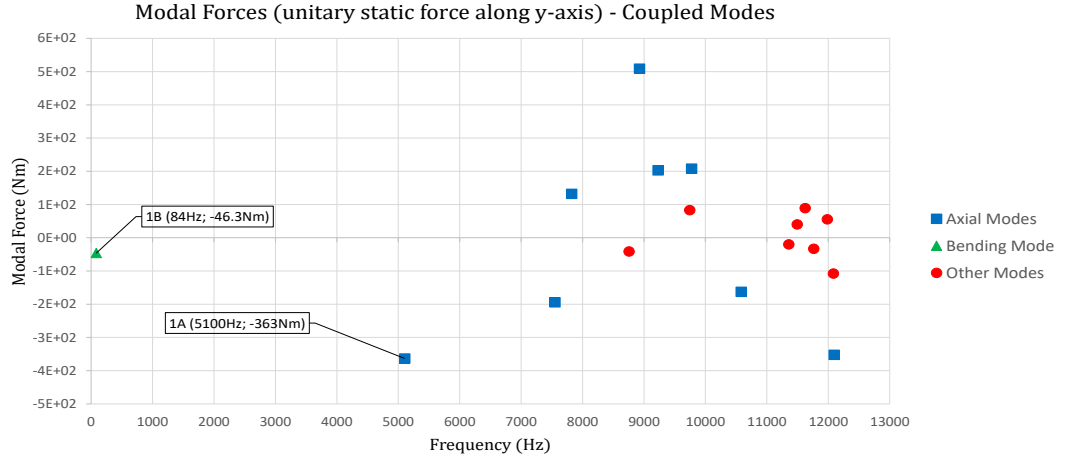
96

Figure 7.12: Coupled Modes in terms of Modal Forces of the Inclined Plate prescribing an Unitary Static Force along y

Mode	Frequency	Modal Force
1B	84 Hz	-46.3 Nm
1A	5100 Hz	-363 Nm

Table 7.3: Selected Modes Inclined Plate

The first bending and axial mode of the plate has been used as internal modes into the RITZ basis, while DY and DZ have been considered as dofs of the boundary node. Imposing a unitary static force along the y-axis also the boundary node along z-axis has been excited, as shown in Tab.7.4.

Direction	Node	Modal Force
x-axis	tip node	7.13E-08 Nm
y-axis	tip node	4.45E+04 Nm
z-axis	tip node	-1.65E+05 Nm

Table 7.4: Modal Forces Boundary Nodes

It has been interested to notice that prescribing the displacement field associated to the internal modes or to the Ritz basis, the same axial modes have been excited, as reported in Fig.7.13.
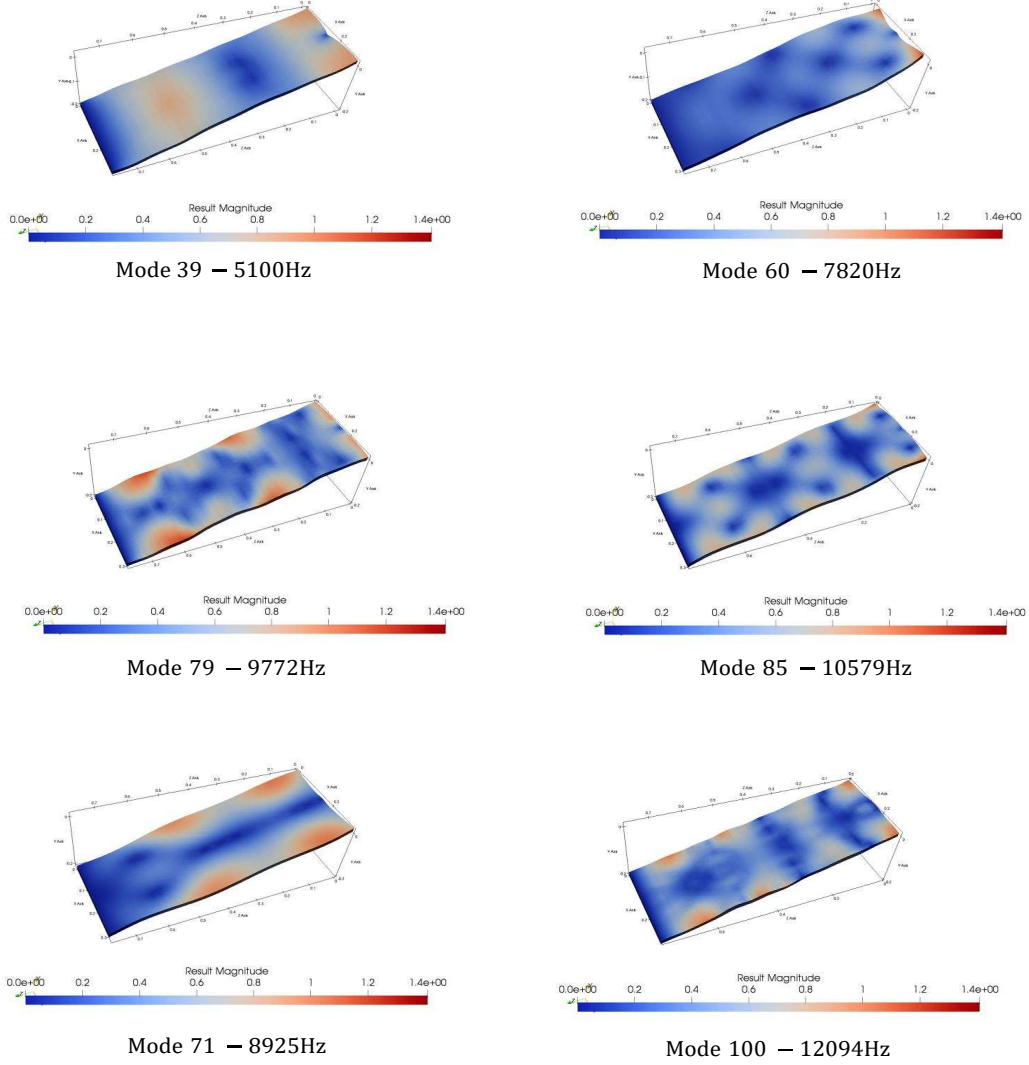
97

Figure 7.13: Axial Mode-Shapes of Inclined Plate

To compare the modal basis $\boldsymbol{\Phi}_{int}$ with the RITZ basis $\mathbf{R}$, only two modes (1B,1A) plus the static contribution along y and z-axis have been considered in the ROM. The comparison between the nonlinear forced responses in frequency domain has been shown in Fig.7.14 and 7.15.
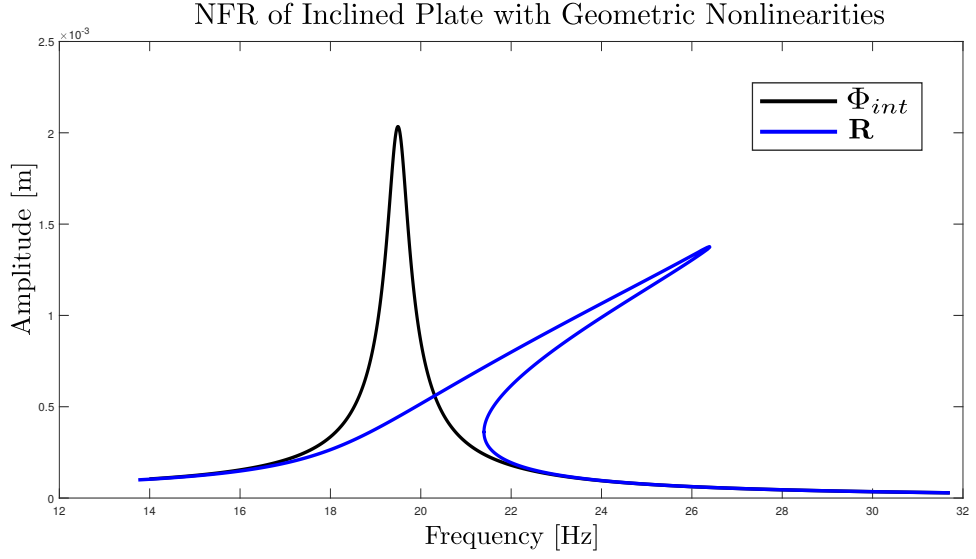
Figure 7.14: Nonlinear Forced Response of Tip Contact Node along z-axis including Geometric Nonlinearities - H=5, F_0=20 N.
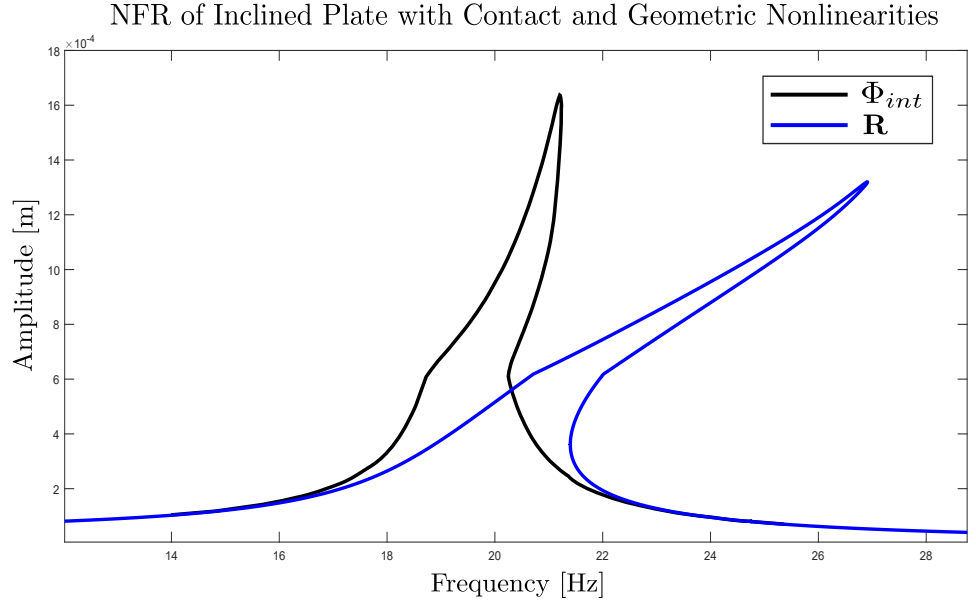

Figure 7.15: Nonlinear Forced Response of Tip Contact Node along z-axis including Contact and Geometric Nonlinearities - H=5, F_0=20 N, gap=0.6 mm, ϵ_n=0.5, μ=0.1, k_c=10^6 N/m.

Once again, the basis of internal modes is not suitable to capture the geometric nonlinearities at the boundary node, therefore the Ritz basis must be adopted in case of a dynamics problem including the tip-rubbing and large deformation.

The geometric nonlinearities have a stiffening effect on the structure due to the coupling between the bending and axial mode-shapes. The large Deformation leads to have a bending-membrane coupling and gives rise to membrane stretching (in plane stresses) when out-of-plane loading is applied.

7.2.2 HEXA20 and DKT Elements for NL Vibrations

In the previous section, the nonlinear forced response of an inclined plate modelled with HEXA20 elements has been shown. Nevertheless, the stiffening effect applying a force of $20N$ along the y-axis at tip-node is too high, therefore the nonlinearities are not well representing the behaviour of the structure. For this reason, a comparison between the isoparametric solid and shell element has been studied in this section. The idea is to compare the nonlinear frequency response of the inclined plate using the HEXA20 and DKT element. Each node of a shell element has 6 degrees of freedom $(DX, DY, DZ, DRX, DRY, DRZ)$ instead of 3 (DX, DY, DZ) as in case of brick element; the DKT inclined plate has 2479 active nodes, and so 14874 active dofs.

The Ritz basis has been used within the STEP method to evaluate the nonlinear stiffness tensors where only one node has been considered as boundary node for applying Craig-Bampton. Prescribing a unitary static force along the y-axis, the values of the modal forces of the first 100 modes have been reported in Fig.7.16. The first bending and axial mode of the plate have been used as internal modes into the RITZ basis, while DY, DZ and DRX have been considered as dofs of the boundary node. Imposing a unitary static force along the y-axis also the boundary node along z-axis has been excited, as shown in Tab.7.6.

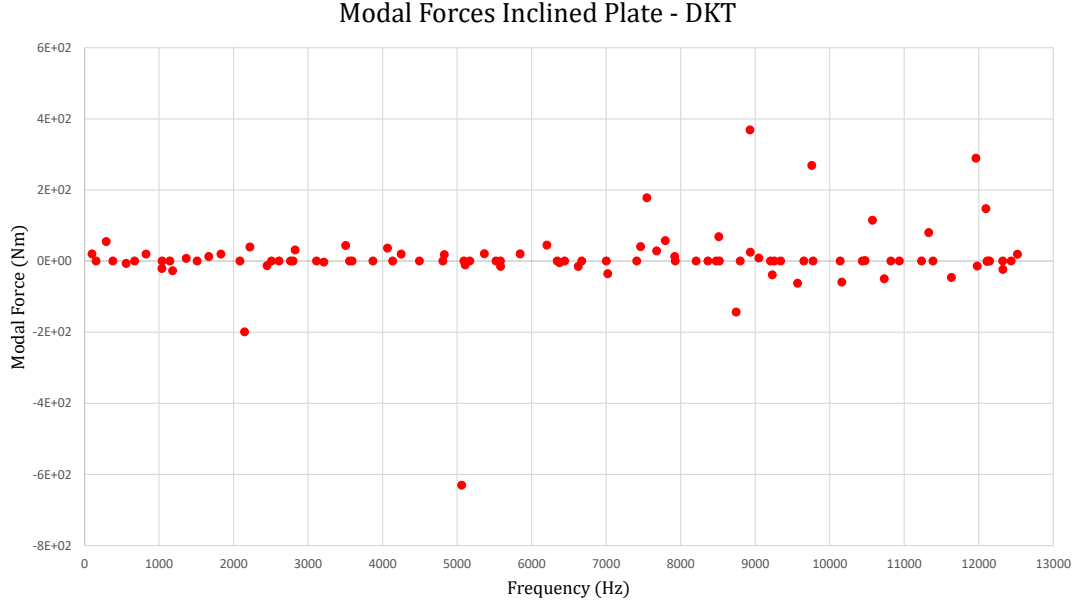| Mode	Frequency	Modal Force
1B	99.38 Hz	2E+01 Nm
1A	2147.4 Hz	-1.99E+02 Nm

Table 7.5: Selected Modes DKT Inclined Plate

Figure 7.16: Modal Forces DKT Inclined Plate prescribing a Unitary Static Force along y-axis

Direction	Node	Modal Force
DX	tip node	-1.21E-09 Nm
DY	tip node	4.27E+04 Nm
DZ	tip node	-1.58E+05 Nm
DRX	tip node	-6.32E+01 Nm
DRY	tip node	4.66E-11 Nm
DRZ	tip node	-1.76E-10 Nm

Table 7.6: Modal Forces Boundary Nodes DKT plate

To evaluate the entries of nonlinear tensor, the amplitude of the internal modes and boundary nodes must be proper selected before using the STEP method. The amplitude used for the computation of the modal forces of DKT inclined plate are reported in Tab.7.7.

	Coordinate	Amplitude
Internal Modes	$\boldsymbol{x}_L$	1E-03
Boundary Nodes	$\boldsymbol{x}_B$	1E-02

Table 7.7: Amplitude of Internal and Boundary nodes for STEP method

101

As shown in Fig.7.17, the nonlinear response of HEXA20 plate seems to over-estimate the nonlinear frequency response for a force magnitude of 20 N applied at tip-node. It has been possible to notice that the maximum displacement along the y-axis of the plate is around 5 millimetres with an increase in frequency due to nonlinearities of 7 Hz. The issue is that for a displacement of 5 mm, the dimensions of the plate are such that it should work in linear region with a small stiffening effect.
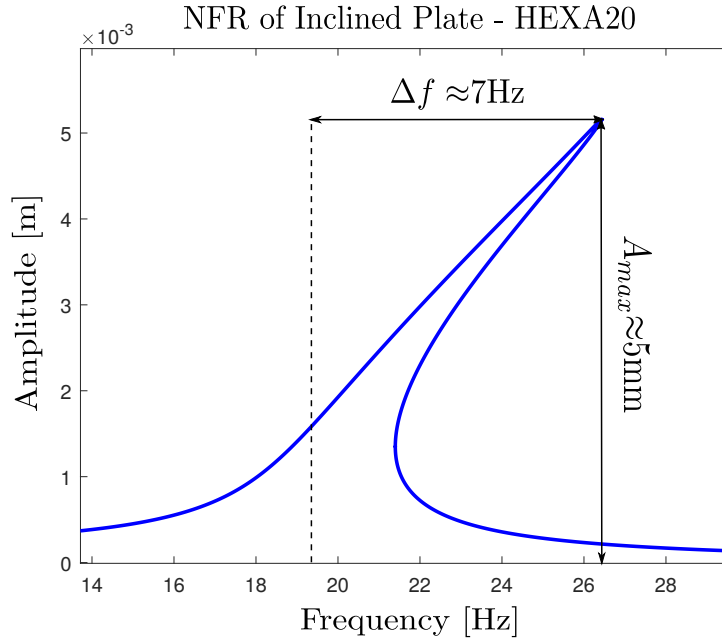

Figure 7.17: Nonlinear Forced Response of Tip Contact Node HEXA20 Plate along y-axis - H=5, F_0=20 N.

In Fig.7.18, the nonlinear forced response of DKT plate has been plotted; in this case the nonlinearities well representing the behaviour of nonlinear structure with a periodic forcing amplitude of 20 N. As expected, the increase in frequency for an amplitude of 4 mm is equal to 0.5 Hz; this is the proof that the inclined plate for a displacement of 4 millimetres behaves as a linear structure. The expected increase in frequency ($f \approx 5 \div 10$ Hz) and amplitude ($A_{max} \approx 10^{-2}m$) corresponding to the large deformation have been achieved for a periodic external force of 100 N along y-axis, as shown in Fig.7.19.
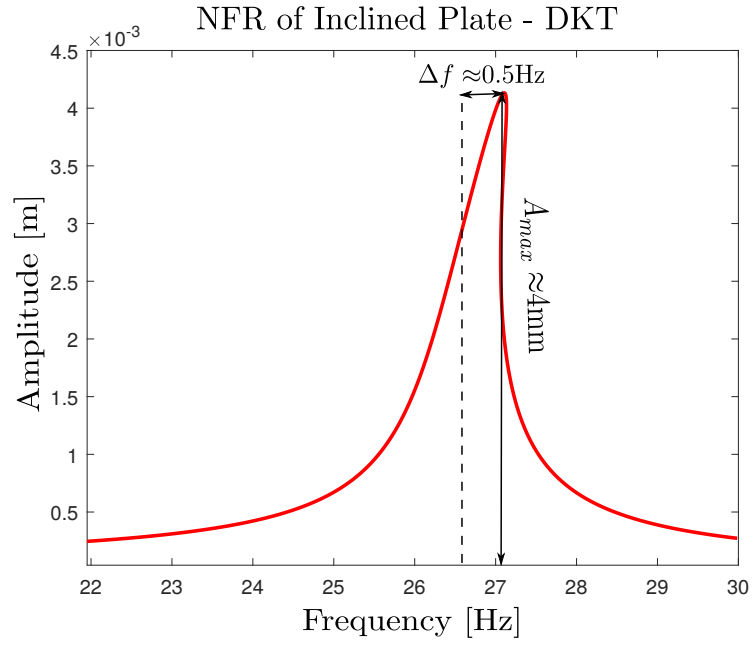
Figure 7.18: Nonlinear Forced Response of Tip Contact Node DKT Plate along y-axis - H=5, F_0=20 N.

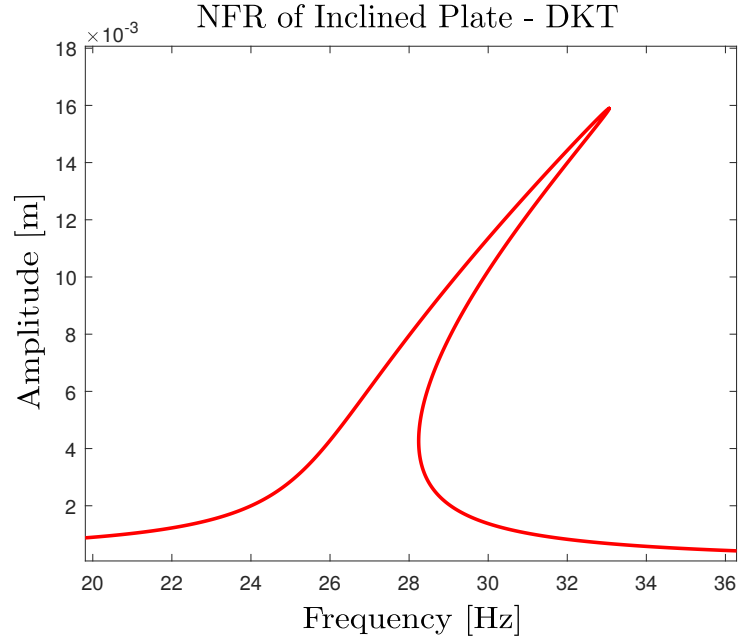Figure 7.19: Nonlinear Forced Response of Tip Contact Node DKT Plate along y-axis - H=5, F_0=100 N.
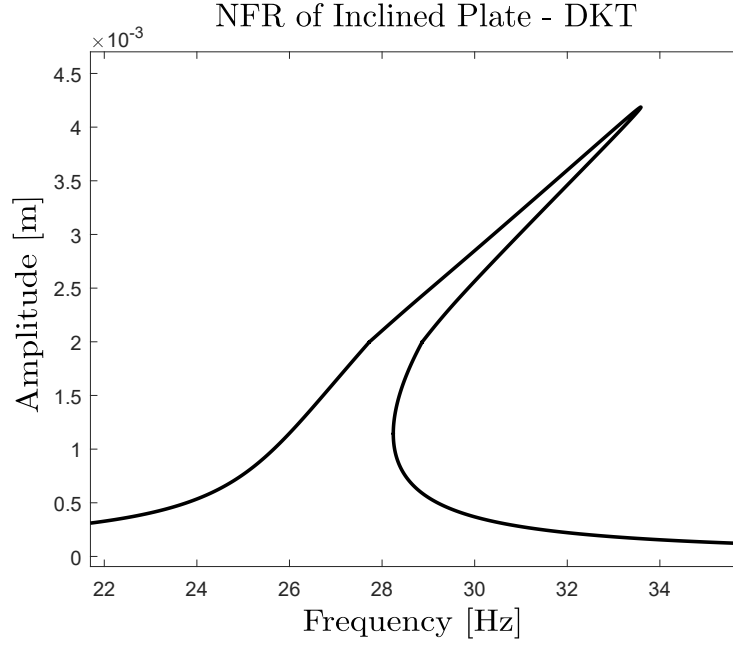
103

Figure 7.20: Nonlinear Forced Response of Tip Contact Node DKT Plate along z-axis H=5, F_0=100 N, gap=2 mm, ϵ_n=0.5, μ=0.1, k_c=10^6 N/m.
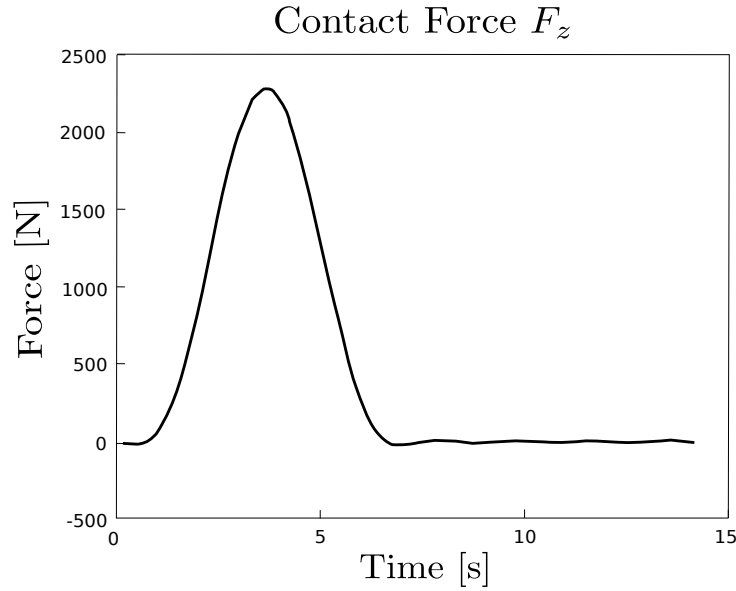

Figure 7.21: Contact Force at Tip Contact Node DKT Plate along z-axis - H=5, F_0=100 N, gap=2 mm, ϵ_n=0.5, μ=0.1, k_c=10^6 N/m.

The nonlinear frequency response including contact of the inclined DKT plate has been shown in Fig.7.21, where it has been plotted the maximum contact force over time when the plate touches the casing. Based on these results, it seems that the shell elements better approximate the behaviour of nonlinear structure due to a less stiffening effect of the plate. In Fig.7.22 the geometrically nonlinear response of the plate has been plotted to show that increasing the amplitude of the external periodic force, the peaks lie always on the same line called "skeleton" or "backbone curve" of nonlinear response.
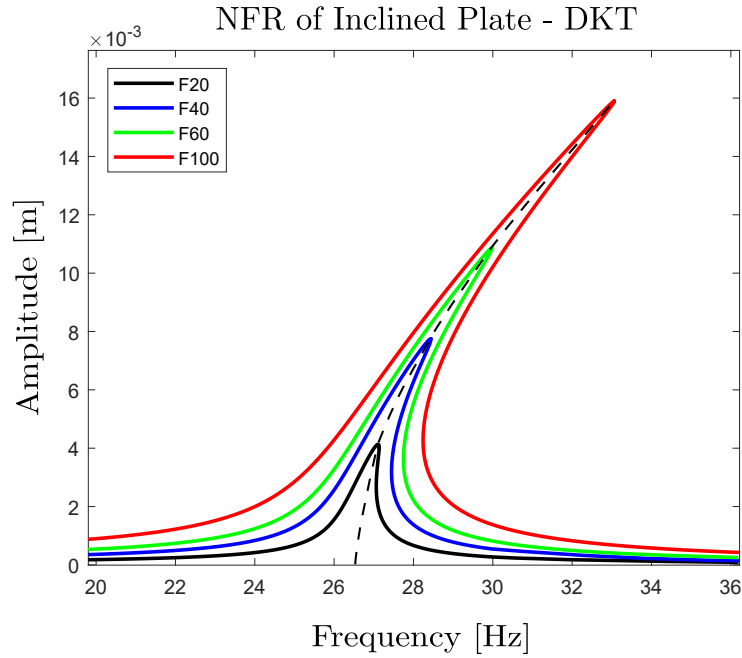
Figure 7.22: Nonlinear Forced Response of Tip Contact Node DKT Plate along y-axis increasing the forcing amplitude F_0 - s=15 mm, H=5.

Nevertheless, the natural frequencies of the linear system in case of DKT and HEXA20 are different, as reported in Tab.7.8; for this reason a further investigation is strictly needed. The idea is to reduce the thickness of the HEXA20 plate in order to have the same dynamics of the structure in terms of natural frequencies. In Fig.7.23 have been plotted the nonlinear forced response of DKT and HEXA20 plate with a thickness of 5 mm. It has been necessary to reduce the thickness of the plate because the strongest assumption of DKT element is that the cross section remains perpendicular to the neutral axis of the plate.
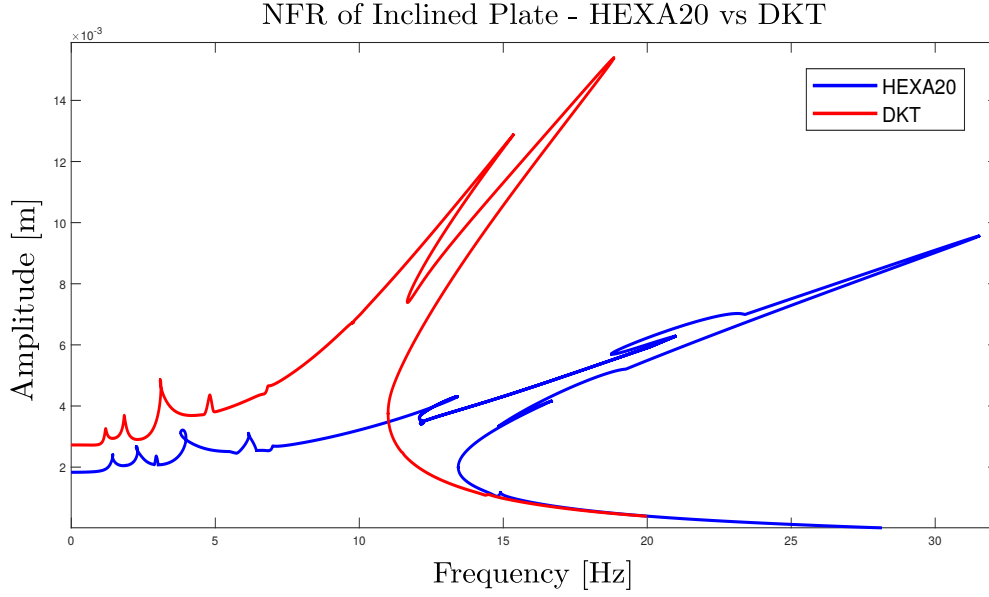
Figure 7.23: Nonlinear Forced Response of Tip Contact Node DKT Plate along y-axis - s=5 mm H=7, F_0=20 N.

Element	f_n (s=15 mm)	f_n (s=5 mm)
HEXA20	19.5 Hz	6.5 Hz
DKT	26.5 Hz	6.7 Hz

Table 7.8: 1st Natural Frequency of HEXA20 and DKT Inclined Plate

The HEXA20 plate shows a remarkable hardening behaviour with respect to the DKT plate. In both cases the internal resonances appear in NFR of the plate, anyway to better understand the nature of the internal resonances a deeper analysis of the nonlinear normal modes (NNMs) is needed, but it is not part of this project. The nonlinear forced response has been plotted considering 7 harmonics to capture the nonlinearities of the super-harmonic resonances. The super-harmonics have a non-negligible amplitude contribution in case of the contact dynamics.

As in case of 3D clamped-clamped beam, only two modes are not enough to properly describe the dynamics of the full structure. One of the possible reasons could be that there are non-negligible modal forces at high frequency in the spectrum, in such a way that the first bending mode couples with in-plane high frequency modes. Nevertheless, a further investigation has been done in Chapter 8, where it has been discovered that all the high frequency modes are the so called "thickness modes".

106

Chapter 8

NFR of 3D FE Reduced Order Model

In this chapter a further investigation on the coupled modes of 3D FE beam model has been done to find out why a ROM, using the linear modes as reduced basis, is not enough to capture the dynamics of the geometrically nonlinear structure. A comparison between different techniques, to proper select the reduced basis, has been done in order to build a ROM able to predict the nonlinear behaviour of the structure, including contact and geometric nonlinearities. The 3D model of a geometrically nonlinear beam has been used as test case.

8.1 Geometrically Nonlinear 3D Beam Model

A clamped-clamped 3D beam, with the same material properties and dimensions of the beam analysed in Section 6.1, has been used as test case to investigate on the high-frequency modes coupling. In this case the beam has been meshed using the isoparametric solid element HEXA20, dividing the domain of the structure in 15 elements along the length and $2{\times}2$ on the cross section. The clamped-clamped beam has 429 active nodes for a total of 1287 dofs. Adopting the same scheme used during the validation procedure in Chapter 6 and checking the nonlinear modal forces calculated during the STEP, seemed reasonable to consider only 2 modes (1B; 4A) as modal basis within the ROM. Nevertheless, the nonlinear forced response of the system shows a predominantly hardening behaviour with respect to the full model. The idea is to plot all the spectrum of the nonlinear modal forces $\tilde{\boldsymbol{F}}_{NL}$ to check if the first bending coupled with high-frequency mode-shapes.

Modal Forces – 3D Beam
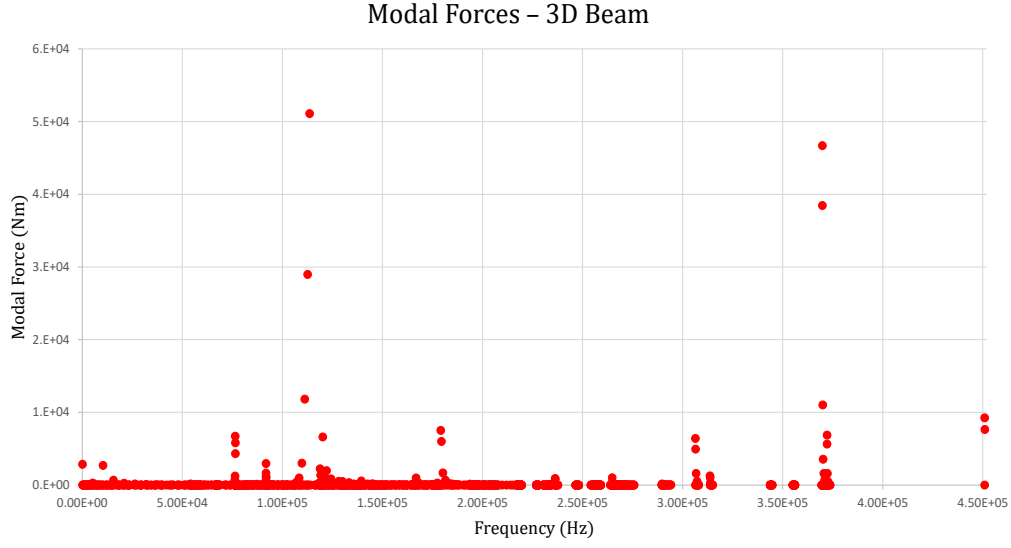
Figure 8.1: Nonlinear Modal Forces 3D FE Beam prescribing 1B

Modal Forces (displacement field 1B) - coupled modes

Figure 8.2: Nonlinear Modal Forces 3D FE Beam prescribing 1B - Coupled Modes

The Fig.8.1 and Fig.8.2 show that the first bending (1B) coupled with high-frequency modes in the spectrum, so that they can not be neglected during the computation of nonlinear stiffness. The 1st bending and the 4th axial modes are not enough to simulate the dynamics of full system due to a non-negligible modal-coupling at high frequencies.

The linear modes that should be considered within the reduction basis are listed in Tab.8.1.

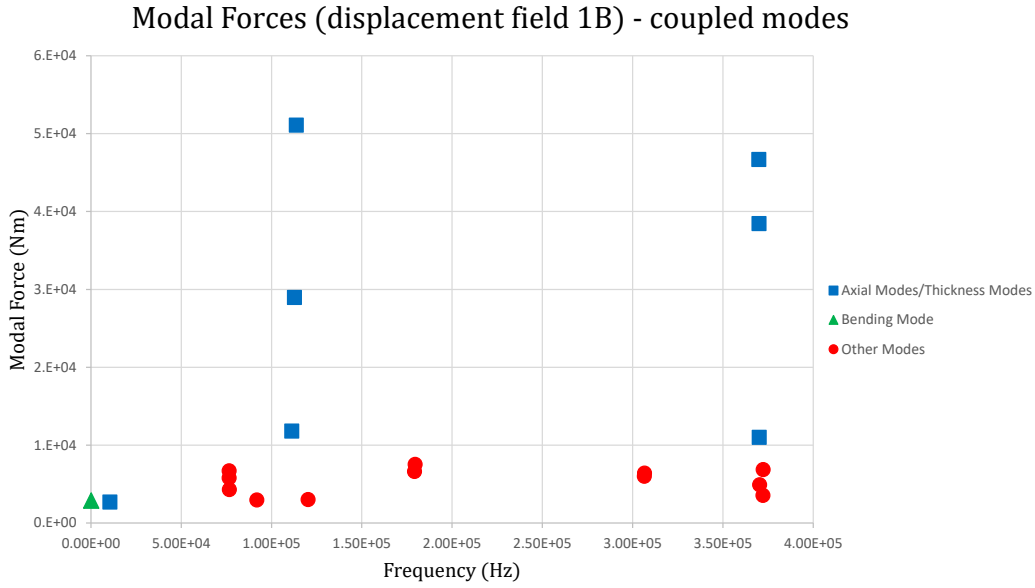| Mode	Frequency	Modal Force
1	1.61E+02	2.85E+03
34	1.04E+04	2.68E+03
167	7.64E+04	6.71E+03
170	7.65E+04	5.80E+03
172	7.65E+04	4.31E+03
252	9.19E+04	2.95E+03
320	1.10E+05	3.01E+03
324	1.11E+05	1.18E+04
328	1.13E+05	2.90E+04
330	1.14E+05	5.11E+04
370	1.20E+05	6.61E+03
629	1.79E+05	7.52E+03
633	1.80E+05	6.00E+03
1064	3.06E+05	6.41E+03
1066	3.07E+05	4.92E+03
1143	3.70E+05	4.67E+04
1147	3.70E+05	3.85E+04
1151	3.70E+05	1.10E+04
1157	3.70E+05	3.54E+03
1176	3.72E+05	6.86E+03
1178	3.72E+05	5.63E+03
1190	4.51E+05	9.23E+03
1192	4.51E+05	7.64E+03

Table 8.1: Selected Modes 3D FE Beam throughout the whole Spectrum

It is also interested to notice that all the modes included into the reduced basis, with high nonlinear modal force, are axial and thickness in-plane modes, as shown in Fig.8.3.

Mode 324

Mode 328

Mode 330

Mode 1143

Mode 1151

Mode 1192
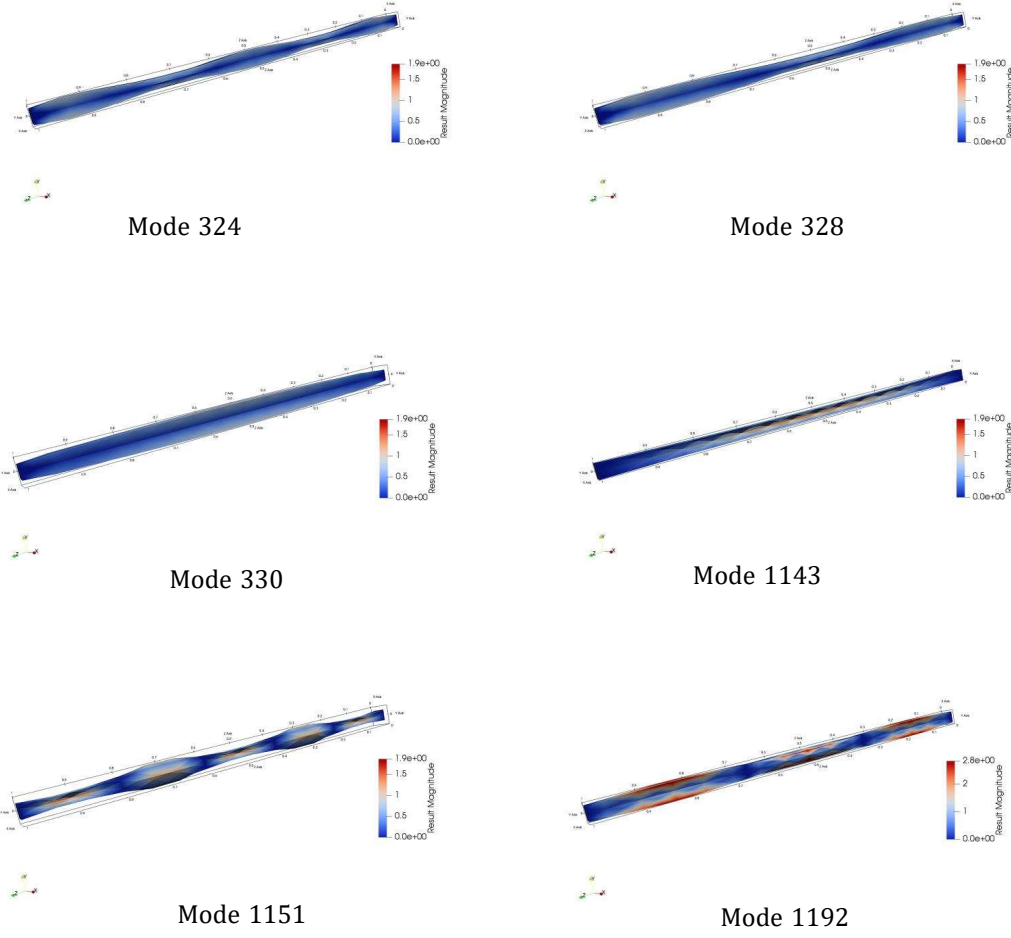
Figure 8.3: Mode-Shapes of Thickness Modes

A convergence study has been done considering the high-frequency modes with higher nonlinear modal force as reduction basis. In Fig.8.4 have been plotted the NFRs of 3D FE beam model. It has been possible to demonstrate that including the high-frequency in-plane modes the NFR of the reduced model tends to the full one. Three different bases have been used in the convergence study including the following linear modes:

$$
\begin{aligned}
\Phi_0 &= [1,34] \\
\Phi_1 &= [1,34,324,328,330] \\
\Phi_2 &= [1,34,324,328,330,1143,1147,1151,1190,1192]
\end{aligned}
\tag{8.1}
$$

NFR of 3D FE Beam

Figure 8.4: Convergence Study of Nonlinear Frequency Response of 3D FE Beam centre node along y-axis - H=3, F_0=200 N.

The idea is to check if the coupling between the first bending and the high-frequency modes is due to the Poisson's ratio or related to a locking in FEM. The loc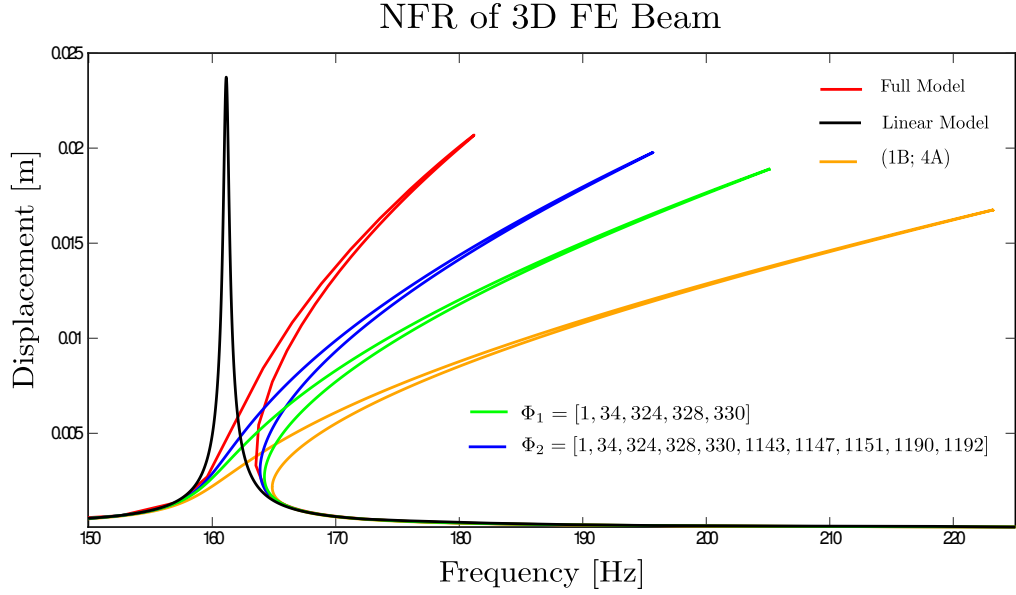king phenomenon may be caused, for instance, by a wrong interpolation of the nodal displacement values along the shape function used within the finite element method. To understand the connection between the Poisson's ratio and the thickness modes, the nonlinear modal forces have been calculated assuming the Poisson's ratio equal to zero. The linear modes with ν=0 are listed in Tab.8.2 while the whole spectrum has been plotted in Fig.8.5.

Mode	Frequency	Modal Force
1	1.60E+02	2.81E+03
32	1.04E+04	2.69E+03
211	8.67E+04	7.98E+03
216	8.68E+04	7.32E+03
219	8.68E+04	2.25E+04
1040	3.12E+05	2.11E+04
1048	3.13E+05	1.40E+04
1055	3.13E+05	5.46E+03

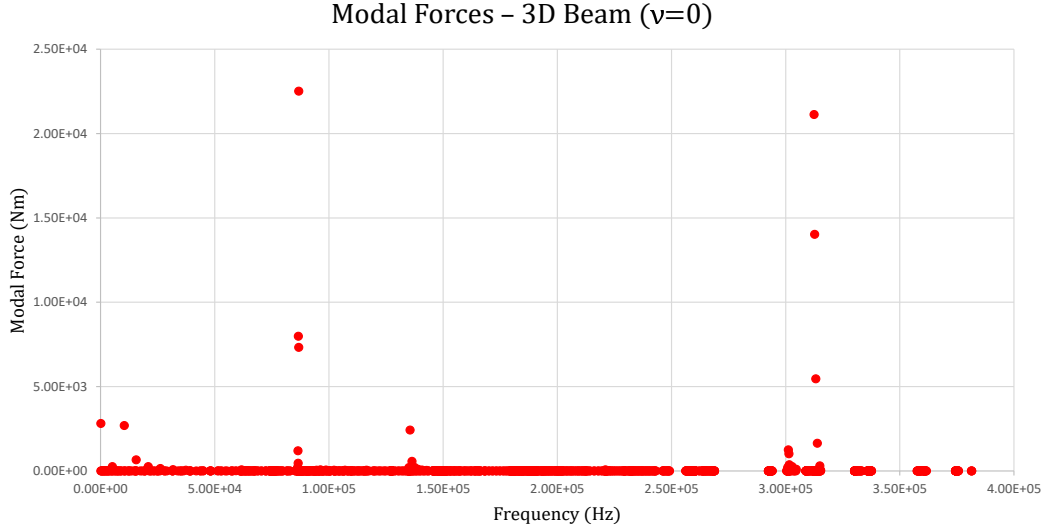Table 8.2: Coupled Modes 3D FE Beam with nil Poisson's ratio ($\nu = 0$)

Figure 8.5: Nonlinear Modal Forces 3D FE Beam with nil Poisson's ratio (ν=0) prescribing 1B

Even if the Poisson's ratio is equal to zero, the 1st bending couples with high frequency modes which can not be neglected within the computation of ROM due to the high amplitude of the nonlinear modal forces.

The main issue of the STEP method using the linear modes as reduction basis is that all the frequency spectrum must be computed to proper select the coupled modes. For large FE structures, even if the modes are linear, the calculation of the eigenvectors as well as the ANM continuation method within the MANLAB code may be very expensive in terms of computational time. The idea is to condensed all the coupled modes in one single factor that corrects the value of cubic nonlinear stiffness (β^1_{111}) associated to the excited mode (1B), so that only the first bending can be considered during the computation of nonlinear tensors. Overall, the issues to overcome are reported below:

1) Impossibility to run the STEP method to evaluate the nonlinear tensors for a large set of selected modes.

2) Avoid the computation of the whole spectrum to select the linear modes considered within the reduction basis.

8.1.1 Nonlinear Static Condensation

The nonlinear static condensation is the solution to the first issue, it allows to condensed all the coupled modes within a factor that corrects the overestimated value of β^1_{111}, responsible of the extremely large hardening behaviour of the NFR of the beam. Considering a nonlinear dynamical system governed by the Eq.8.2.

$$\boldsymbol{M}\ddot{\boldsymbol{X}} + \boldsymbol{C}\dot{\boldsymbol{X}} + \boldsymbol{K}\boldsymbol{X} + \boldsymbol{F}_{nl}(\boldsymbol{X}) = \boldsymbol{F}_{ext} \tag{8.2}$$

with $\boldsymbol{A}_2$ and $\boldsymbol{B}_3$ the quadratic and cubic tensors, respectively.

$$\boldsymbol{F}_{nl}(\boldsymbol{X}) = \boldsymbol{A}_2\boldsymbol{X}\boldsymbol{X} + \boldsymbol{B}_3\boldsymbol{X}\boldsymbol{X}\boldsymbol{X} \tag{8.3}$$

The response of the system may be written as [22]:

$$\boldsymbol{X} \approx \boldsymbol{\Gamma} = \boldsymbol{\Phi}\boldsymbol{q} + \boldsymbol{\Psi}\boldsymbol{p} + \boldsymbol{\Xi}\boldsymbol{h} \tag{8.4}$$

then:

$$\boldsymbol{X} = \sum_{r=1}^{N_B} \boldsymbol{\phi}_r q_r + \sum_{s=N_B+1}^{N_T} \boldsymbol{\psi}_s p_s \tag{8.5}$$

where $\boldsymbol{\Phi}$, $\boldsymbol{\Psi}$ are the excited and coupled modes, respectively; while $\boldsymbol{\Xi}$ represents all the other modes in the spectrum that give a negligible contribution into the NFR of the system. In this case the reduction basis is $\boldsymbol{P}=[\boldsymbol{\Phi} \quad \boldsymbol{\Psi}]$, and so the reduced system can be written as:

$$\boldsymbol{P}^T\boldsymbol{M}\ddot{\boldsymbol{\Gamma}} + \boldsymbol{P}^T\boldsymbol{C}\dot{\boldsymbol{\Gamma}} + \boldsymbol{P}^T\boldsymbol{K}\dot{\boldsymbol{\Gamma}} + \boldsymbol{P}^T\boldsymbol{F}_{nl}(\boldsymbol{\Gamma}) = \boldsymbol{P}^T\boldsymbol{M}\boldsymbol{\Phi}\boldsymbol{F}_{ext} \tag{8.6}$$

The Eq.8.6 may be developed by component, it yields:

$$
\ddot{q}_r + 2\zeta_r\omega_r\dot{q}_r + \omega_r^2 q_r + \sum_{i=1}^{N_B}\sum_{j=i}^{N_B}\alpha_{ij}^r q_i q_j + \sum_{i=1}^{N_B}\sum_{l=N_B+1}^{N_T}\alpha_{il}^r q_i p_l + \sum_{l=N_B+1}^{N_T}\sum_{m=l}^{N_T}\alpha_{lm}^r p_l p_m +
$$

$$
+ \sum_{i=1}^{N_B}\sum_{j=i}^{N_B}\sum_{k=j}^{N_B}\beta_{ijk}^r q_i q_j q_k + \sum_{i=1}^{N_B}\sum_{j=i}^{N_B}\sum_{l=N_B+1}^{N_T}\beta_{ijl}^r q_i q_j p_l + \sum_{i=1}^{N_B}\sum_{l=N_B+1}^{N_T}\sum_{m=l}^{N_T}\beta_{ilm}^r q_i p_l p_m +
$$

$$
+ \sum_{l=N_B+1}^{N_T}\sum_{m=l}^{N_T}\sum_{n=m}^{N_T}\beta_{lmn}^r p_l p_m p_n = f_{ext}^r
$$

$$(8.7)$$

$$
\ddot{p}_s + 2\zeta_s\omega_s\dot{p}_s + \omega_s^2 p_s + \sum_{i=1}^{N_B}\sum_{j=i}^{N_B}\alpha_{ij}^s q_i q_j + \sum_{i=1}^{N_B}\sum_{l=N_B+1}^{N_T}\alpha_{il}^s q_i p_l + \sum_{l=N_B+1}^{N_T}\sum_{m=l}^{N_T}\alpha_{lm}^s p_l p_m +
$$

$$
+ \sum_{i=1}^{N_B}\sum_{j=i}^{N_B}\sum_{k=j}^{N_B}\beta_{ijk}^s q_i q_j q_k + \sum_{i=1}^{N_B}\sum_{j=i}^{N_B}\sum_{l=N_B+1}^{N_T}\beta_{ijl}^s q_i q_j p_l + \sum_{i=1}^{N_B}\sum_{l=N_B+1}^{N_T}\sum_{m=l}^{N_T}\beta_{ilm}^s q_i p_l p_m +
$$

$$
+ \sum_{l=N_B+1}^{N_T}\sum_{m=l}^{N_T}\sum_{n=m}^{N_T}\beta_{lmn}^s p_l p_m p_n = 0
$$

$$(8.8)$$

In case of symmetric structures, the coupling between the out-of-plane and in-plane modes generates high value of alpha coefficients rather than beta. The quadratic terms will be generated, during the stiffness evaluation procedure, and the sign of nonlinear modal forces does not change when the nodal displacement field of the first mode-shape will be projected on the other modes. More precisely, changing the sign of the prescribed nodal displacement field the nonlinear modal forces do not change the sign; as it has been possible to notice from the 1st loop within the STEP method explained in Section 3.3.3.

Neglecting the terms that produce quasi-zero contribution in terms of nonlinearities, the Eq.8.7 and Eq.8.8 may be written as:

$$\ddot{q}_r + 2\zeta_r\omega_r\dot{q}_r + \omega_r^2 q_r + \sum_{i=1}^{N_B}\sum_{l=N_B+1}^{N_T}\alpha_{il}^r q_i p_l + \sum_{i=1}^{N_B}\sum_{j=i}^{N_B}\sum_{k=j}^{N_B}\beta_{ijk}^r q_i q_j q_k$$

$$+\sum_{i=1}^{N_B}\sum_{l=N_B+1}^{N_T}\sum_{m=l}^{N_T}\beta_{ilm}^r q_i p_l p_m = f_{ext}^r \tag{8.9}$$

$$\ddot{p}_s + 2\zeta_s\omega_s\dot{p}_s + \omega_s^2 p_s + \sum_{i=1}^{N_B}\sum_{j=i}^{N_B}\alpha_{ij}^s q_i q_j + \sum_{l=N_B+1}^{N_T}\sum_{m=l}^{N_T}\alpha_{lm}^s p_l p_m$$

$$+\sum_{i=1}^{N_B}\sum_{j=i}^{N_B}\sum_{l=N_B+1}^{N_T}\beta_{ijl}^s q_i q_j p_l + \sum_{l=N_B+1}^{N_T}\sum_{m=l}^{N_T}\sum_{n=m}^{N_T}\beta_{lmn}^s p_l p_m p_n = 0 \tag{8.10}$$

Assuming that the beta coefficients are negligible with respect the alpha ones, and considering only the alpha terms that couple with the excited modes, the Eq.8.10 may be rewritten as:

$$\ddot{p}_s + 2\zeta_s\omega_s\dot{p}_s + \omega_s^2 p_s + \sum_{i=1}^{N_B}\sum_{j=i}^{N_B}\alpha_{ij}^s q_i q_j = 0 \tag{8.11}$$

Since the coupled modes are all membrane modes, the in-plane inertia of these modes can be neglected. Moreover, the forcing frequency is in proximity of the low resonance frequencies, and so the dynamics of the coupled modes can be neglected as well.

$$p_s = -\sum_{i=1}^{N_B}\sum_{j=i}^{N_B}\frac{\alpha_{ij}^s}{\omega_s^2}q_i q_j, \quad p_l = -\sum_{j=i}^{N_B}\sum_{j=k}^{N_B}\frac{\alpha_{jk}^l}{\omega_l^2}q_j q_k, \quad p_m = -\sum_{y=k}^{N_B}\sum_{y=z}^{N_B}\frac{\alpha_{yz}^m}{\omega_m^2}q_y q_z \quad (8.12)$$

substituting in Eq.8.9, it yields:

$$\ddot{q}_r + 2\zeta_r\omega_r\dot{q}_r + \omega_r^2 q_r - \sum_{i=1}^{N_B}\sum_{j=i}^{N_B}\sum_{k=j}^{N_B}\sum_{l=N_B+1}^{N_T}\frac{\alpha_{il}^r\alpha_{jk}^l}{\omega_l^2}q_iq_jq_k + \sum_{i=1}^{N_B}\sum_{j=i}^{N_B}\sum_{k=j}^{N_B}\beta_{ijk}^r q_iq_jq_k +$$

$$+ \sum_{i=1}^{N_B}\sum_{j=i}^{N_B}\sum_{k=j}^{N_B}\sum_{y=k}^{N_B}\sum_{z=y}^{N_B}\beta_{ilm}^r\frac{\alpha_{jk}^l\alpha_{yz}^m}{\omega_l^2\omega_m^2}q_iq_jq_kq_yq_z = f_{ext}^r \tag{8.13}$$

Neglecting the terms that generate the nonlinearities of the fifth order, the Eq.8.13 may be written as:

$$\ddot{q}_r + 2\zeta_r\omega_r\dot{q}_r + \omega_r^2 q_r + \sum_{i=1}^{N_B}\sum_{j=i}^{N_B}\sum_{k=j}^{N_B}\left(\beta_{ijk}^r - \sum_{l=N_B+1}^{N_T}\frac{\alpha_{il}^r\alpha_{jk}^l}{\omega_l^2}\right)q_iq_jq_k + \mathcal{O}(q_i^5) = f_{ext}^r \tag{8.14}$$

where N_B and N_T are the number of the excited and total modes, respectively; while $N_M = N_T - N_B$ is the number of the coupled modes. Applying the static condensation, the size of the obtained system has been drastically reduced including only cubic nonlinearities. The symmetry of the quadratic tensor $\boldsymbol{A_2}$ allows to avoid the computation of the whole tensor, computing only the combination of q_i and q_j during the STEP method, so that:

$$\alpha_{il}^r = 2\boldsymbol{\phi}_r^T\mathbf{A_2}\boldsymbol{\phi}_i\boldsymbol{\psi}_l = 2\boldsymbol{\psi}_l^T\mathbf{A_2}\boldsymbol{\phi}_r\boldsymbol{\phi}_i = \begin{cases} \alpha_{ir}^l, & \text{if } r > i \\ 2\alpha_{ii}^l, & \text{if } r = i \\ \alpha_{ri}^l, & \text{if } r < i \end{cases} \tag{8.15}$$

From the Eq.8.14 it has been possible to identify the factor $C_{ijk}^r{}^{(l)}$ as:

$$C_{ijk}^r{}^{(l)} = \begin{cases} \dfrac{\alpha_{ir}^l\alpha_{jk}^l}{\omega_l^2}, & \text{if } r > i \\[2ex] 2\cdot\dfrac{\alpha_{ii}^l\alpha_{jk}^l}{\omega_l^2}, & \text{if } r = i \\[2ex] \dfrac{\alpha_{ri}^l\alpha_{jk}^l}{\omega_l^2} & \text{if } r < i \end{cases} \tag{8.16}$$

116

The correction factor ${C_{ijk}^r}^{(l)}$ is a parameter to measure the contribution of the coupled modes on the excited ones, so that the value of the beta coefficients will be corrected by the quantities expressed by the Eq.8.16. The idea is to weight the contribution of the correction factor of all the modes of 3D FE beam model described in Section 8.1. Since only the first bending mode has been considered as excited mode, the normalised modal correction factor $\frac{2(\alpha_{11}^n/\omega_n^2)}{\beta_{111}^1}$ has been reported in Fig.8.6.
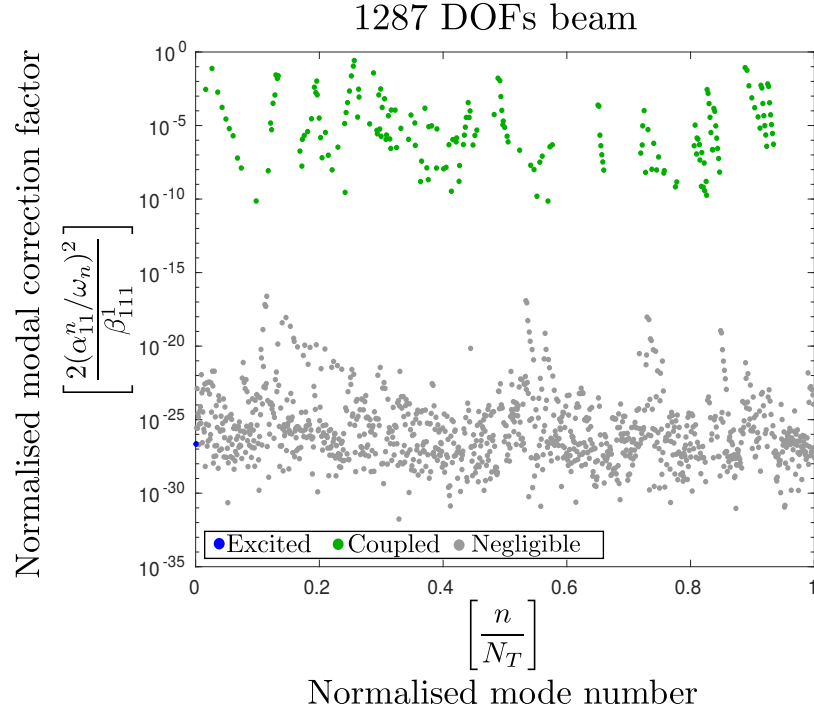

Figure 8.6: Normalised Modal Correction Factor on the 1B excited mode.

In Fig.8.8 the modes sorted by normalised modal correction factor have been reported to demonstrate that only a small percentage ($\approx 20\%$) of the total number of modes participates in the nonlinear forced response of the structure. The coupled modes are spread throughout the whole frequency domain and they show an absolutely independence from the mesh refinement, as reported in Fig.8.7 and Fig.8.8. Moreover, it has been possible to identify a threshold for a significant contribution of the normalised modal correction factor around 10^{-15}.

Considering all the coupled modes above the threshold ($\approx 10^{-15}$), the reduced order model of 3D beam converges to the full one thanks to the contribution of the coupled modes within the correction factor. The overestimate hardening effect was caused by not having included enough coupled modes in the reduction basis.
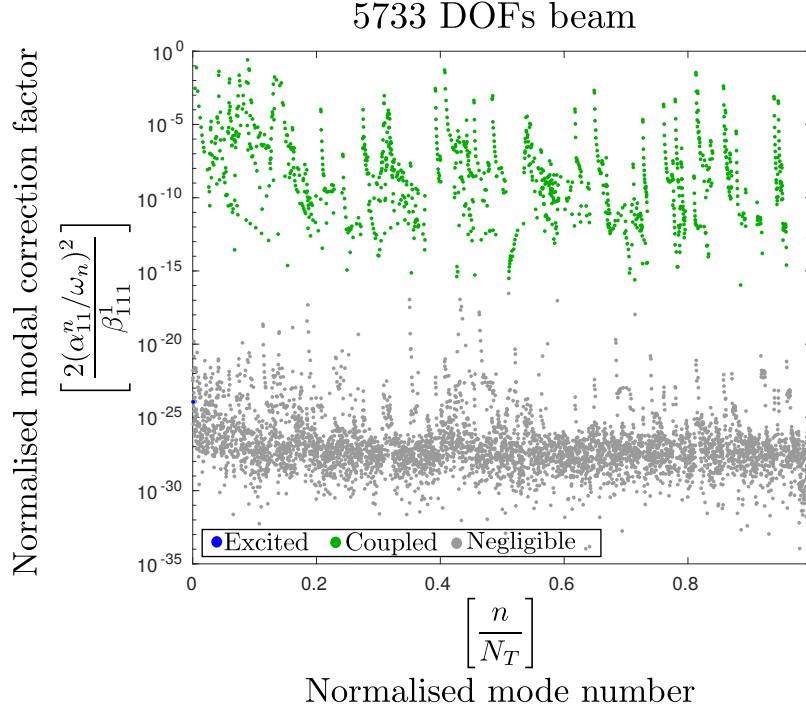

Figure 8.7: Normalised Modal Correction Factor on the 1B excited mode - Mesh Refinement: 20 HEXA20 elements along the length and 3×3 elements on the cross section.

Therefore, the static condensation allows to consider only the first bending and all the coupled modes condensed within the correction factor $C_{ijk}^{r}{}^{(l)}$, so that it has been possible to run only the first loop of the STEP method and to have only the excited modes, plus the correction factor, within the reduction basis. This approach drastically reduced the size of the nonlinear system making the stiffness evaluation procedure and the ANM continuation method faster in terms of computational time.

118
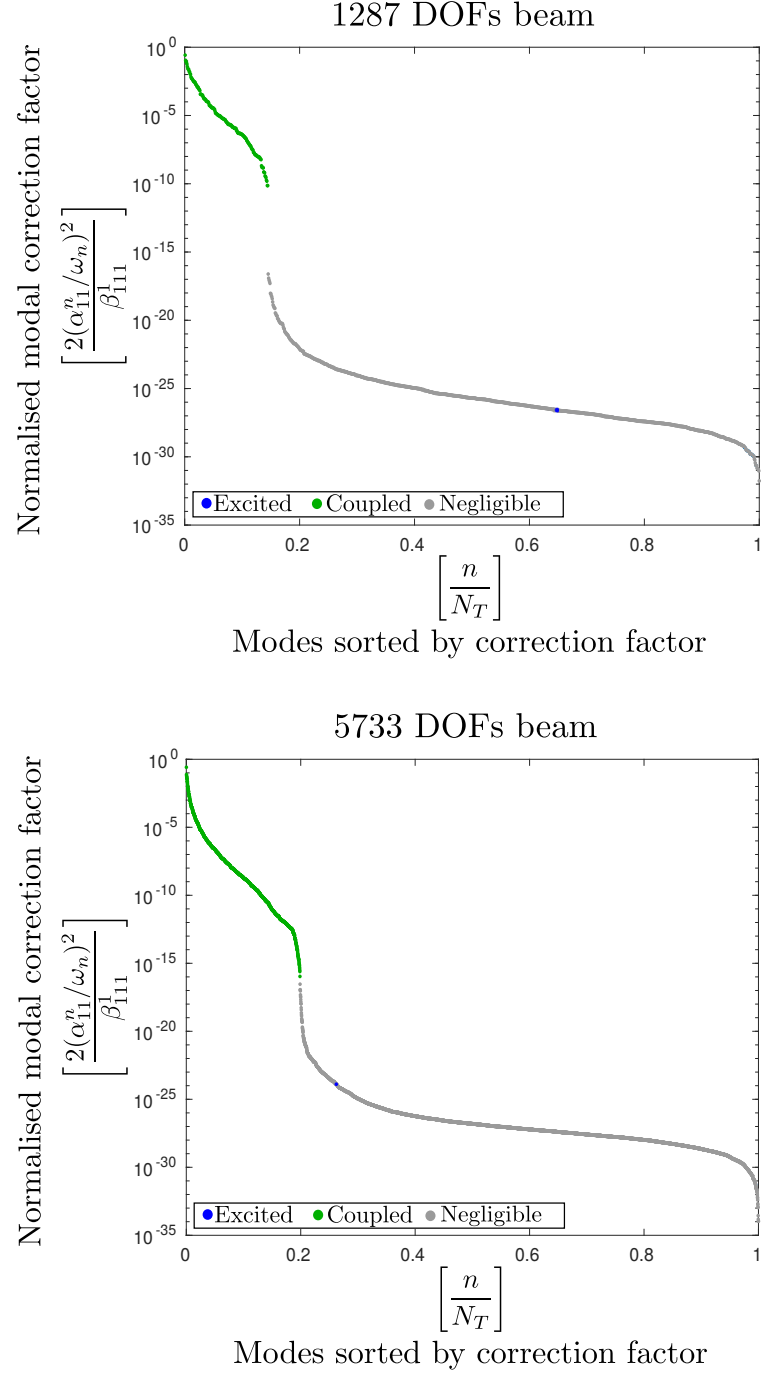
Figure 8.8: Modes Sorted by Normalised Modal Correction Factor on the 1B excited mode.
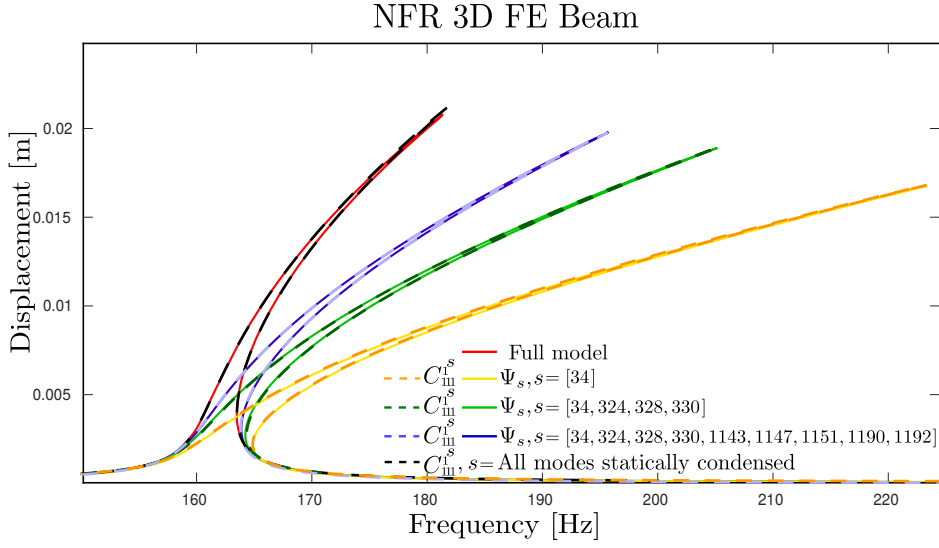
NFR 3D FE Beam

Figure 8.9: NFR of 3D FE beam (center node along y-axis) with 1287 dofs - comparison between the ROM using the nonlinear static condensation and the full beam model - H=3, F_0=200 N.

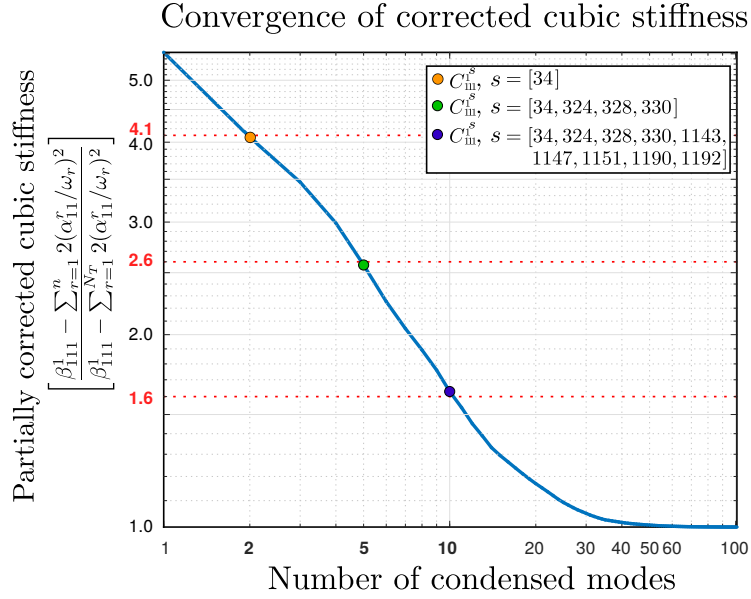Convergence of corrected cubic stiffness

Figure 8.10: Convergence Study of corrected cubic stiffness increasing the number of the modes statically condensed.

The nonlinear forced response in frequency domain has been plotted in Fig.8.9 to show the convergence of the ROM to the full one, where all the modes with a correction factor above 10^{-15} has been statically condensed (black dashed-line). It is also possible to notice a perfect overlapping between the generic set of coupled modes statically condensed and the same modes included within the reduction basis as internal modes, as explained in Section 8.1. It has been calculated that 68 out of 1287 modes must be statically condensed to have a relative error of 0.1% with respect to the full model.

8.1.2   Static Modal Derivative

The static modal derivatives follow the same logic of the static condensation because they are both based on the non-intrusive method to evaluate the nonlinear stiffness tensors. The modal derivatives allow to accurately approximate the dynamics of the structure considering the linear modeshapes and their modal derivatives as basis of reduction. The definition of static modal derivative has been formulated as [24]:

$$\boldsymbol{\theta}_{ij} = \frac{\partial \boldsymbol{\phi}_i}{\partial q_j} = -\mathbf{K}^{-1} \frac{\partial}{\partial q_j} \left(\nabla \mathbf{F}(\boldsymbol{\phi}_j q_j) \right) \bigg|_{q_j=0} \cdot \boldsymbol{\phi}_i \tag{8.17}$$

where the nonlinear stiffness matrix $\nabla \mathbf{F}$ may be defined starting from the restoring force vector $\mathbf{F}(\mathbf{X})$ as function of the quadratic and cubic nonlinear tensors; while $\nabla \mathbf{F}(\boldsymbol{\phi}_j q_j)$ represents the nonlinear stiffness matrix projected along the mode ϕ_j.

$$\mathbf{F}(\mathbf{X}) = \mathbf{K}\mathbf{X} + \mathbf{A_2}\mathbf{X}\mathbf{X} + \mathbf{B_3}\mathbf{X}\mathbf{X}\mathbf{X} \tag{8.18}$$

$$\nabla \mathbf{F}(\mathbf{X}) = \mathbf{K} + 2\mathbf{A_2}\mathbf{X} + 3\mathbf{B_3}\mathbf{X}\mathbf{X} \tag{8.19}$$

$$\nabla \mathbf{F}(\boldsymbol{\phi}_j q_j) = \mathbf{K} + 2\mathbf{A_2}\boldsymbol{\phi}_j q_j + 3\mathbf{B_3}\boldsymbol{\phi}_j \boldsymbol{\phi}_j q_j^2 \tag{8.20}$$

Thus the static modal derivative $\boldsymbol{\theta}_{ij}$ can be written as:

$$\boldsymbol{\theta}_{ij} = -\mathbf{K}^{-1}\left(2\mathbf{A_2}\boldsymbol{\phi}_j\right) \cdot \boldsymbol{\phi}_i = \boldsymbol{\theta}_{ji} \tag{8.21}$$

The modal derivative is defined as combination of two excited modes ϕ_i and ϕ_j, whereas the symmetry of the modal derivatives arises from the symmetry of the quadratic tensor. Therefore, for N_{B} excited modes, the number of linearly independent static modal derivatives is equal to $N_{\mathrm{SMD}} = N_{\mathrm{B}}(N_{\mathrm{B}} + 1)/2$. The idea is to build the reduced order basis (ROB) comprising N_B excited modes and N_{SMD} static modal derivatives that subsequently can be used within the STEP method. The reduction basis of any finite element structure may be wrtitten as $\mathbf{P} = [\boldsymbol{\Phi}\ \ \boldsymbol{\Theta}]$, where the equation of motion and the reduced system have the same shape of the Eq.8.2 and Eq.8.6. In this case the response of the system has been represented by a reduction on a linear manifold:

$$\mathbf{X} \approx \boldsymbol{\Gamma} = \boldsymbol{\Phi}\mathbf{q} + \boldsymbol{\Theta}\mathbf{z} \tag{8.22}$$

The equation of motion can be expanded as follows:

$$\begin{aligned}
\ddot{\mathbf{q}} + \boldsymbol{\zeta}_{\Phi}\dot{\mathbf{q}} &+ \boldsymbol{\Omega}_{\Phi}^2\mathbf{q} + \boldsymbol{\Phi}^T\mathbf{M}\boldsymbol{\Theta}\ddot{\mathbf{z}} + \boldsymbol{\Phi}^T\mathbf{C}\boldsymbol{\Theta}\dot{\mathbf{z}} + \boldsymbol{\Phi}^T\mathbf{K}\boldsymbol{\Theta}\mathbf{z} + \\
&+ \boldsymbol{\Phi}^T\mathbf{A_2}\boldsymbol{\Phi}\mathbf{q}\boldsymbol{\Phi}\mathbf{q} + 2\boldsymbol{\Phi}^T\mathbf{A_2}\boldsymbol{\Phi}\mathbf{q}\boldsymbol{\Theta}\mathbf{z} + \boldsymbol{\Phi}^T\mathbf{A_2}\boldsymbol{\Theta}\mathbf{z}\boldsymbol{\Theta}\mathbf{z} + \\
&+ \boldsymbol{\Phi}^T\mathbf{B_3}\boldsymbol{\Phi}\mathbf{q}\boldsymbol{\Phi}\mathbf{q}\boldsymbol{\Phi}\mathbf{q} + 3\boldsymbol{\Phi}^T\mathbf{B_3}\boldsymbol{\Phi}\mathbf{q}\boldsymbol{\Phi}\mathbf{q}\boldsymbol{\Theta}\mathbf{z} + 3\boldsymbol{\Phi}^T\mathbf{B_3}\boldsymbol{\Phi}\mathbf{q}\boldsymbol{\Theta}\mathbf{z}\boldsymbol{\Theta}\mathbf{z} + \\
&+ \boldsymbol{\Phi}^T\mathbf{B_3}\boldsymbol{\Theta}\mathbf{z}\boldsymbol{\Theta}\mathbf{z}\boldsymbol{\Theta}\mathbf{z} = \mathbf{f_{ext}}
\end{aligned} \tag{8.23}$$

$$\begin{aligned}
\mathbf{I}_{\Theta}\ddot{\mathbf{z}} + \boldsymbol{\zeta}_{\Theta}\dot{\mathbf{z}} &+ \boldsymbol{\Omega}_{\Theta}^2\mathbf{z} + \boldsymbol{\Theta}^T\mathbf{M}\boldsymbol{\Phi}\ddot{\mathbf{q}} + \boldsymbol{\Theta}^T\mathbf{C}\boldsymbol{\Phi}\dot{\mathbf{q}} + \boldsymbol{\Theta}^T\mathbf{K}\boldsymbol{\Phi}\mathbf{q} + \\
&+ \boldsymbol{\Theta}^T\mathbf{A_2}\boldsymbol{\Phi}\mathbf{q}\boldsymbol{\Phi}\mathbf{q} + 2\boldsymbol{\Theta}^T\mathbf{A_2}\boldsymbol{\Phi}\mathbf{q}\boldsymbol{\Theta}\mathbf{z} + \boldsymbol{\Theta}^T\mathbf{A_2}\boldsymbol{\Theta}\mathbf{z}\boldsymbol{\Theta}\mathbf{z} + \\
&+ \boldsymbol{\Theta}^T\mathbf{B_3}\boldsymbol{\Phi}\mathbf{q}\boldsymbol{\Phi}\mathbf{q}\boldsymbol{\Phi}\mathbf{q} + 3\boldsymbol{\Theta}^T\mathbf{B_3}\boldsymbol{\Phi}\mathbf{q}\boldsymbol{\Phi}\mathbf{q}\boldsymbol{\Theta}\mathbf{z} + 3\boldsymbol{\Theta}^T\mathbf{B_3}\boldsymbol{\Phi}\mathbf{q}\boldsymbol{\Theta}\mathbf{z}\boldsymbol{\Theta}\mathbf{z} + \\
&+ \boldsymbol{\Theta}^T\mathbf{B_3}\boldsymbol{\Theta}\mathbf{z}\boldsymbol{\Theta}\mathbf{z}\boldsymbol{\Theta}\mathbf{z} = \boldsymbol{\Theta}^T\mathbf{M}\boldsymbol{\Phi}\mathbf{f_{ext}}
\end{aligned} \tag{8.24}$$

where:

$$\mathbf{I}_{\Theta} \doteq \boldsymbol{\Theta}^T\mathbf{M}\boldsymbol{\Theta}, \qquad \boldsymbol{\zeta}_{\Theta} \doteq \boldsymbol{\Theta}^T\mathbf{C}\boldsymbol{\Theta}, \qquad \boldsymbol{\Omega}_{\Theta}^2 \doteq \boldsymbol{\Theta}^T\mathbf{K}\boldsymbol{\Theta}$$

The reduced system formulated including the static modal derivatives within the reduced basis will be much smaller compared to the non-intrusive method (displacement based) and faster to solve with respect to the static condensation, because it is not necessary to compute the eigenproblem of the full system.

The modal derivatives can be thought as a substitute of the coupled modes within the reduction basis. Under the same assumptions used to formulate the nonlinear static condensation in Section 8.1.1, it has been possible to evaluate the modal amplitude of the static modal derivatives:

$$p_s = -\sum_{i=1}^{N_B} 2\frac{\alpha_{ii}^s}{\omega_s^2} z_{ii} - \sum_{i=1}^{N_B}\sum_{j=i+1}^{N_B} \frac{\alpha_{ij}^s}{\omega_s^2} z_{ij} \tag{8.25}$$

Recalling the Eq. 8.12 the modal amplitude of the coupled modes that has been used to condensed all the coupled modes in a single factor, it has been shown that the amplitude of the coupled modes is a function of the excited modes [23].

$$p_s = -\sum_{i=1}^{N_B}\sum_{j=i}^{N_B} \frac{\alpha_{ij}^s}{\omega_s^2} q_i q_j \tag{8.26}$$

Comparing the Eq.s 8.25 and 8.26 the relation between the amplitude of the modal derivatives and the modal amplitude of the excited modes can be found [25]:

$$z_{ii} = \frac{1}{2}q_i^2, \qquad z_{ij} = q_i q_j \tag{8.27}$$

In this way the quadratic manifold relation may be found [24]:

$$\mathbf{\Gamma}(\mathbf{q}) = \mathbf{\Phi}\mathbf{q} + \frac{1}{2}\mathbf{\Theta}\mathbf{q}\mathbf{q} \tag{8.28}$$

The quadratic manifold is the logic evolution of the linear manifold, where the reduced system is built projecting the excited modes and the equation of motion onto the quadratic subspace $\mathbf{\Gamma}(\mathbf{q})$.

The strength of using the modal derivatives is to avoid the computation of the full eigenproblem to find the coupled modes. The modal derivatives are directly related to the excited modes ϕ_i; therefore, only the computation of the excited modes is needed to build the reduced order model of the structure. The idea is to isolate the quadratic terms and to impose the nodal displacement following the non-intrusive method.

$$2\mathbf{A_2}\phi_i\phi_i = \mathbf{F}(\phi_i) + \mathbf{F}(-\phi_i) \tag{8.29}$$

Pre-multiplying the nodal forces evaluated within the finite element software by the inverse of the stiffness matrix $\mathbf{K}$, the modal derivatives can be found. The SMDs with different indices have been calculated following the same procedure.

$$\boldsymbol{\theta}_{ii} = -\mathbf{K}^{-1}2\mathbf{A_2}\phi_i\phi_i \tag{8.30}$$

Since the static modal derivatives has the dimension of a displacement, it has been interesting to plot (Fig.8.11) the shape of the SMD associated to the first excited bending mode of the 3D clamped-clamped beam.

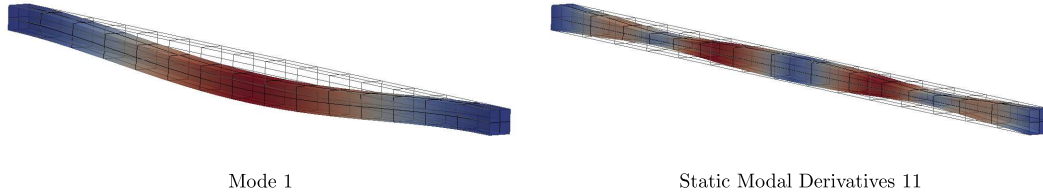Mode 1   Static Modal Derivatives 11

Figure 8.11: First Bending Mode of 3D Clamped-Clamped Beam and its Static Modal Derivative

It is possible to notice that the static modal derivative has the same shape of an in-plane mode, this means that within the SMDs there are all coupled modes that could not be neglected in the STEP method to build the reduced model of the structure. The stiffness evaluation procedure remains always the same, as described in Section 3.3.3, what has been changed are the sets of the imposed nodal displacements that in case of linear and quadratic manifold comprising the excited modes $\boldsymbol{\Phi}$ and their modal derivatives $\boldsymbol{\Theta} = [\theta_{11}\ \theta_{22}\ldots\theta_{12}\ \theta_{13}\ldots\theta_{23}]$.

Overall, the equivalent nonlinear tensors can be always evaluated with the STEP method applied to the reduction basis including the excited modes and the SMDs.

The reduced system may be formulated making the same assumptions done in case of static condensation, neglecting the terms which generate the nonlinearities of the fifth order:

$$
\ddot{q}_r + \zeta_r \dot{q}_r + \omega_r^2 q_r + \sum_{i=1}^{N_B} \sum_{l=N_B+1}^{N_T} a_{il}^r q_i z_l + \sum_{i=1}^{N_B} \sum_{j=i}^{N_B} \sum_{k=j}^{N_B} b_{ijk}^r q_i q_j q_k +
$$
$$
+ \sum_{i=1}^{N_B} \sum_{l=N_B+1}^{N_T} \sum_{m=l}^{N_T} b_{ilm}^r q_i z_l z_m = f_{ext}^r \tag{8.31}
$$

$$
\sum_{l=N_B+1}^{N_T} \mathrm{I}_{ls} \ddot{z}_s + \sum_{l=N_B+1}^{N_T} \zeta_{ls} \dot{z}_s + \sum_{l=N_B+1}^{N_T} \Omega_{ls}^2 z_s + \sum_{i=1}^{N_B} \sum_{j=i}^{N_B} a_{ij}^s q_i q_j + \sum_{l=N_B+1}^{N_T} \sum_{m=l}^{N_T} a_{lm}^s z_l z_m +
$$
$$
+ \sum_{i=1}^{N_B} \sum_{j=i}^{N_B} \sum_{l=N_B+1}^{N_T} b_{ijl}^s q_i q_j z_l + \sum_{l=N_B+1}^{N_T} \sum_{m=l}^{N_T} \sum_{n=m}^{N_T} b_{lmn}^s z_l z_m z_n = 0 \tag{8.32}
$$

Unfortunately, the terms I_{ls}, ζ_{ls}, and Ω_{ls}^2 are not diagonal because the static modal derivatives do not respect the orthogonality conditions (i.e. the SMDs are not **M**-orthogonal and **K**-orthogonal). Finally, the nonlinear forced response of the 3D clamped-clamped beam has been plotted in Fig. 8.12. The nonlinear response has been obtained by considering the first bending mode and its static modal derivatives within the reduced basis. Moreover, the response perfectly overlaps the solution got using the static condensation approach in perfect agreement with the response of the full model.
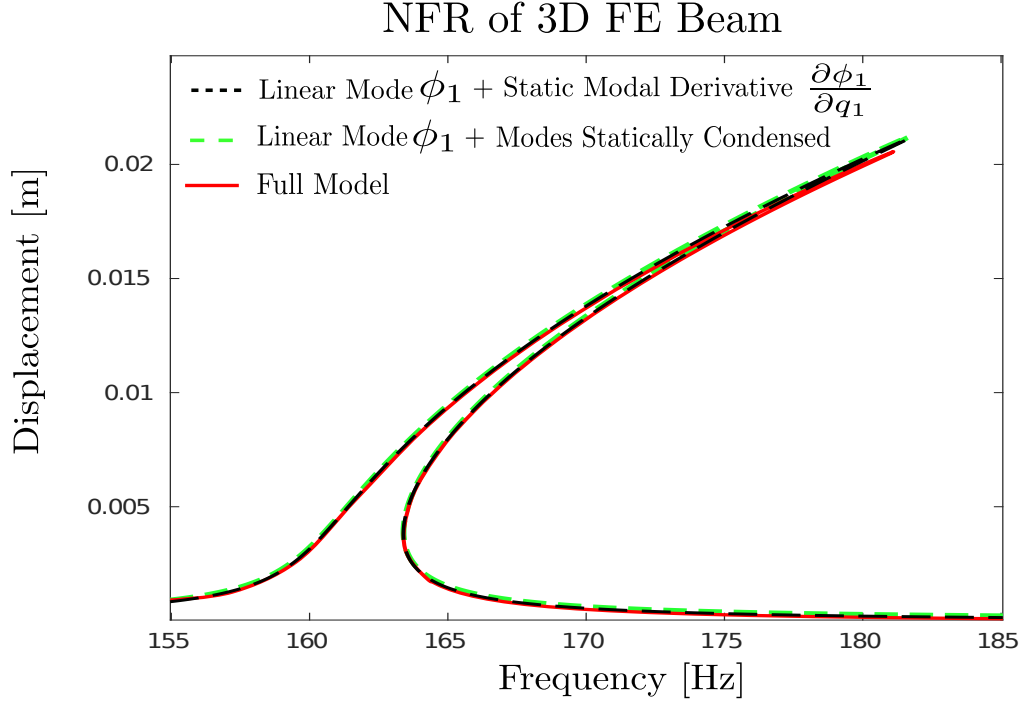
NFR of 3D FE Beam

Figure 8.12: Nonlinear Forced Response of 3D clamped-clamped beam; comparison between the ROMs using the static modal derivatives, the nonlinear static condensation and the full beam model.

Chapter 9

Conclusions

The linear reduction methods presented in Section 3.2 cannot be applied to a nonlinear system. Therefore, the computation of a reduced basis must be formulated using proper methods able to capture the geometric nonlinearities of the structure. The non-intrusive displacement based method has been applied to evaluate the nonlinear stiffness quadratic and cubic coefficients, so that the coupling between the out-of-plane (bending) and in-plane (membrane) modeshapes has been properly caught, as widely explained in Chapter 8. The stiffness evaluation procedure has been validated against the simply supported plate [1] and the 3D clamped-clamped beam [2] with a relative error less that 3 percent comparing the quadratic and cubic tensors' coefficients. Nevertheless, the nonlinear forced response of the geometrically nonlinear structure appeared very sensitive to the inclusion of the high modes (i.e. membrane and thickness modeshapes) in the reduced order basis. For this reason, the low frequency modes have not been enough to simulate the dynamics of the full nonlinear system, due to a non-negligible coupling at high frequencies. The nonlinear forced response of the 3D clamped-clamped beam showed a convergence to the full model when more coupled modes have been included within the reduced basis. The coupled modes are widespread throughout the whole spectrum of the linear model. Moreover, it has been demonstrated that the existence of the thickness modes is independent of the mesh refinement.

The main issue is that the computation of the nonlinear response becomes extremely slow increasing the number of coupled modes within the reduction basis. This procedure is computationally expensive due to the high number of nonlinear static displacements that must be performed to calculate the nonlinear stiffness tensors. Two approaches have been presented to overcome this problem reducing the size of the system and speeding up the entire procedure to build a reduced order model.

The first method is the so called "nonlinear static condensation" that allowed to drastically reduce the full model condensing all the coupled modes in one single correction factor that measures the contribution of the coupled modes on the excited ones. In this way, the computation of the nonlinear response is extremely fast, because within the reduced basis have been considered only the first bending (excited mode) and the correction factor comprising all the coupled modes. However, the pre-processing to select the coupled modes is still time consuming, because the full eigenproblem of the structure must be computed.

The second approach is based on the "static modal derivatives" that can be thought as the logical evolution of the static condensation. Under the hypothesis of the negligible inertia of the coupled modes, the solution of the eigenproblem is not needed anymore. The modal derivatives allow to accurately approximate the dynamics of the structure considering the linear modeshape and its modal derivatives as basis of reduction.

The stiffness evaluation procedure remains always the same, as described in Section 3.3.3, what has been changed are the fields of the imposed nodal displacements that in case of linear manifold comprising the excited modes $\mathbf{\Phi}$ and their modal derivatives $\mathbf{\Theta}$. Overall, the equivalent nonlinear tensors can be always evaluated with the non-intrusive method applied to the reduction basis including the excited modes and the static modal derivatives.

Finally, the Asymptotic Numerical Method (ANM) continuation algorithm based on the Taylor expansion, has been adapted to solve regularized non-smooth dynamics problems like vibrating systems with contact conditions and friction laws. The ANM continuation algorithm has been used to trace the nonlinear forced response of the system including the contact and the geometric nonlinearities. An inclined straight cantilever plate has been used as test case where the contact has been modelled as smooth function to simulate the tip-rubbing phenomenon. Once again, the basis of internal modes is not suitable to capture the geometric nonlinearities at the boundary node, therefore the Ritz basis must be adopted in case of a dynamics problem including the tip-rubbing and large deformation. In this way, it has been possible to study how the geometric nonlinearities have been activated in case of tip-rubbing phenomenon. The geometric nonlinearities have a stiffening effect on the structure due to the bending-membrane interaction; while the tip-rubbing is the responsible of the curvature change of the nonlinear forced response when the tip touches the casing.

Bibliography

[1] Muravyov A.A., Rizzi S.A. *Determination of nonlinear stiffness with application to random vibration of geometrically nonlinear structures*, Computers and Structures, 81(15), 1513–1523, 2003.

[2] Grolet A. *Dynamique non-linéaire des structures mécaniques : application aux systémes à symétrie cyclique*, PhD Thesis, 155-159, 2013.

[3] Hughes T. *The finite element method*, Prentice Hall, 1987.

[4] Batoz, J.L., Dhatt G. *Modeling of the structures by finite elements: beams and plates*, Hermes, 1992.

[5] Genta G. *Vibration Dynamics and Control: The finite element method*, Springer, 363-396, 2009.

[6] Genta G. *Vibration Dynamics and Control: Reduction of the Number of Degrees of Freedom*, Springer, 213-220, 2009.

[7] Grolet A. *Model Order Reduction for Nonlinear Structural Dynamics*, PhD Thesis, 21-38, 2017.

[8] Young J.T. *Primer on the Craig-Bampton Method*, 2000.

[9] Rutzmoser J.B. *Model Order Reduction for Nonlinear Structural Dynamics*, PhD Thesis, 118-121, 2017.

[10] Mignolet M.P., Przekop A., Rizzi S.A., Spottswood S.M. *A review of indirect/non-intrusive reduced order modeling of nonlinear geometric structures*,J Sound Vib, 332(10), 2437-2460, 2013.

[11] Genta G. *Vibration Dynamics and Control: Forced Response of Damped Nonlinear Systems*, Springer, 519-550, 2009.

[12] Krack M., Gross J. *The Harmonic Balance Method and its application to nonlinear vibrations: Introduction and current state of the art*, Istitute of Aircraft and Propulsion Systems, University of Stuttgart, Germany, 2018.

[13] Cochelin B., Damil N., Potier-Ferry M. *Asymptotic-Numerical Method and Pade Approximants for Non-Linear Elastic Structures*, John Wiley & Sons, 1994.

[14] Ajjarapu V. *Computational Techniques for Voltage Stability Assessment and Control*, Springer, 19-44, 2007.

[15] Seydel R. *Practical Bifurcation and Stability Analysis*, Springer, 2010.

[16] Lazarus A., Thomas O. *A harmonic-based method for computing the stability of periodic solutions of dynamical systems*, Comptes Rendus Mecanique, 338(2010), 510–517, 2010.

[17] Cochelin B., Vergez C. *A high order purely frequency-based harmonic balance formulation for continuation of periodic solutions*, Journal of Sound and Vibration, 324 (1-2), 243-262, 2009.

[18] Guillot L., Cochelin B., Vergez C. *A generic and efficient Taylor series–based continuation method using a quadratic recast of smooth nonlinear systems*, hal-01827832, 2018.

[19] Nayfeh A.H., Balachandran B. *Applied Nonlinear Dynamics*, John Wiley & Sons, 83-128, 1995.

[20] Vizzaccaro A., Salles L., Peng C. *Time finite element methods for the periodic solution of blade-tip casing interaction*, European Conference on Computational Mechanics (ECCM 6), 2018.

[21] Salles L., Peng C., Schwingshackl C.W. *Analysis of blade-tip casing interaction using harmonic balance method*, EUROMECH Colloquium 573 Coupling and Nonlinear interactions in Rotating Machinery, 2015.

[22] Idelsohn S.R., Cardona A. *A reduction method for nonlinear structural dynamic analysis*, Computer Methods in Applied Mechanics and Engineering, 49(3), 253-79, 1985.

[23] Givois A., Grolet A., Thomas O., Deü J.-F. *On the frequency response computation of geometrically nonlinear flat structures using reduced-order finite element models*, Nonlinear Dynamics, Springer, 1-35, 2019.

[24] Jain S., Tiso P., Rutzmoser J.B., Rixen D.J. *A quadratic manifold for model order reduction of nonlinear structural dynamics*, Computers & Structures, 188, 80-94, 2017.

[25] Rutzmoser J.B., Rixen D.J., Tiso P., Jain S *Generalization of quadratic manifolds for reduced order modeling of nonlinear structural dynamics*, Computers & Structures, 192, 196-209, 2017.

[26] Géradin M., Rixen D. *Mechanical Vibrations: Theory and Applications to Structural Dynamics*, John Wiley & Sons, 2015.

[27] Lazarus A., Thomas O., Deü J.-F. *Finite element reduced order models for nonlinear vibrations of piezoelectric layered beams with applications to NEMS*, Finite Elements in Analysis and Design, 49(1):35-51, 2012.

[28] Touzé C. , Vidrascu M., Chapelle D. *Direct finite element computation of non-linear modal coupling coefficients for reduced-order shell models*, Computational Mechanics, 54(2):567-580, 2014.